Parametric study on the lateral structural behaviour of a timber building concept with core-exoskeleton system

An investigation on the performance of complementary stability systems for a mid- and high-rise full timber building concept

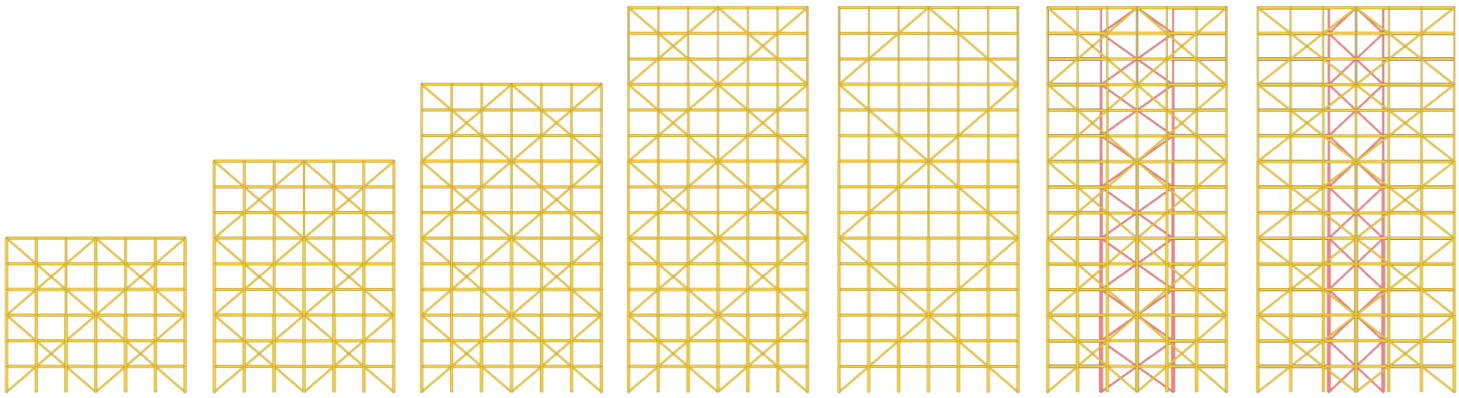

J.N.H. Karsemeijer
5364523
August 28, 2026

TU Delft

VAN ROSSUM RAADGEVENDE INGENIEURS

Parametric study on the lateral structural behaviour of a timber building concept with core-exoskeleton system

An investigation on the performance of complementary stability systems for a mid- and high-rise full timber building concept

By

J.N.H. Karsemeijer

In partial fulfilment of the requirements for the degree of:

Master of Science

in Civil Engineering

at the Delft University of Technology

Thesis Committee:	Dr. Ir. G.J.P. Ravenshorst	TU Delft, Main Supervisor
	Prof. Dr. Ir. J.W.G. van de Kuilen	TU Delft, Supervisor
	Dr. Ir. G. Pagella	TU Delft, Supervisor
	Dr. Ir. H.R. Schipper	TU Delft, Supervisor
	Ir. J.S. Van Hulst	Van Rossum, Supervisor

Preface

This thesis, titled ‘Parametric study on the lateral structural behaviour of a timber frame high-rise building concept with core-exoskeleton system’, marks the conclusion of my Master in Civil Engineering at TU Delft. The research is part of a consortium called the WoodCore project, which aims to develop a cost-effective and low-emission building concept. From November 2025 to August 2026, I invested a lot of time and effort into this project.

I have learned a lot during my thesis. Not only regarding technical aspects, such as modelling in SCIA Engineer and coding with Python, but also how to communicate with many different parties and how a structural engineering firm operates.

This thesis would not have been possible without the guidance and expertise of many people.

First of all, I want to thank my main supervisor Geert Ravenshorst, my second supervisor Giorgio Pagella, and Jan Willem van de Kuilen from the timber department of TU Delft for their guidance, suggestions and for sharing their expertise on timber during my project. I also would like to express my gratitude Roel Schipper for his guidance and feedback on the parametric design aspect of this report, as well as his general guidance throughout the completion process.

I am also very thankful for the everyday guidance and support of Jeffrey van Hulst, my supervisor at Van Rossum Ingenieurs. I really appreciated that I was always able to ask questions, and I am grateful for the time he invested in me. Furthermore, I want to thank the other people at Van Rossum for their warm welcome and for showing interest in my project. And I want to thank Van Rossum for giving me the opportunity to complete my internship there and for offering me a job as a structural engineer.

Lastly, I want to thank my family and friends for their support throughout my studies and the writing of this thesis.

Jan Karsemeijer
Delft, August 2026

Abstract

The Netherlands is currently facing a severe housing shortage. As the supply of new homes cannot keep up with the demand, housing prices have increased significantly in recent years (CBS, 2024). At the same time, the construction sector must comply with increasingly strict climate requirements, such as the Paris Agreement and Dutch Climate Act, to reduce CO2 emissions. Timber is a construction material with low carbon emissions, but to build higher than 6 stories, a concrete core or CLT is needed, which contribute significantly to CO2 emissions and increase construction costs, respectively (Saxion, 2025). To fill this gap, the WoodCore consortium was founded to develop a low-emission and affordable building concept.

This thesis is part of this consortium and aims to study the lateral stability and stiffness system of the building concept consisting of a timber exoskeleton, a braced timber core, and timber frame shear walls. The main objective of this report is therefore to investigate, through a parametric study, the extent to which the various stability systems of a timber building concept, comprising an exoskeleton, a braced core, and timber frame shear walls, influence the horizontal deflection of the building and how these systems can be optimized.

To achieve this objective, a parametric workflow has been developed. The workflow uses the finite element software SCIA Engineer. Within SCIA Engineer, models of the timber building concept were created and exported to XML files. By modifying these XML files using a Python script and running them using SCIA OpenAPI modules, many different parameter configurations could be studied. Since running a single configuration still takes approximately two minutes, and thousands of parameter configurations had to be executed, the workflow was expanded with a surrogate model. A surrogate model is a mathematical model that mimics the results of the finite element analysis, allowing for a significant expansion of the number of parameter configurations while reducing the total computational time.

With this approach, the influence of seven different parameters on the horizontal displacement of the building, and therefore the lateral stiffness of the building, was investigated across different variants with a varying number of stories and diagonal layouts. The parameters that were considered for both the exoskeleton and the braced core are: the dimensions of the timber diagonals, the dimensions of the timber columns, and the axial stiffness of the connections in the diagonals. In addition, the influence of the stiffness of the timber frame shear walls on the horizontal displacement of the building was studied.

To study the influence of the parameters, two sensitivity analyses were performed for every variant: a local sensitivity analysis using the One-At-a-Time method and a global sensitivity analysis using the Variance-based Sobol method. In addition, the economic and environmental influence of every parameter was studied using a material and shadow costs comparison and optimisation.

The local sensitivity analysis shows that for each variant, the exoskeleton has a significantly larger influence on the horizontal deflection than the braced core. Furthermore, it followed that the dimensions of the diagonals and the stiffness of the connections have a greater influence than the dimensions of the columns. The influence of each parameter remains mostly constant for variants with a different

number of stories. The diagonal configuration has a larger influence on the resulting deflection of the building, but for the investigated variants, the exoskeleton continues to dominate this deflection. The influence of the stiffness of the timber frame shear walls is highly dependent on the chosen parameter ranges.

The global sensitivity analysis also shows that the dimensions of the diagonals and the stiffness of the connections within the diagonals have the largest influence on the horizontal deflection. In this analysis, the influence of the diagonals and connection stiffness has become even more pronounced. This demonstrates that the influence of each parameter is highly dependent on the chosen parameter range and baseline model. Additionally, the GSA reveals that parallel linked parameters, such as the diagonals of the exoskeleton and braced core interact, meaning that the influence of these parameters are dependent on each other.

The cost-effectiveness analysis and optimization indicate that changing the dimensions of the diagonals and the axial stiffness of the connections not only has a major influence on the deflection but is also effective regarding material and shadow costs. This does not apply to the columns and applies to a lesser extent to the timber frame shear walls. Although the influence of the diagonals and connections in the braced core on the lateral stiffness is significantly lower than in the exoskeleton, the material and shadow cost-effectiveness of these parameters is comparable in both systems.

Based on these results, it can be concluded that the exoskeleton has a significantly larger influence on the deflection than the braced core and the timber frame shear walls. Furthermore, it can be concluded that the diagonals and axial connection stiffness have a significantly larger influence on the stiffness than the columns and beams in the exoskeleton and braced core. It can also be concluded that the influence of each parameter is highly dependent on the chosen parameter ranges and geometry, and that the number of stories does not necessarily influence the results. Optimal parameter configurations for material costs are characterized by minimal column dimensions and low stiffness of the timber frame shear walls. Despite the influence of the diagonals and connections in the exoskeleton on the deflection being significantly larger, it can be concluded that the cost-effectiveness of the diagonals and connection stiffnesses of the braced core are similar to the diagonals and connection stiffness in the exoskeleton.

Contents

Preface iv

Abstract v

1 Introduction 1
- 1.1 Problem Description 1
  - 1.1.1 Housing Shortage 1
  - 1.1.2 Environmental impact of the construction industry 1
  - 1.1.3 Inefficient construction and design process 2
  - 1.1.4 Limitations of timber frame buildings 2
  - 1.1.5 Problem Statement 2
- 1.2 Design Objective 3
- 1.3 Research questions 3
- 1.4 Scope 3
  - 1.4.1 Inclusions research 3
  - 1.4.2 Exclusions research 3
  - 1.4.3 Inclusions parametric model 4
  - 1.4.4 Exclusions parametric model 4

2 Literature Review 5
- 2.1 Designing with timber 5
  - 2.1.1 Mechanical properties timber 5
  - 2.1.2 ULS Verification 6
  - 2.1.3 SLS Verification 8
- 2.2 Timber connections 9
  - 2.2.1 Slotted steel connections 9
  - 2.2.2 General failure modes 9
  - 2.2.3 Brittle failure modes 11
  - 2.2.4 Minimum bolt distances 11
  - 2.2.5 Stiffness of connections according to EuroCode 12
  - 2.2.6 Stiffness of connection according to Malo 12
- 2.3 Current state of technology of timber buildings 14
  - 2.3.1 Mjøstarnet, Norway 14
  - 2.3.2 Treet, Norway 15
  - 2.3.3 Sara Kulturhus, Sweden 16
  - 2.3.4 HAUT, The Netherlands 17
  - 2.3.5 1430 Q Street, United States of America 18
  - 2.3.6 Summary State-of-the-art 19

3 Case-study description 21
- 3.1 Original case-study WoodCore 21
- 3.2 Description of the base-line model 22
  - 3.2.1 Used materials in the base-line model 24

3.2.2 Dimensions of the base-line model 25

4 Methodology 26
4.1 Research approach 26
4.2 Investigated parameters 26
4.3 Investigated variants 27
4.4 Parametric workflow 29
4.4.1 Evaluation of workflow alternatives 29
4.4.2 Description parametric workflow 30

5 Finite element modelling 32
5.1 Schematization and modelling of the building concept 32
5.1.1 Schematisation and modelling of Kerto-Ripa Floors 32
5.1.2 Schematisation and modelling of timber frame shear walls 33
5.1.3 Schematisation and modelling of connections 36
5.1.4 Schematisation of the foundation stiffness 37
5.1.5 Mesh setup 38
5.2 Load definition 39
5.2.1 Applied loads 39
5.2.2 Overview load cases and load combinations 41
5.3 Design of structural elements of the base-line model 42
5.3.1 Design and verification of columns 42
5.3.2 Design and verification of beams 42
5.3.3 Design and verification of floors 43
5.3.4 Design and verification of diagonals 44
5.4 Validation of the finite-element model 45
5.4.1 Reaction Forces on the foundation: 45
5.4.2 Deformation of individual elements and use of modification factors 46
5.4.3 Global deformation pattern of the building 48

6 Sensitivity Analyses 52
6.1 Local vs Global Sensitivity Analysis 52
6.2 Definition parameter ranges 53
6.2.1 Overview definition parameter ranges 53
6.2.2 Lower- and upper bound of columns in the exoskeleton and braced core 54
6.2.3 Lower- and upper bound of diagonals in the exoskeleton and braced core 55
6.2.4 Lower- and upper bound dimensions equivalent diagonal shear walls 56
6.2.5 Lower- and upper bound relative connection stiffness of connections in exoskeleton and braced core 57
6.2.6 Resulting lower- and upper-bound values of the baseline model 60
6.3 Local sensitivity analysis: One-At-a-Time method 61
6.3.1 Description of OAT method 61
6.3.2 Results of the OAT-method for the base-line variant 61
6.3.3 Results of the OAT-method for main additional variants 64
6.3.4 Exploratory studies of the building 69
6.3.5 Interpretation of the results of the OAT-method 71
6.3.6 Conclusion local sensitivity analysis 74

6.4 Global sensitivity analysis: Sobol-method 75
6.4.1 Description of the Sobol-method 75
6.4.2 Description and validation of the Gaussian Processing surrogate model 77
6.4.3 Global sensitivity analysis of the base-line variant 80
6.4.4 Global sensitivity analysis of additional variants 82
6.4.5 Interpretation of the results of the global sensitivity analysis 86
6.4.6 Conclusion global sensitivity analysis 88
6.5 Costs-effectiveness analysis 89
6.5.1 Material and shadow costs calculation framework 89
6.5.2 Costs versus influence comparison 90
6.5.3 Costs optimalisation of the base-line model 92
6.5.4 Conclusion cost-effectiveness analysis 95

7 Discussion 96

8 Conclusions and recommendations 98
8.1 Conclusions 98
8.2 Recommendations 101
8.2.1 Practical design recommendations 101
8.2.2 Recommendations for future research 102

Bibliography 103

Appendix A – Calculation wind load on the building 106
A.1 Wind pressure distribution over the height 106
A.2 General formula characteristic wind-load 107
A.3 Determination structural factor $c_s c_d$: 107
A.4 Determination expected wind velocity v_m and peak wind pressure q_p 107
A.5 Determination of force coefficient c_f 109

Appendix B – Design of timber members 111
B.1 Material properties timber 111
B.2 Overview verification 111
B.3 Design calculation for the governing failure mode 115

Appendix C – Modelling of floors 116

Appendix D – Modelling of timber frame walls 119

Appendix E – Additional results 121
E.1 Results global sensitivity analysis of the base-line model with average lower-bounds 121

Appendix F – Access to parametric model 122

1 Introduction

This chapter describes the societal and technical challenges that the construction industry is currently facing. In addition, the main design objective and additional research questions are formulated.

1.1 Problem Description

1.1.1 Housing Shortage

The Netherlands is currently facing a severe housing shortage. As the supply for new homes cannot keep up with the demand, housing prices have increased significantly in recent years and waiting lists for rental properties have grown (CBS, 2024). In particular, the demand for affordable houses is high which makes it more difficult for young adults to find a home for themselves, forcing them to delay important life stages.

The Dutch Ministry of Housing and Spatial Planning has calculated that in 2024 the national housing shortage was equal to 401,000 homes, which corresponds to 4.8% of the total housing supply. For the housing market to function at an acceptable level, the housing shortage should be significantly lower at approximately 2%. To reach this threshold, the Ministry has estimated that a total of 1.108 million new homes will need to be constructed by 2038 to account for the growing number of households (Ministerie van Volkshuisvesting en Ruimtelijke Ordening, 2024). It is evident that this presents an enormous challenge for the Dutch building sector, which needs to adopt efficient strategies to increase the output to keep up with the demand.

The housing shortage in the Netherlands has several causes (Ministerie van Volkshuisvesting en Ruimtelijke Ordening, 2023). Firstly, the population growth increases the demand for housing. At the same time, household types are changing, creating a higher demand for smaller and more affordable housing. In addition, the Netherlands is densely populated, with limited space available for building homes. The increasing housing prices are also caused by rising construction costs and lengthy administrative procedures which slow down construction. Lastly, obtaining building permits has become more difficult due to the nitrogen crisis in the Netherlands.

1.1.2 Environmental impact of the construction industry

In addition to the ambitious goals to solve the housing shortage, the construction sector must simultaneously comply with the climate requirements. In the Paris Agreement, it is stated that the global warming may not exceed a 2°C boundary, while aiming to limit the warming to 1.5°C (Copper8, et al., 2024). In addition to these international goals, the Dutch government approved a climate act which states that the CO_2 emissions in the Netherlands should be reduced with 55% by 2030, compared to the emission in 1990 and should be completely climate neutral by 2050 (Rijksoverheid, n.d.).

The building sector plays a significant role in the reduction of CO_2. At this moment, the building industry is responsible for approximately 11% of the total carbon dioxide emissions in the Netherlands (Copper8, et al., 2024). Additionally, the sector is the largest producer of waste in the Netherlands, generating approximately 22% of the total waste by mass (CBS, 2024). To deal with these challenges, the building

sector will need to develop and shift toward methods that encourage efficient working practices and the use of sustainable materials.

1.1.3 Inefficient construction and design process

The engineering and construction industry remain slow in adapting to technological innovation, resulting that the productivity growth lags behind the global economy (F. Barbosa, 2017). A reason for this is that the traditional way of working in the construction sector is optimized for linear progression. Consequently, it is often time-consuming and inefficient to adopt the design when changes need to be implemented at a later stage. In addition, the number of different alternatives that can be considered is limited as costs would increase. This is strongly contrasting with the need for fast and affordable construction to deal with the housing demand. A parametrized workflow adopted by the architecture, engineering and construction industry could streamline the design and construction process and could be an important step towards the industrialization of construction to fulfil the current needs (O. Lang, 2019).

1.1.4 Limitations of timber frame buildings

At the moment, the construction of timber frame buildings without a CLT or concrete core is naturally restricted to approximately four to six storeys (TKI, 2025). This limitation is caused by numerous reasons. Firstly, the compressive strength of timber perpendicular to the grain for platform-based construction methods could be a restriction as the loads on the elements increase. Additionally, for increasing height of the building, the lateral stiffness of the building will be more difficult to guarantee. Lastly, fire safety regulations become stricter when the number of occupants in buildings increases which makes it more difficult to meet the separation requirements (CWC, n.d.). In addition to structural limitations, also procedural obstacles such as limited awareness of emerging timber technologies hold back the use of timber-frames in multi-storey buildings (Xia & O'Neill, 2014).

To implement timber in mid- and high-rise buildings often a concrete core or cross laminated timber (CLT) is used. However, these methods also have drawbacks. Solutions with concrete have larger carbon emissions, while solutions using CLT are often 15% more expensive than timber frame buildings (TKI, 2025). If the technical difficulties can be resolved, mid- and high-rise timber frame buildings using a core-exoskeleton system could be a cost-effective and environmentally friendly solution.

1.1.5 Problem Statement

In summary, the problem can be described by the following bottlenecks:

- To meet the substantial housing demand and comply with climate agreements, low-emission and cost-effective construction methods must be adapted.
- Due to inefficient linear design and construction process, changes to the design can cause significant delays and less configurations can be considered.
- Due to technical restrictions current timber frame buildings with core-exoskeleton systems are generally limited to approximately four storeys.

1.2 Design Objective

The objective of this report is to investigate, through a parametric study, the extent to which the various stability systems of a timber building concept, comprising an exoskeleton, a braced core and timber frame shear walls influence the horizontal deflection of the building and how these systems can be optimized.

1.3 Research questions

In addition to the design objective, the following research questions are formulated:

- What is the current state of technology of timber buildings?
- How can a parametric workflow be developed to study the horizontal deflection of the timber building concept?
- Which stabilizing system contributes most to the lateral stiffness of the building?
- How does the influence of the stability systems change when varying the number of storeys or the structural geometry?
- How can the stability systems be optimized to minimize material costs and environmental impact?

1.4 Scope

This paragraph defines the scope of the project to ensure the assignment can be completed within the available timeframe and to provide clarity to the different parties involved regarding the expected outcome. Firstly, the inclusions and exclusions regarding the research objectives are defined. Subsequently, the inclusions and exclusions regarding the parametric model will be described.

1.4.1 Inclusions research

The research as part of this project includes the following aspects:

- Although timber frame buildings have multiple limitations for high-rise structures as described in Section 1.1.4, this study focuses on the lateral stiffness and horizontal deformation of the building under wind loads in the Serviceability Limit State (SLS).
- Multiple sensitivity analyses will be conducted to quantify how much every stability system contributes to the lateral stiffness of the building.

1.4.2 Exclusions research

The following aspects of the research will not be included in this project:

- Fire safety will not be considered for this project as this study focusses on the lateral stiffness in SLS.
- The analysis is limited to static wind loads excluding dynamic effects such as natural frequencies and accelerations.
- Seismic loading will not be considered for this research.
- Time-dependent effects on the lateral behaviour of the building will not be considered.

1.4.3 Inclusions parametric model

The parametric model is the main tool for this research. The following aspects are included in the parametric model:

- The following parameters will be implemented in the parametric model:
    - Dimensions of elements in exoskeleton
    - Dimensions of elements in core
    - Stiffness of timber frame shear walls
    - Stiffness of connections
- The influence of these parameters on the horizontal displacement will be analysed for both the x and y direction of the building.
- The influence of these parameters will be analysed for the same building with 6, 9 and 12 storeys, in addition to the reference model of 15 storeys.

1.4.4 Exclusions parametric model

The following aspects will not be part of the parametric model:

- The analysis will be based on a constant structural geometry, with exceptions of the number of stories and the diagonal structure in the exoskeleton.
- The floor plan layout is also maintained, meaning the grid does not change during the analysis.

2 Literature Review

2.1 Designing with timber

2.1.1 Mechanical properties timber

Anatomy of wood:

To understand the mechanical behaviour of timber, a solid understanding of the anatomy of the wood is needed. Wood is an organic material which consists of cellulose, hemicellulose, lignin and other constituents. Due to the elongated structure of the cells and orientation of cell walls, physical properties of the wood depend on the angle at which a load is applied with respect to the grain directions. Timber is therefore called anisotropic material (Blaß & Sandhaas, 2017).

Although wood is an anisotropic material, for structural purposes it is assumed to be orthotropic, which means that it is assumed that timber has directional properties in three perpendicular orthogonal axes (J. Porteus, 2007). In Figure 2.1, the longitudinal (L), radial (R) and the tangential (T) directions are displayed for a tree trunk (a) and for a piece of timber (b). Timber is noticeably stronger and stiffer in the longitudinal direction. The properties of timber in tangential and radial direction are very similar and are therefore combined in one direction called perpendicular to the grain (J. Porteus, 2007).

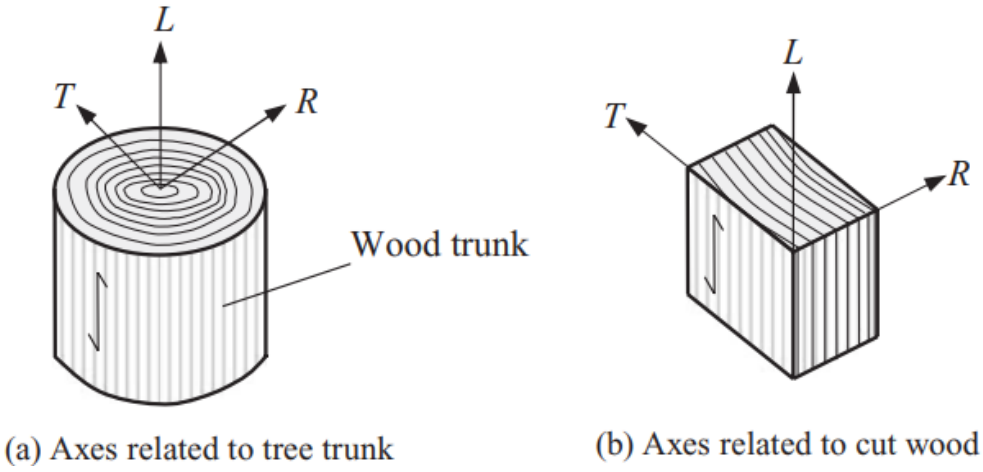

Figure 2.1: Orthogonal directions of wood (J. Porteus, 2007).

However, as a timber element can also be loaded under an angle to the grain, Hankinson proposed equation 2.1 to determine the compressive and tensile strength of a timber element under an angle α. The formula assumes a linear interaction between the strength parallel and perpendicular to the grain (Blaß & Sandhaas, 2017). The tensile strength under an angle can be found by replacing f_c with f_t.

$$f_{c,\alpha} = \frac{f_{c,0} * f_{c,90}}{f_{c,0} * \sin^2(\alpha) + f_{c,90} * cos^2(\alpha)} \quad (2.1)$$

Where:

α	[°]	=	angle between the load and grain direction
$f_{c,0}$	[MPa]	=	compressive strength parallel to the grain
$ft_{,0}$	[MPa]	=	compressive strength parallel to the grain

Material properties glulam:

The building concept where this thesis focuses on using Glued Laminated (glulam) timber for the main structural elements. glulam is fabricated from timber sections which are bonded together using adhesives (Blaß & Sandhaas, 2017). All timber sections are laminated parallel to the longitudinal axis. In Figure 2.2 an illustration of a glulam beam is displayed. The characteristic material properties of glulam which will be used for the design of the building are displayed in Appendix B.1 (EN 14080, 2013).



Figure 2.2: Glued Laminated Beam (Blaß & Sandhaas, 2017).

2.1.2 ULS Verification

Design resistance:

The Eurocode standards are based on limit states which should not be exceeded to comply with the design requirements. The first limit state taken into consideration is the ultimate limit state (ULS), which when exceeded, in case of structural failure, may put personal safety at risk (Blaß & Sandhaas, 2017). In the ULS, the design value of the action or load should not exceed the design value of the resistance as is visualized in Figure 2.3.

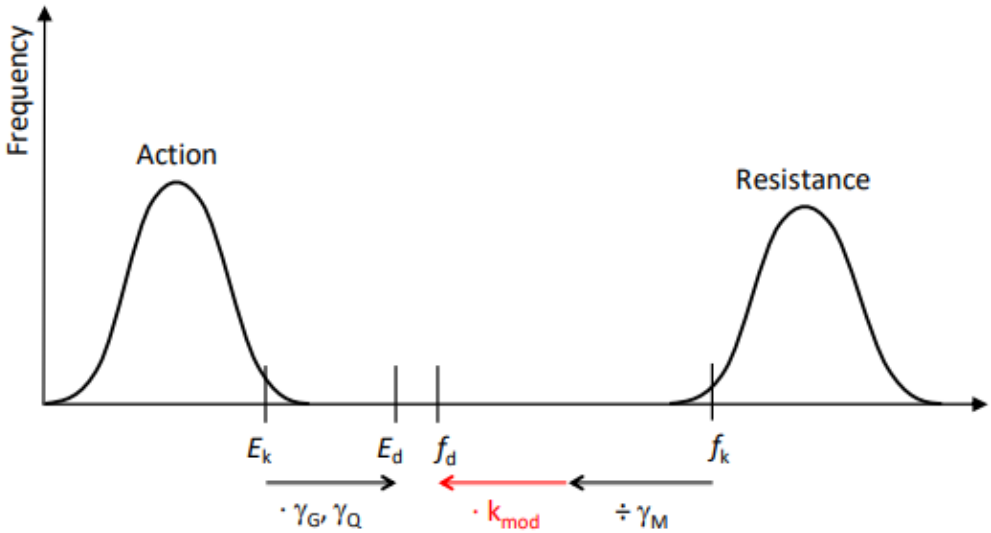

Figure 2.3: Reduction of probability of failure through partial safety factor and k_{mod} (Blaß & Sandhaas, 2017).

To determine the design value X_d for a material property with characteristic value X_k equation 2.2 can be used. For glulam members smaller than 600 mm, the characteristic value for bending ($f_{m,k}$) and tension parallel to the grain ($f_{t,0,k}$) should be multiplied with factor k_h to account for the size-effect (NEN-EN-1995-1-1, 2011).

$$X_d = k_{mod} * \frac{X_k}{\gamma_M} \quad (2.2)$$

Where:

X_k	[MPa]	=	the characteristic value of a strength property
k_{mod}	[-]	=	modification factor which takes the load duration and moisture content into consideration
γ_M	[-]	=	partial safety factor for the material property

ULS Checks:

In Table 2.1, an overview of the ULS checks is displayed which are needed for verification of the resistance of the timber elements (NEN-EN-1995-1-1, 2011).

	Compression	Tension	Buckling pure compression	Buckling compression + bending	Shear	Bending + tension	Vertical deflection
Beams Exoskeleton	X	X		X		X	X
Columns Exoskeleton	X	X	X				
Diagonals Exoskeleton	X	X	X				
Beams Core	X	X		X		X	X
Columns Core	X	X	X				
Diagonals Core	X	X	X				
Beams Wall	X			X	X	X	X
Beams Floor	X			X	X	X	X
Columns Remaining	X	X	X				

Table 2.1: Overview Ultimate Limit State verification checks.

2.1.3 SLS Verification

The second limit state taken into consideration is the serviceability limit state (SLS) which compromises deformations or vibrations which could impact or damage the planned usage of a structure (Blaß & Sandhaas, 2017). For this project vibrations and acoustics are not taken into account. The two SLS verifications that are considered are the total horizontal deformation of the building and the vertical deflection of beams.

The total horizontal deformation of the building is defined as the maximum displacement the top of the building will have to the critical characteristic load. In equation 2.3, the SLS check for the total deformation is displayed (NEN-EN-1990-NB, 2019).

$$u \leq \frac{H}{500} \tag{2.3}$$

Where:

H [mm] = The total height of the building

In addition to the maximum horizontal deformation of the entire building, the displacement of each storey subjected to the critical characteristic load should also be limited. In equation 2.4, the SLS check for the deformation for each storey is displayed (NEN-EN-1990-NB, 2019).

$$u_i \leq \frac{H_i}{300} \tag{2.4}$$

Where:

H_i [mm] = The height of the critical storey

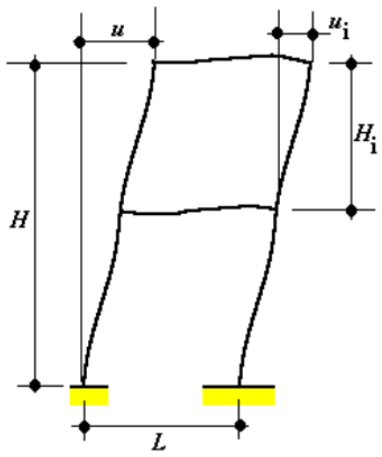

Figure 2.4: Overview horizontal displacements in SLS (NEN-EN-1990-NB, 2019).

In addition to the deflection of the building, the vertical deflection of the beams and the floors were verified according to the EuroCode (NEN-EN-1995-1-1, 2011) as described in Section 5.3.

2.2 Timber connections

2.2.1 Slotted steel connections

To connect the timber columns, beams and diagonals in the exoskeleton and the core skeleton slotted-in steel plate connections will be used. Slotted-in steel plates are commonly used in large timber structures due to their high resistance. Another advantage of slotted-in steel-to-timber connections is that the timber protects the steel to improve fire resistance (Leur, 2023). To construct these connections, grooves are cut in the timber members. Subsequently steel plates with bolt holes are placed in these grooves. The steel plates and timber elements are connected using steel dowels. In Figure 2.5, an example of a slotted-in steel connection is shown.

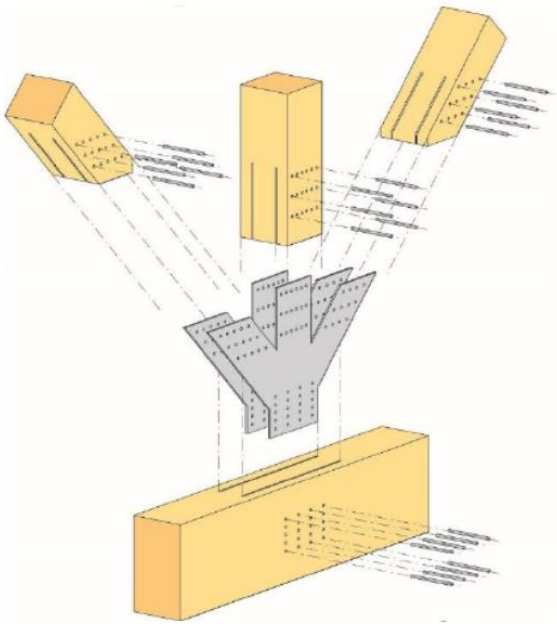

Figure 2.5: Example slotted-in steel timber connection (Crocetti, 2016).

2.2.2 General failure modes

For the ULS verification of the connections, the new timber Eurocode is used (NEN-EN-1995-1-1, 2025). The connections in the building will be designed such that failure mode D is the governing failure mode. In this failure mode plastic hinges form inside the stainless-steel dowels. By designing the connections this way, it can be guaranteed that the connections will show ductile failure. Therefore, signs of failure can be recognized before the structure collapses.

Failure mode D is the equivalent of failure mode f for multiple shear planes. In Figure 2.6, failure mode D is displayed on the left, while failure mode f is shown on the right. For the slotted-in steel-to-timber connections which are considered for this study, the parts in the connection denoted with a 2 represent the steel p[lates. The outer timber members are denoted with a 1 and the inner timber members are denoted with a 3.

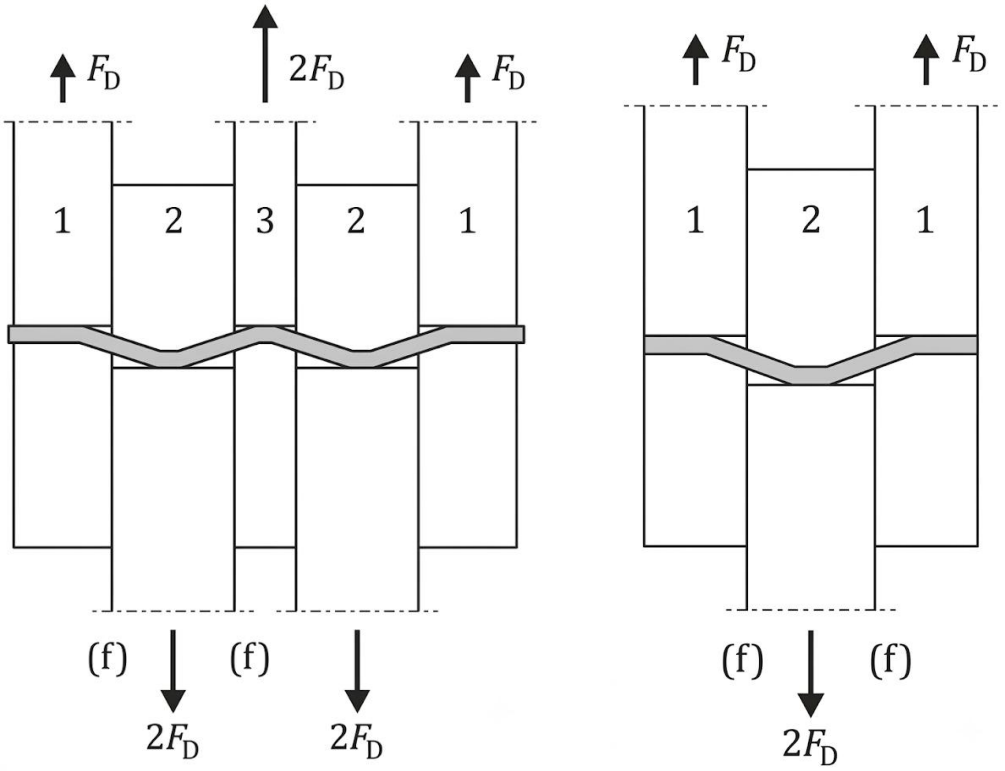

Figure 2.6: Considered failure modes for steel-to-timber connections: failure mode D on the left for multiple steel plates and failure mode f for a single steel plate on the right (NEN-EN-1995-1-1, 2025).

To calculate the characteristic resistance per shear plane of the connection for failure mode f, equation 2.5 can be used.

$$F_{D,k} = 1{,}15 * \sqrt{\frac{2 * \beta}{1 + \beta}} * \sqrt{2 * M_{y,k} * f_{h,1,k} * d} \qquad (2.5)$$

$$\beta = \frac{f_{h,2,k}}{f_{h,1,k}}$$

Where:

$M_{y,k}$	[Nmm]	=	The characteristic yield moment
$f_{h,1,k}$	[MPa]	=	The characteristic embedment strength of glulam
$f_{h,2,k}$	[MPa]	=	The characteristic embedment strength of steel = 600
d	[mm]	=	The diameter of the steel dowel

To guarantee that failure mode f will occur, the distances between the steel plates and the distance between the steel plate and the edge of the connection must me sufficient such that plastic hinges occur in the steel dowels. To calculate these distances the Eurocode proposes equation 2.6 (NEN-EN-1995-1-1, 2025).

$$t_{h,req} = 1{,}15 * 4 * \sqrt{\frac{M_{y,k}}{f_{h,k} * d}} \qquad (2.6)$$

2.2.3 Brittle failure modes

In addition to the general ductile failure modes described in paragraph 2.2.2, brittle failure modes such as splitting, row shear, block shear, net tensile failure and plug shear should be taken into account for the design of the slotted-in steel to timber connections. The revised Eurocode proposes a simplified approach to prevent the brittle failure modes. The brittle failure modes can be neglected provided that the minimum spacings a_1, a_2, and end distance $a_{3,t}$ is multiplied with factor k_{br} (NEN-EN-1995-1-1, 2025). This factor to increase the spacing and loaded end distance can be calculated using equation 2.7.

$$k_{br} = \max \begin{Bmatrix} 1.0 \\ \left(1 + k_{rp,2}\right) * k_{pos} * n_0^{0.5} * n_{90}^{0.3} * d^{-0.2} \end{Bmatrix} \quad (2.75)$$

Where:

$k_{rp,2}$	[-]	=	The limitation of the rope-effect contribution, for smooth dowels = 0
k_{pos}	[-]	=	Factor related to the timber member position, for combination of inner and outer members = 1.0
n_0	[-]	=	The number of dowels in row parallel to the grain
n_{90}	[-]	=	The number of dowels in row perpendicular to the grain
d	[mm]	=	The diameter of the dowel

2.2.4 Minimum bolt distances

To prevent splitting of the timber and to ensure a more even stress distribution, the dowels in the connection should have sufficient spacing between each other and between the edge and end of the connection. In Table 2.2, the minimum distances between the dowels and the edges is displaced as a function of the dowel diameter d (NEN-EN-1995-1-1, 2025). The dowels used in the slotted-in steel timber connection are predrilled steel dowels. Figure 2.7, the minimum distances are indicated.

Dowel Type	$a_{1,min}$	$a_{2,min}$	$a_{3,t,min}$ (loaded end)	$a_{3,c,min}$ (unloaded end)	$a_{4,t,min}$ (loaded edge)	$a_{4,c,min}$ (unloaded edge)
Dowels and bonded-in rods	5d	3d	max(7d; 80mm)	4d	4d	3d

Table 2.2: Minimum spacings, edge and end distanced for glulam connection with dowels.

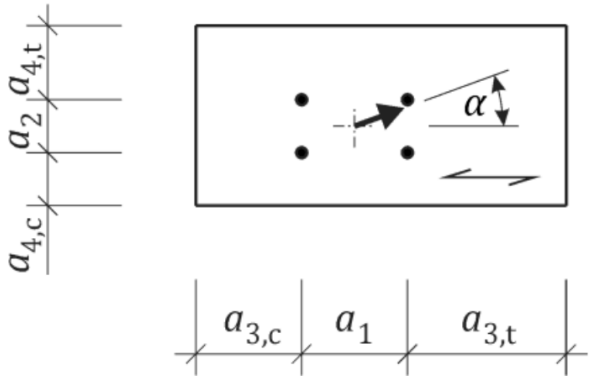

Figure 2.7: Minimum spacings, edge and end distances (NEN-EN-1995-1-1, 2025).

2.2.5 Stiffness of connections according to EuroCode

The stiffness of the connections is a very important parameter for the lateral stiffness of the building. For this study, only the longitudinal stiffness of the connection will be considered. It is assumed that de rotational connection stiffness of the connection between the main load bearing elements does not influence the global lateral deformation of the building. The connections of the main load bearing elements of the exoskeleton and the timber frame core are designed such that the centre lines of the elements connect in the same location. Therefore, the bending moments in the connections will be equal to zero and the rotational stiffness would not influence the total lateral behaviour. The timber connections will therefore be modelled as hinged with only springs in the direction of the elements.

The slip modulus or stiffness of the connection in longitudinal direction can be calculated using equation 2.8, which is revised in the new Eurocode for timber (NEN-EN-1995-1-1, 2025).

$$K_{SLS,v} = \sum_{i=1}^{n_{90}} \min\{n_{0,i}; 6\} * m * K_{SLS,v,i} \tag{2.6}$$

Where:

$n_{0,i}$	[-]	=	The number of fasteners in a row parallel to the grain
n_{90}	[-]	=	The number of fasteners in a row perpendicular to the grain
m	[-]	=	The number of shear planes per fastener
$K_{SLS,v,i}$	[N/mm]	=	The slip modulus of a single fastener per shear plane

The slip modulus of a single steel dowel per shear plane should be calculated according to equation 2.9 (NEN-EN-1995-1-1, 2025). The slip modulus of steel-to-timber connections can be multiplied with factor 2.

$$K_{SLS,v,i} = \rho_{mean}^{1.5} * \frac{d}{23} \tag{2.9}$$

Where:

ρ_{mean}	[kg/m^3]	=	The mean density of timber
d	[mm]	=	The diameter of the dowel

The long-term effects on the lateral stiffness of the building will not be accounted for in this study for the calculation of the global lateral stiffness of the building. It is assumed that the long-term effects will not have a significant impact on the horizontal deformation of the building as they mainly are affected by long-term permanent loading which are only applied on vertical direction. Long-term effects will be accounted for in the design of the beams of the structure.

2.2.6 Stiffness of connection according to Malo

In the calculation of the stiffness of the slotted-in steel-to-timber connections according to the Eurocode, the total stiffness of the connection can be obtained by linearly multiplying the stiffness per shear plane with the total number of shear planes, with a maximum of 6 dowels in parallel direction (NEN-EN-1995-1-1, 2025) as described in Section 2.2.5. According to Malo, this method overestimates the stiffness of the connection for large timber connections which was found during the design of the Mjøstarnet. Therefore, Malo proposed an exponential relationship between the number of dowels and the total stiffness of the connection (Malo, 2023).

Using the method proposed by Malo, the total stiffness of the connection can be determined using Equation 3.0 (Malo, 2023).

$$K_{ser,mod} = k_{ser} * m * n_{spd} * n_0 * (q_{0,1} + q_{0,2} * e^{\frac{1-n_0}{r_0}}) * n_{90} * (q_{90,1} + q_{90,2} * e^{\frac{1-n_{90}}{r_{90}}}) \tag{1.0}$$

In this formula K_{ser} is determined according to NEN-EN 1995-1-1 as described in Section 2.2.5 and n_{spd} is equal to the number of shear planes per dowel. The remaining factors can be determined using Table 2.3. It should be noted that these factors are determined for dowels with a diameter of 12 mm. In this study also dowels with diameters of 10 and 14 mm are considered for the design of the timber connections. As the diameter of the dowels is accounted for in k_{ser} and as the connection stiffness is only calculated to determine the lower- and upper bound of the parameter ranges, it is assumed that this does not influence the results of the study.

	Along grain			**Perpendicular grain**		
Number of dowels	n_0			n_{90}		
Model symbols	$q_{0,1}$	$q_{0,2}$	r_0	$q_{90,1}$	$q_{90,2}$	r_{90}
Model values	0.3	0.7	2	0.3	0.7	4
Loading direction	$m = 2.5$			$m = 1.3$		

Table 2.3: Model parameters for calculating the connection stiffness according to Malo for dowels with a diameter of 12 mm (Malo, 2023).

2.3 Current state of technology of timber buildings

In this paragraph, the structural system and design characteristics of some of the highest buildings which use load bearing timber are described. This provides an overview of the current 'state-of-the-art' of timber buildings to gain knowledge on different lateral stability systems and to obtain reference values to compare with the obtained values for the design and verification of the model. The buildings that will be considered are Mjøstarnet, Treet, Sara Kulturhus, HAUT and 1430 Q street.

2.3.1 Mjøstarnet, Norway

Mjøstarnet, translated to Mjøsa tower, is an 18-storey timber building which is located in Norway near the Mjøsa lake. Upon completion in 2019, the building was the highest timber building in the world with a height of 84.4 meters. The building has a footprint of about 17 by 37 meters with a net area of 11300 m^2 and will provide space for offices, apartments, a hotel, a restaurant and a roof terrace (Abrahamsen R. , 2017).

Structural system:

The structural load bearing system of the Mjøstarnet is entirely made of timber. The large-scale glulam trusses along the facades and the internal columns and beams as displayed in Figure 2.8 are the main load bearing elements. The glulam trusses provide the necessary horizontal stiffness of the building. The CLT walls in the building are only secondary load bearing elements for the elevators and staircases and do not contribute to the lateral stiffness of the building (Abrahamsen R. , 2017). To reduce peak accelerations, timber-concrete composite floors are implemented from level 12 to 18. The maximum calculated horizontal deflection of the top of the building is 140 mm. The wind loading turned out to be the dominating load in the design combinations. The wind load was applied as a static load (Abrahamsen R. , 2017).

The building uses slotted-in steel connections to connect the glulam trusses with steel grade S355, see Figure 2.8 (Abrahamsen R. , 2017). The steel plates and dowels are embedded deep into the timber to protect the steel from fire. For the glulam elements strength classes GL30c and GL30h is used and designed for climate class 1. Typical dimensions of the corner columns are 1485 x 625 mm^2 and for internal columns 725 x 810 mm^2. The beams below the timber floors have a general dimension of 395 x 675 mm^2 (Abrahamsen R. , 2017).

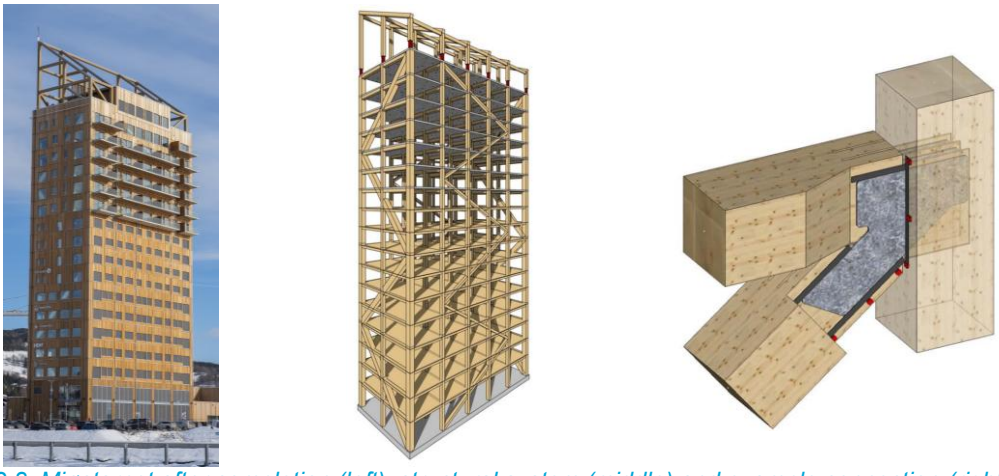

Figure 2.8: Mjøstarnet after completion (left), structural system (middle) and example connection (right) (Abrahamsen R. , 2017), (Moelven Limtre As, 2019).

2.3.2 Treet, Norway

Treet, translated to 'the tree' is a fourteen-storey building located in Bergen, Norway. The building was completed in 2015 and was at the time the highest timber building in the world with a height of 45 meters. The building has a total net area of 5830 m^2 and provides space to 62 apartments (Abrahamsen & Malo, 2014).

Structural system:

The structural system of the building consists of glulam trusses and prefabricated residential modules. To explain the structural design of the building an analogy to a cabinet rack filled with drawers can be used, where the large glulam trusses can be seen as the cabinet rack and the prefabricated residential modules as the drawers. The glulam trusses along the façade provide the horizontal stiffness of the building. The CLT core and the prefabricated residential modules do not contribute to the horizontal stiffness. Level 5 and 10 are so-called 'power-storeys' which are strengthened with a large glulam truss system. On top of the power-storeys prefabricated concrete slabs are placed which carry four levels of stacked residential modules, see Figure 2.9 (Abrahamsen & Malo, 2014).

All glulam elements are connected using slotted-in steel plates and dowels. Typically, 8 mm plates with a steel grade of S355 and 12 mm dowels are used for the connection. Most structural timber is covered behind glass and metal sheeting. Climate class 1 is used for members that are indoors. For the glulam members strength classes GL30c and GL30h are used (Abrahamsen & Malo, 2014). Typical dimensions for the columns are 305x650 mm^2 and 495x495 mm^2. The diagonal bracing has a typical bracing of 405x405 mm^2.

Modelling and Analysis:

For verification the building was modelled using Robot Structural Analysis Professional 2013 computer-software. The glulam trusses are modelled with their actual geometry and stiffness. The connections of the trusses are modelled with pinned joints between all members. Slip in the connections was not included in the design as every connection consists of a considerable number of dowels The highest found compression force in a column was equal to 4287 kN and the highest tension force in a column is equal to 296 kN. The highest tension force in a diagonal is 930 kN. Under the design wind load, the maximum horizontal deflection at the top of the building is equal to 71 mm. which equals L/634 and therefore satisfies the requirement of L/500 (Abrahamsen & Malo, 2014).



Figure 2.9: Overview 'Treet' Norway (Abrahamsen & Malo, 2014) (BOB, 2015).

2.3.3 Sara Kulturhus, Sweden

The Sara Kulturhus is a 20-storey timber building located in Skelleftea, Sweden. The building was completed in 2001 and has a height of 72.8 m. The building houses a museum, theatre, library and hotel. The hotel is located on the upper 16 storeys which have a footprint of 40.0 x x15.0 m^2 (Yan & Chen, 2025).

Structural System:

The upper 16 storeys of the main tower of the building uses two CLT cores on both sides of the building for stability of the building. In between the CLT cores CLT room modules are placed, see Figure 2.10. The room modules are prefabricated and stacked up-on each other at the construction-site. Glulam columns on the corners of the modules carry the vertical load. The roofs of the modules are connected to each other and the CLT cores to enable diaphragm action to improve the horizontal stability (Yan & Chen, 2025).

Below the hotel, on the 5th floor, a steel framework is located to enable a large open space near the main entrance. The steel truss rests on glulam beams with dimensions of approximately 400x600 m^2. On the 19th and 20th floor, heavy concrete slabs are installed to reduce horizontal acceleration of the building due to the wind load. To reduce noise from fans on the technical plant area concrete floors have also been installed on floors 5 and 6 (Yan & Chen, 2025).

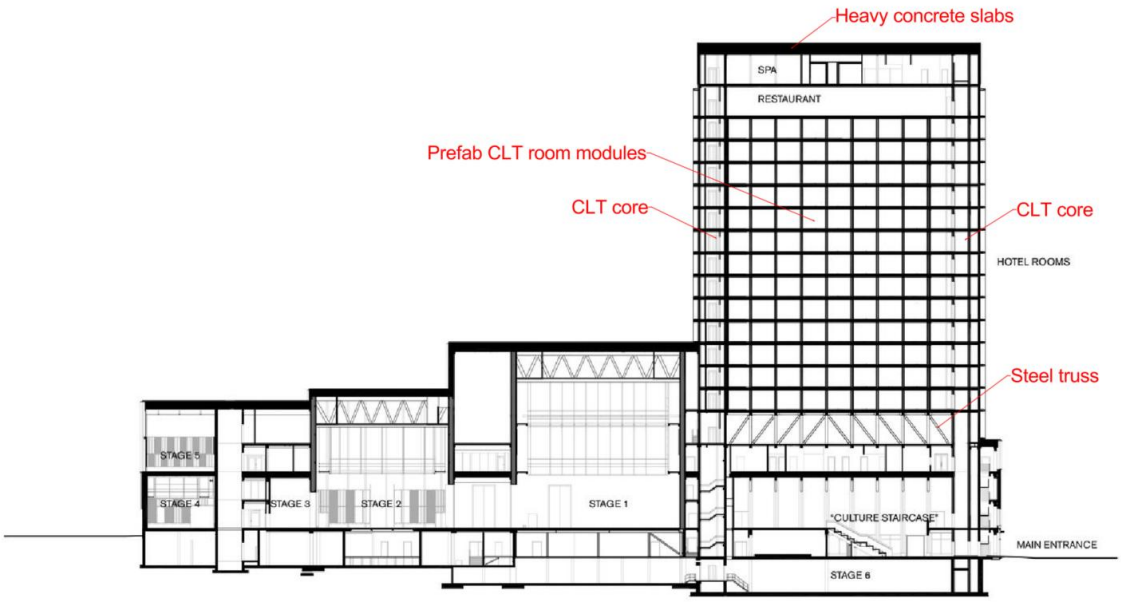

Figure 2.10: Front view structural elements Sara Kulturhus (CLT Rezult, 2024).

2.3.4 HAUT, The Netherlands

HAUT, is a 21-storey building located in Amsterdam, The Netherlands. The building was completed in 2021 and has a height of 73 meters, making it the highest (hybrid) timber structure in the Netherlands upon completion. The residential building has a total net floor area of 14,500 m^2 (Verhaegh, 2021).

Structural system:

One of the aims of the architects was to have unobstructed views from the residential compartments. To achieve this a load-bearing façade structure was ruled out at an early stage (Verhaegh, 2021). The use of a CLT core was also investigated but was ruled out as it would demand a high steel use to achieve very stiff connections. For the final design a solution using a concrete core and two CLT shear walls was chosen. For architectural reasons the concrete core would be placed eccentrically which introduces torsional effects under wind loads and increasing lateral deflections. To reduce these effects the CLT walls were chosen. In addition, the concrete core is extended with flanges up to certain heights, see (Verhaegh, 2021).

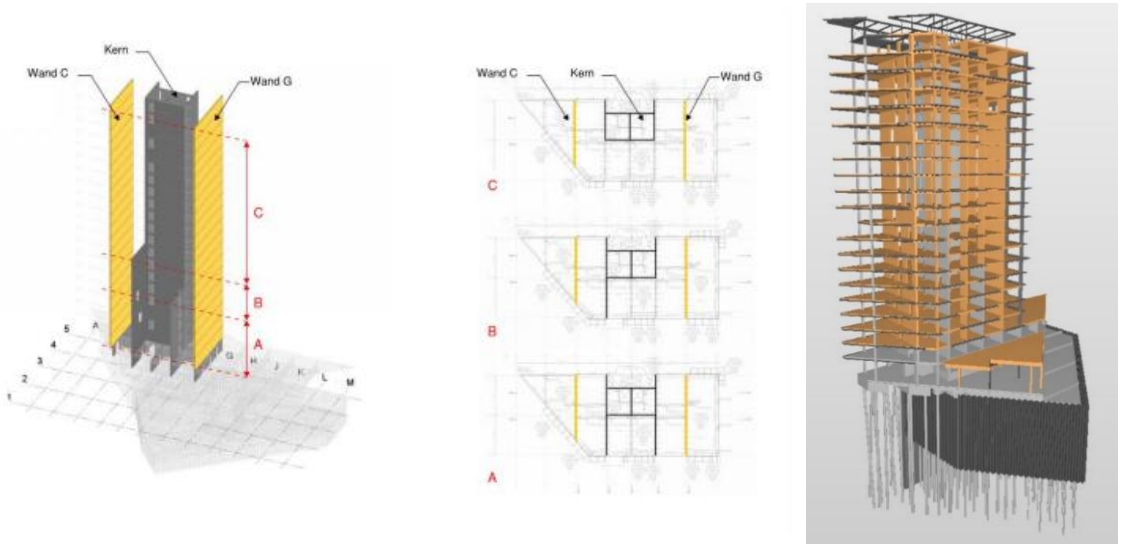

Figure 2.11: Lateral stability system HAUT (left) and the building structure (right) (Verhaegh, 2021).

To reduce peak accelerations and improve acoustics, timber-concrete composite (TCC) floors were used for the building. To enable diaphragm action in the floors the individual TCC floors are connected in-plane (Verhaegh, 2021). On the locations where the floor edges are not supported by a load bearing wall, the floors are carried by glulam beams with approximate dimensions of 450x900 mm^2 and strength class GL28h-GL32h (Yan & Chen, 2025).

2.3.5 1430 Q Street, United States of America

The 1430 Q Street building in Sacramento, California is the first residential two-over-six storey light timber-frame building in the United States of America (WoodWorks, 2020). The building has a total height of 29 meters, making it the tallest timber frame light timber-frame building in the United States upon completion in 2020. The footprint of the building is approximately 36.9 x 49.0 m^2 and provides a total net area of 15144 m^2 (Miller, 2019). In Figure 2.12, the building is displayed during construction and after it was completed.

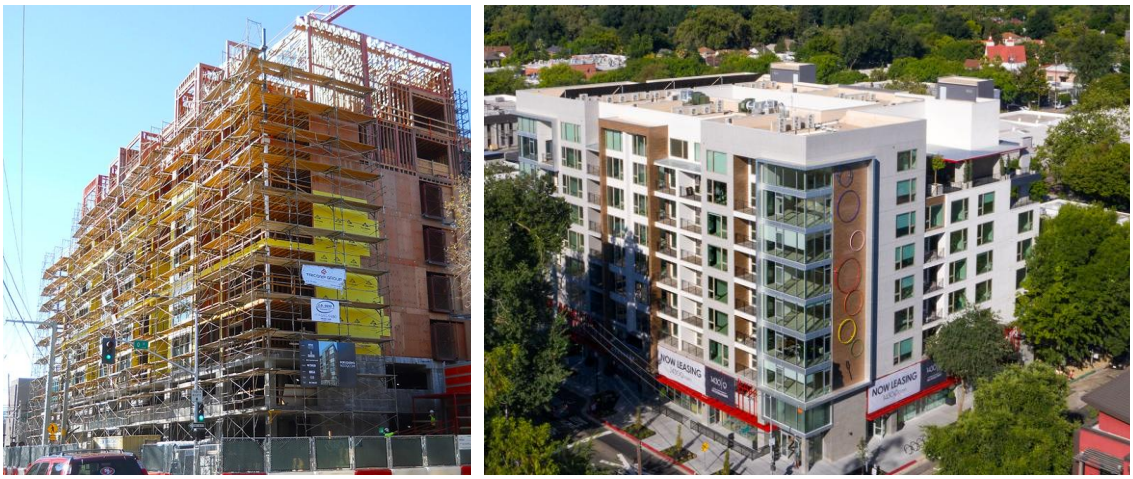

Figure 2.12; 1430 Q Street building during construction (Buehler, 2019) and after completion (Folkins).

Structural System:

As explained, building uses a six-over-two building system where 6 storeys of timber-framed floors are placed on top of a concrete podium. The concrete shear walls where extended until the third floor above the concrete podium. This was done to comply with the local code limitation where a maximum of 5 timber frame stories is allowed to be placed on top of a concrete podium or foundation (Miller, 2019). Above the third floor, all shear walls are made of timber frames as displayed in Figure 2.13. The timber frame walls are loading bearing and transfer the vertical load to the concrete podium. In addition, the timber frame walls are also shear walls to provide lateral stability to the building. The shear walls are only located on in residential dividing walls. Some walls at the bottom of the timber frame superstructure are double sided to increase the shear stiffness (WoodWorks, 2020).

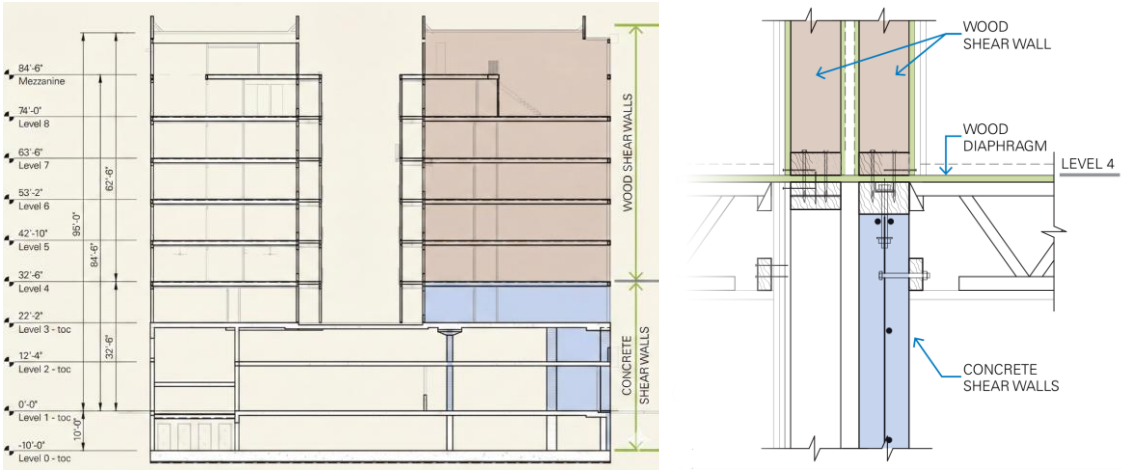

Figure 2.13: Location shear walls and detail of connection between timber and concrete shear walls (WoodWorks, 2020).

One of the biggest challenges was to connect the double shear walls to the concrete shear walls (Miller, 2019). The load of the timber shear wall which is not placed directly above the concrete shear wall through a segment of the timber diaphragm sheathing. To prevent rocking of the walls, a continuous tie-down rod system is used for hold-downs as displayed in Figure 2.13. All timber frames which were used for the superstructure where prefabricated. The structural timber walls were framed with 2x6 (38mm x 140mm) and 3x6 (64mm x 140mm) studs with a common spacing of 300 mm. The timber frame walls were covered with 20 mm plywood panels (WoodWorks, 2020).

2.3.6 Summary State-of-the-art

This paragraph summarizes the main findings of the literature study. In Table 2.4, the height and lateral stability systems of the timber buildings are summarized. It can be concluded that buildings using light-weight timber frame shear walls for the lateral stability is limited to approximately 6 storeys. Using alternatives such as a concrete core or CLT cores, a much higher building height can be reached until approximately 73 meters. The highest timber building is made using a large-scale glulam truss system to guarantee lateral stability, reaching a height of 85.4 meters. Based on the heights that can be achieved using the different lateral stability systems, the reference building, with a height of 45 meters, which combines a timber frame exoskeleton, a timber frame core and timber frame shear walls should be feasible given that the timber frame walls are not overloaded in both vertical and horizontal direction.

Timber Building	Height [m]	Storeys	Lateral stability system
Mjøstarnet	85.4	18	Large-scale glulam truss
Treet	45	14	Glulam truss with two ‘power-storeys’
Sara Kulturhus	72.8	16	Two CLT cores with CLT modules in between
Haut	73	21	Concrete core in combination with two CLT shear walls
1430 Q Street	29	8	Light-weight timber frame superstructure on top of a two-storey concrete podium

Table 2.4: Overview lateral systems and height of state-of-the-art timber buildings.

In Table 2.5, some of the dimensions and material classes that were used for the design of the state-of-the-art timber buildings are displayed. These reference values and used material classes can be used for first indication and comparison for the design of the reference building of the case-study. From the overview it can be concluded that glulam beams with strength class GL30c & GL30h are often used for the main load bearing elements. For the connections between the glulam elements, often slotted-in connections are used with a strength class of S355.

Timber Building	Reference dimensions	Material classes
Mjøstarnet	*Glulam corner columns:* 1485x625 mm^2 *Glulam internal columns:* 725x810 mm^2 *Glulam beams:* 395x675 mm^2 *Glulam diagonal bracing*: 625x990 mm^2	*Timber truss*: GL30c & GL30h *Slotted-in steel connection*: S355
Treet	*Glulam elements:* Column: 305x650mm^2 and 495x495mm^2 Diagonal bracing: 405x405 mm^2 *Slotted-in connections:* Steel plates: 8 mm Dowels: 12 mm	*Timber truss*: GL30c & GL30h *Slotted-in connections*: Steel plates: S355 Stainless steel dowels: f_y=755 MPa
Sara Kulturhus	*Glulam columns carrying truss:* 400x600 mm^2	*Glulam columns*: GL30c
Haut	*Glulam edge beams*: 450x900 mm^2	*Edge beams*: GL28h-GL32h
1430 Q Street	*Timber frame studs:* 64x140mm^2 and 64x140mm^2 *General spacing studs*: 300 mm *Timber frame panels*: 20 mm plywood	

Table 2.5: Overview reference dimensions and material classes of state-of-the-art timber buildings.

3 Case-study description

3.1 Original case-study WoodCore

This study is part of a consortium called the WoodCore Project. This consortium aims to develop a full timber building concept. For this concept a indicative model was developed. A number of changes has been made to the indicative model to make the model both structurally as architectural more feasible. This results in the reference model which will be used for this study. The changes and the resulting reference model are described in Section 3.2 were also the used materials, material dimension, schematisation and modelling of the reference building is described in more detail.

In Figure 3.1, the indicative model of the 15-storey building is displayed. The building has a rectangular footprint of 23.5 by 21.5 meters and reaches a height of approximately 45 meters. The structural elements, which are made of Glulam, and timber frame walls will be fully prefabricated to enable rapid assembly and reduce carbon emissions (Saxion, 2025).

The building combines three systems to efficiently improve the lateral stiffness of the building as shown in Figure 3.2.On the perimeter of the building an exoskeleton is located and in the centre a timber core is placed. Between the core and the exoskeleton, timber frame shear walls are located which help to transfer the loads between the exoskeleton and the timber core.

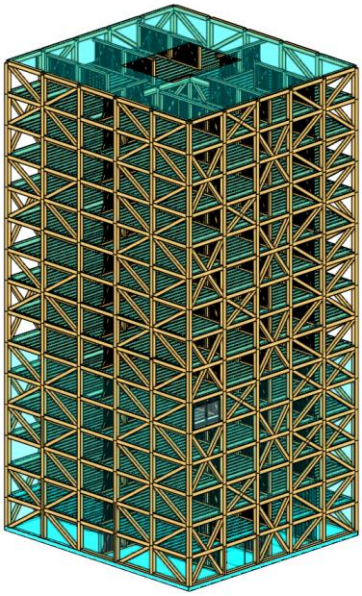

Figure 3.1: General design of the reference building.

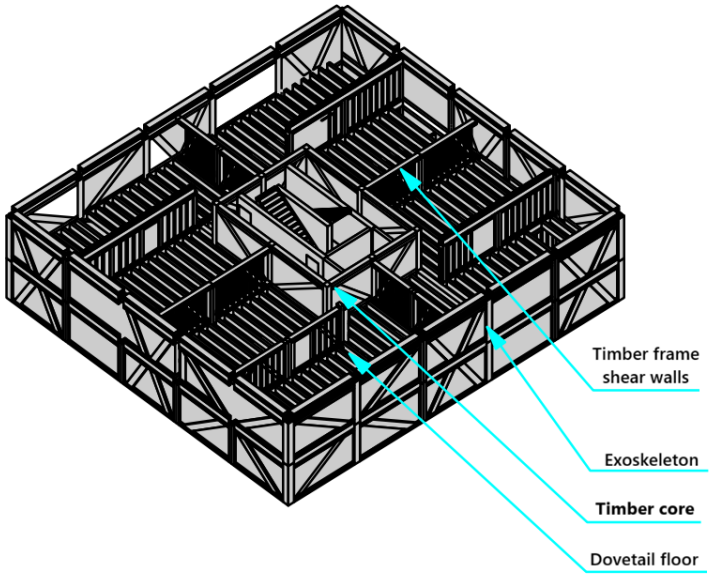

Figure 3.2: Overview lateral stability systems.

3.2 Description of the base-line model

To make the indicative model of the Woodcore-project more structurally and architecturally more feasible, a number of changes has been made. The resulting model is called the base-line model which will be used for the parametric analysis.

While the overall building and core dimensions remain the same with respect to the indicative model, a number of changes has been made. First of all, the irregular diagonal layout of the indicative model was changed to a more regular layout. This was done to make the results of the analyses more generally applicable. Furthermore, the locations of exterior columns were given an even spacing for each façade, ensuring that the diagonals in the exoskeleton have an equal angle. The new diagonal layout in the exoskeleton and braced core of the baseline model are displayed in Figure 3.3 and Figure 3.4.

In Figure 3.5, the new floor plan of the baseline building is displayed. The same floor plan is used for all additional variants. In the figure the location of the braced timber core is indicated with red, the location of the timber frame shear walls is indicated in right. In the floor plan also the global x- and y-direction is denoted which is the notation which is used for this report. All floors span in the global x-direction. The floor beams in y-direction are supported by internal columns which are indicated with a grey colour. In the indicative model the timber frame shear walls did not align with the core and interrupted the open space in the residential apartments. To prevent this only timber frame shear walls have been placed at the separation of the apartments.

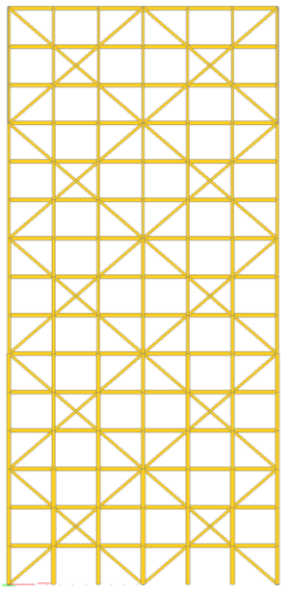

Figure 3.3: Exoskeleton diagonal lay-out of the baseline variant.

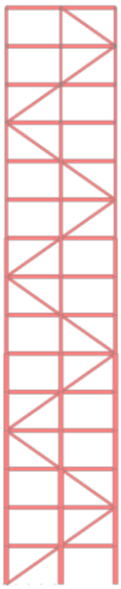

Figure 3.4: Braced core diagonal lay-out of all variants.

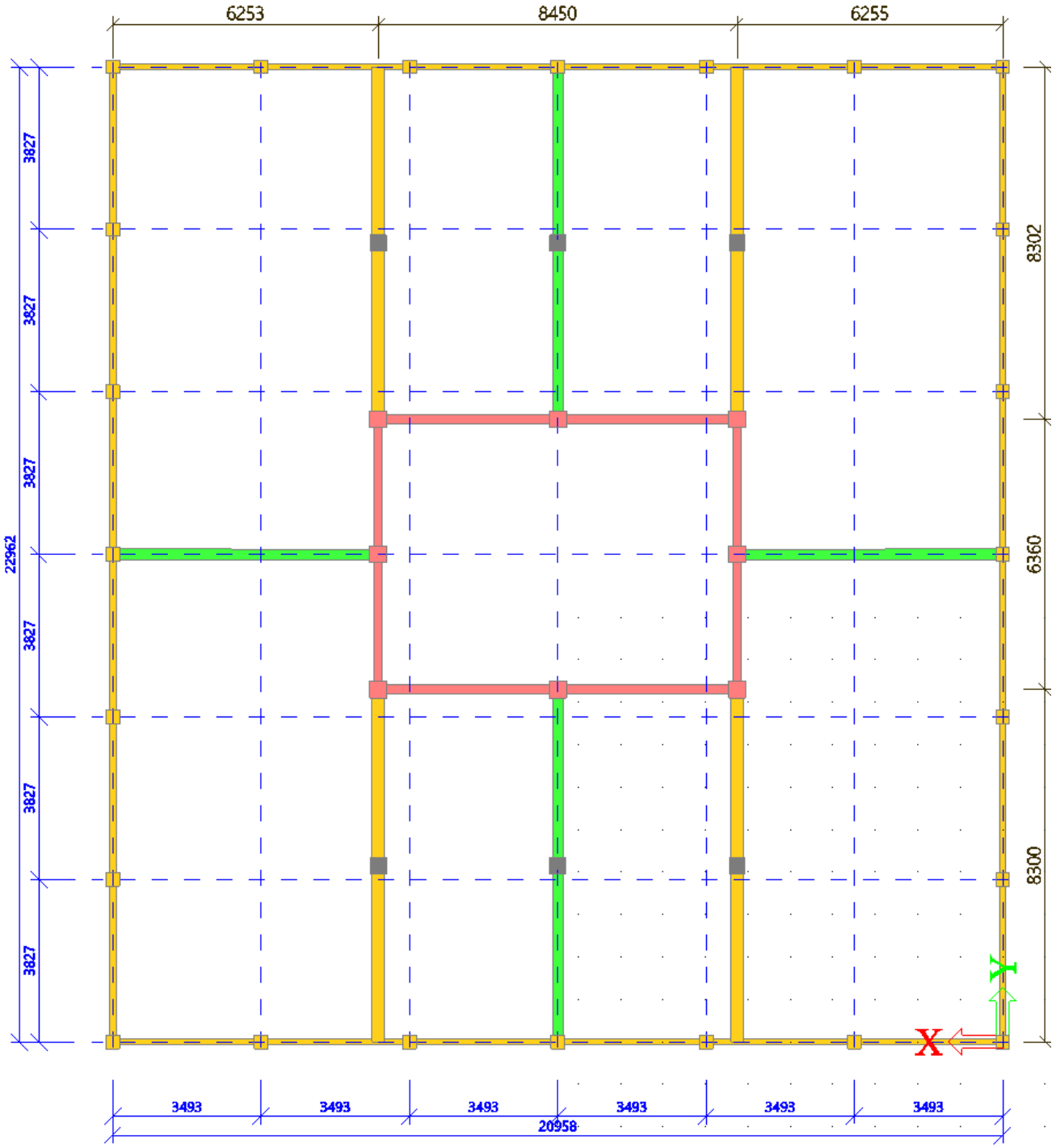

Figure 3.5: Floor plan of the baseline variant and all additional variants.

3.2.1 Used materials in the base-line model

In this section the materials which are used for the base-line model for which the parametric studies are performed are described and justified.

The primary load-bearing elements, the columns, beams and diagonals of the exoskeleton and the core are made of glulam members with a strength class of GL24h. Glulam was chosen as it is commonly used for mid and high-rise timber buildings as described in Section 2.3. The used strength class of GL24h is also commonly used for glulam members and was chosen as it was used in the indicative model of the WoodCore Project.

For the floors in the building, Kerto-Ripa box elements are used which consists of LVL Q cross-laminated veneer plates which are connected using LVL S longitudinal plated ribs. These floors are chosen as the timber beam floors are chosen as reference point in the indicative model. The Kerto-Ripa floor elements have the same orthotropic properties as a timber beam floor. In addition, the Kerto-Ripa floors provide a high bending stiffness such that their effective height can be reduced.

The timber frame shear walls are made of sawn timber studs and rails with a strength class of C24, which is common practice (De Graaf & Banga, 2000). In the base-line model triplex sheeting was applied. For the parametric study also OSB sheeting with higher stiffness properties is considered. The slotted-in steel-to-timber connections are made using steel plates with a strength class of S355 and stainless-steel dowels with a ultimate characteristic strength of 800 MPa. These materials and strength classes were chosen as they are commonly used in for this type of connection which was found in the literature study in Section 2.3.

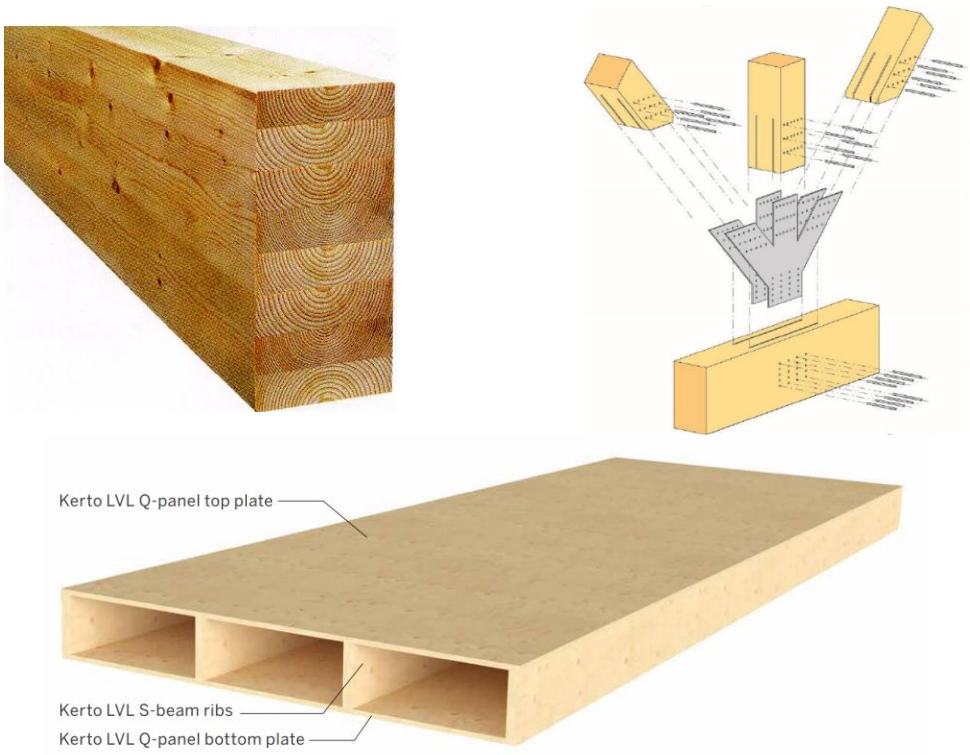

Figure 3.6: Overview of structural elements: glulam beam on the top left (Blaß & Sandhaas, 2017), slotted-in steel-to-timber connection on the top-right (Crocetti, 2016) and a Kerto-Ripa box element floor on the bottom (Metsä, 2025).

Element Type:	Element:	Material:	Strength Class
Members exoskeleton	Beams	Glulam	GL24h
	Columns	Glulam	GL24h
	Diagonals	Glulam	GL24h
Members braced core	Beams	Glulam	GL24h
	Columns	Glulam	GL24h
	Diagonals	Glulam	GL24h
Wall supporting beams	Beams	Glulam	GL24h
Floor supporting beams	Beams	Glulam	GL24h
Floors (Kerto-Ripa Box element)	Top/bottom plate	LVL Q	LVL 36 C
	Beam ribs	LVL S	LVL 48 P
Timber frame shear walls	Studs	Sawn Timber	C24
	Rails	Sawn Timber	C24
	Sheeting	Triplex	ρ_k = 420 kg/m3 G = 600 MPa
Slotted-in steel-to-timber connections	Plates	Steel	S355
	Smooth Dowels	RVS	A4-80 ($f_{u,k}$) = 800 MPa

Table 3.1: Overview strength classes of structural elements.

3.2.2 Dimensions of the base-line model

In addition, to the used materials the dimensions of the elements in the base-line model is shortly described in this section. The dimensions of the glulam members, the Kerto-Ripa floors and the slotted-in steel-to-timber connections are determined using ULS and SLS verifications. For the design and verification of the elements is referred to Section 5.3. The dimensions of the studs and rails in the timber frame shear walls are based on standard dimensions. (De Graaf & Banga, 2000).

Element Type:	Elements:	Dimensions (hxb):
Members exoskeleton	Beams	300x150mm^2
	Columns (bottom)	320x320mm^2
	Diagonals	200x200mm^2
Members braced core	Beams	300x200mm^2
	Columns (bottom)	400x400mm^2
	Diagonals	200x200mm^2
Wall supporting beams	Beams	350x250mm^2
Floor supporting beams	Beams	350x300mm^2
Floors (Kerto-Ripa box element)	Total height	290 mm
	Top/bottom plate	25 mm
	Beam ribs	45x240mm^2
Timber frame shear walls	Studs	46x146mm^2
	Rails	46x146mm^2
	Sheeting	t=18, h=2750, b=1167mm
Slotted-in steel-to-timber connections	Plates	10 mm
	Smooth dowels	12 mm

Table 3.2: Overview of used dimensions of structural elements.

4 Methodology

This chapter outlines the chosen approach to answer the research questions. First, in Section 4.1 a summary of the approach is described. Subsequently in Section 4.2, an overview of the parameters is displayed. In addition to the parameters, also different structural variants have been investigated to study the influence of different geometries on the results. These variants are described in Section 4.3. Lastly, Section 4.4 explains the approach which was applied to construct the parametric model.

4.1 Research approach

To investigate, quantify and optimize the influence of the stability systems in the timber building, a parametric model is developed. Using this parametric model, a local sensitivity analysis is first carried out with the One-At-a-Time method (OAT), in which only one parameter is varied at a time. This method provides a first impression of the influence of the different parameters close to the reference variant.

Since the measured effect of the parameters in the OAT-method depends on the choice of the reference model, also a global sensitivity analysis was performed using the Variance-Based Sobol-Method. This provides a complete picture of the influence of each parameter over the entire parameter range. In addition, interaction between different parameters can be quantified.

Although the sensitivity analyses quantify which parameters dominate the global horizontal deformation of the building, they do not account for the economic and environmental impact of varying these parameters. Therefore, the material and shadow costs of changing every is determined and compared to the influence of every parameter. In addition, a costs optimalisation of the parameters was performed

4.2 Investigated parameters

To study the performance of the exoskeleton, braced core, timber frame shear walls and connection stiffness on the global horizontal deflection of the building, seven different parameters are investigated:

- Dimensions of columns in the exoskeleton
- Dimensions of diagonals in the exoskeleton
- Dimensions of columns in the braced core
- Dimensions of diagonals in the braced core
- Dimensions of equivalent diagonal to model shear stiffness of timber frame walls
- Relative axial connection stiffness of connections in the exoskeleton
- Relative axial connection stiffness of connections in the braced core

The beams of the exoskeleton and braced core are not included as a parameter as a manual sensitivity analysis showed that varying the beams between their lower and upper bound had a negligible influence on the displacement.

In addition, the connection stiffness is defined as a relative rather than an absolute parameter. The relative connection stiffness expresses the utilization ratio of the connection within the timber element in which the connection is located and is varied between 0 and 1. This choice is made because the maximum achievable connection stiffness strongly depends on the dimensions of the timber element,

since sufficient spacing between the bolts and steel plates must be maintained. As a result, the absolute axial connection stiffness can be varied over a much wider range in a large timber member than in a small timber member. By expressing the axial stiffness of the connection as a relative parameter it is ensured that every parameter combination remains feasible.

4.3 Investigated variants

In addition to the parameter variations to investigate the influence of the different stability systems, the study also investigates how the results are affected when different structural variants are considered. For a number of main additional variants, the full local and global sensitivity analyses were performed. In addition, to investigate specific scenarios and building aspects, several exploratory variants were investigated.

The baseline model:
In this report one variant is considered as the reference model. This baseline model is a 15-story building using a dense diagonal structure in the exoskeleton and where the wind is applied in x-direction. A more detailed description of the baseline model is given in Section 3.2 and Section 5.3.

Main additional variants:
In addition to the baseline model the complete local and global sensitivity analyses were performed on additional variants to investigate the influence of varying the number of stories, the geometry of the building and the lower bounds of the parameter ranges for the sensitivity analyses. The main additional variants can therefore be divided into three categories: variants with a varying number of stories, variants with a varying structural geometry and variants with different parameter lower bounds. The main additional variants are listed below.

Variants with varying stories to study the influence of a varying building height on the influence of the investigated parameters. The considered variants are listed below and displayed in Figure 4.1.

- Variant with 15 stories (baseline)
- Variant with 12 stories
- Variant with 9 stories
- Variant with 6 stories

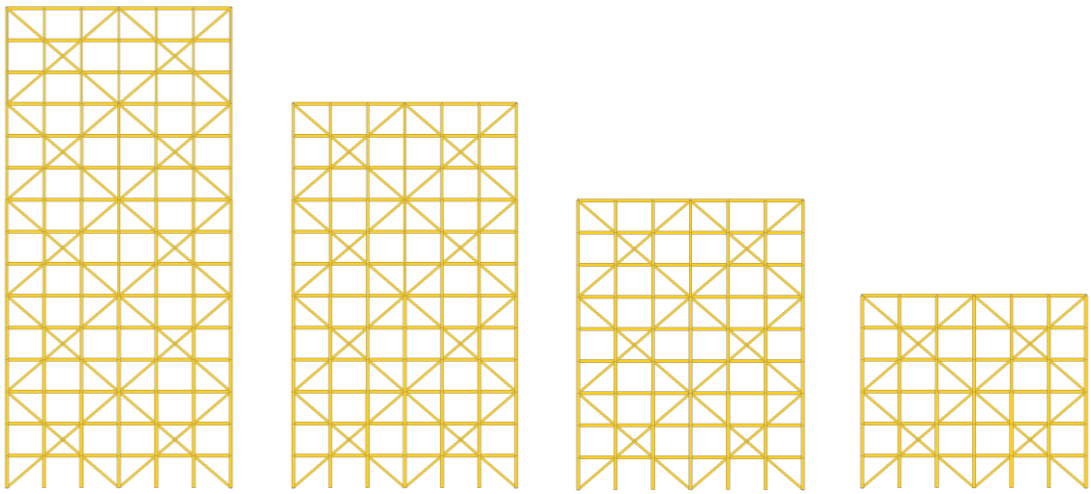

Figure 4.1: Overview of variants with varying stories with 15, 12, 9 and 6 stories.

Variants with varying stories to study the influence of a different building geometries on the influence of the investigated parameters. The considered variants are listed below and displayed in Figure 4.2.

- Variant with a dense diagonal structure in the exoskeleton: in this variant the diagonals intersect the columns every three stories (baseline).
- Variant with an open diagonal structure in the exoskeleton: in this variant the diagonals intersect the columns every six stories.
- Variant where the wind-load is applied in y-direction instead of x-direction: in this direction the braced core is more slender.

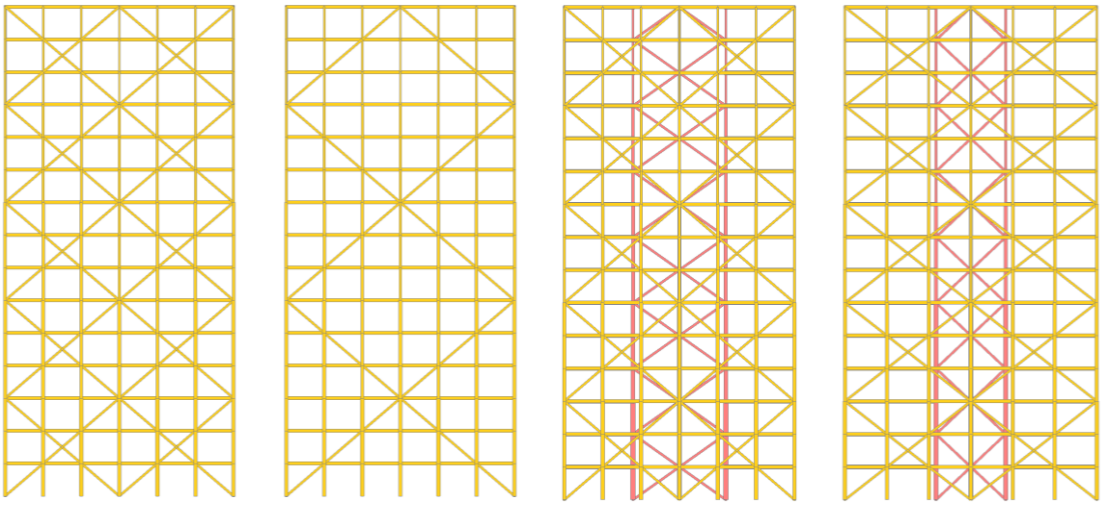

Figure 4.2: Overview of variants with varying structural geometry. The baseline variant in x-direction is displayed in the first and third image. The second image indicates the variant with open diagonal lay-out. The fourth image indicates the design of the building in y-direction with a more slender braced core.

To study the influence of the decision of the lower-bound also three different variants with varying lower bounds for the diagonals and connection stiffness were investigated:

- Variant where the lower bounds are determined based on a conservative ULS verification. For example, the lower-bound of the diagonals in the exoskeleton is equal to 220 mm (baseline).
- Variant where the lower-bounds are set to a near-zero value to simulate complete absence. For example, the lower bounds of the diagonals in the exoskeleton is equal to 1 mm.
- Variant where the lower-bounds are determined to guarantee ductile failure of the connections assuming a dowel-diameter of 10 mm. For example, the lower bounds of the diagonals in the exoskeleton is equal to 100 mm.

Exploratory variants:

In addition to the main variants for which complete analyses were performed, manual investigations were performed for a number of exploratory variants. These exploratory variants are used to investigate specific structural cases and influences. The exploration variants that are considered are:

- Variants to study the influence of foundation stiffness
- Variant containing only the exoskeleton as stability system
- Variant containing only the braced core as stability system
- Variant containing only the timber frame shear walls as stability system

The results of the exploratory analyses are displayed in Section 6.3.4.

4.4 Parametric workflow

4.4.1 Evaluation of workflow alternatives

To develop a parametric tool for the analysis of the building concept, four parametric approaches were considered. For every approach the advantages and disadvantages are shortly explained. In addition, a motivation for the final choice is given.

Grasshopper + Koala + SCIA Engineer:
In this approach the visual code interface of Grasshopper is used in combination with Rhino to develop a model which is connected to the FEM solver of SCIA Engineer using the Koala plug-in for Grasshopper. Advantages of this approach is that Grasshopper has a lower learning curve due to the visual coding interface. In addition, Grasshopper is commonly used for parametric modelling due to the many predefined modules and possibilities to study geometrical relations. Using the Koala plug-in the advanced FEM capabilities of SCIA Engineer in principle can be used.

Disadvantages of this approach is that the number of modules provided by the Koala plug-in is limited. Therefore, many functions of SCIA Engineer cannot be accessed. In addition, the complete model has to be generated in Rhino and Grasshopper, which makes modelling of a full building concept unnecessarily complicated. Lastly, due to the visual programming interface, Grasshopper is less suitable for utilizing advanced Artificial Intelligence (AI) tools for code generation and troubleshooting

Grasshopper + Karamba3D:
In this approach the parametric model and the structural analysis are generated and performed within Grasshopper. Karamba3D is a FEM solver which can directly be implemented as plug-in for Grasshopper. Advantages of this approach is that both the parametric model and FEM analysis are located in a single environment which makes it possible to run configurations quickly.

Disadvantages of this method is that Karamba3D is a lighter FEM engine than SCIA Engineer and has less functionalities. Similar to the previous option, the graphical interface limits the integration of AI coding tools.

Python + SCIA OpenAPI + SCIA Engineer:
In this approach, the model is built in SCIA Engineer and controlled using a Python script through the SCIA OpenAPI modules. Advantages of this approach is that the complete model is directly created in SCIA Engineer, which allows for straightforward modelling of the building and gives access to every functionality that SCIA Engineer offers. Within Python relevant parameters can easily be adjusted using the XML files of the model. Using the OpenAPI modules of SCIA Engineer the approach can be fully automated which makes it possible to run large number of configurations required for the sensitivity analyses. In addition, with the use of AI tools, coding parametric model in Python becomes significantly easier.

The main disadvantage of this approach is that varying the geometry of the parametric model is more difficult to implement by altering the XML-files. However, in hindsight it is expected that this would also be possible using the coding capabilities of AI tools.

Chosen parametric workflow:
Based on this comparison, the combination of Python and SCIA Engineer using the OpenAPI modules was chosen. In this approach the full capabilities of SCIA Engineer can be used and the process can easily be automated. Additionally, this decision was motivated by practical considerations. SCIA Engineer is a commonly used tool at Van Rossum, the structural engineering firm where this project was conducted, which ensured good guidance for the modelling of the finite-element model. A more detailed explanation of the chosen parametric workflow is described in Section 4.4.2.

4.4.2 Description parametric workflow

In this paragraph a more detailed description of the parametric approach is given. As motivated in Section 4.4.1, the parametric workflow couples SCIA Engineer to a Python script through the SCIA OpenAPI modules. The complete workflow is summarized in Figure 4.3: Visualization of the parametric workflow.Figure 4.3 and can be divided in three stages: the set-up stage, the computation stage and the post-processing stage.

In the set-up stage only has to be performed once for every variant. In this stage, the building is first modelled in SCIA Engineer. From this model, an XML file is exported. An XML file is a structured text format that contains all the information of the SCIA model, such as the geometry, cross-sections, connection stiffness and materials. The XML file is subsequently read using a Python script, which locates the parameter properties of the base-line model. In the Python script parameter ranges are defined from which the configurations are generated

In the computation stage the workflow performs the same steps for every parameter configuration. First, the Python script writes a new XML file in which the values of the selected parameters are replaced by their adjusted values. Using the SCIA OpenAPI modules, the existing SCIA model is updated with the newly generated XML file. Next a linear finite element analysis is performed in the background using the SCIA solver. Lastly, relevant results, such as the horizontal deformation of the building are loaded in the Python script and saved in an Excel-file.

After all parameter configurations are computed the saved results can be loaded from the Excel-file and used for post-processing. In the Python script the results of the configurations are used to train the surrogate model, to calculate the Sobol-indices and to visualize the results of the local and global sensitivity analyses.

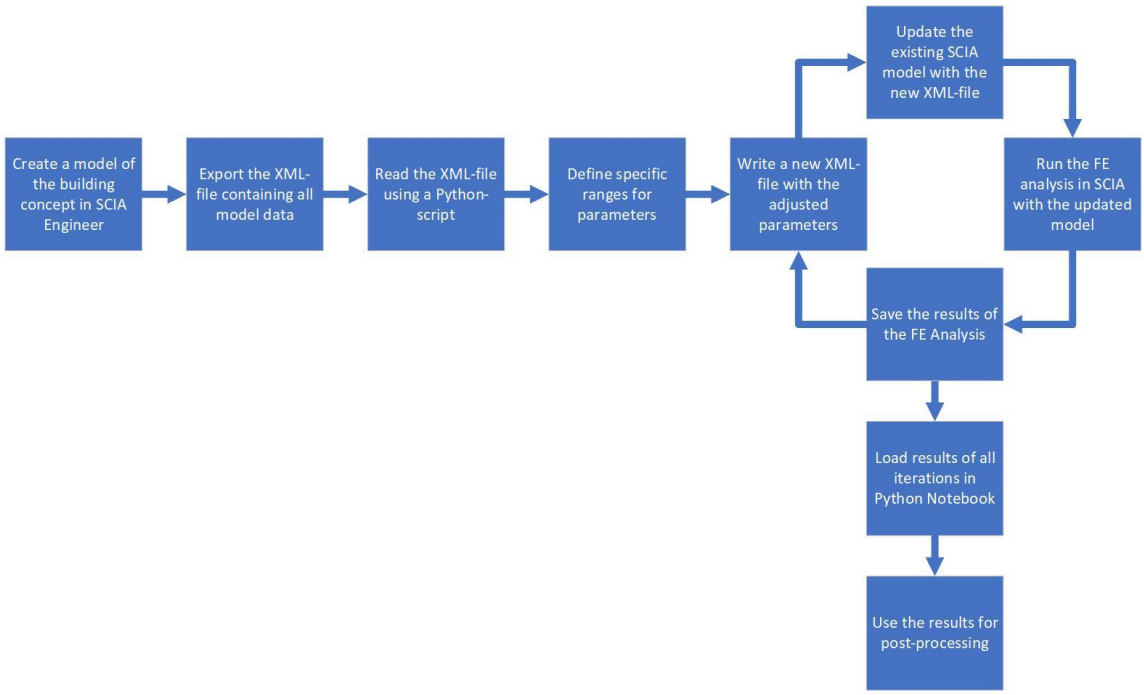

Figure 4.3: Visualization of the parametric workflow.

5 Finite element modelling

5.1 Schematization and modelling of the building concept

This section describes the schematization of the baseline model from Chapter 3 and explains the modelling of the building in the FEM software SCIA Engineer.

5.1.1 Schematisation and modelling of Kerto-Ripa Floors

As described in Section 3.2.2, the floors of the building are constructed with Kerto-Ripa floors. It is assumed that the floor panels are hinged to the adjacent beams, since the floor panels are connected only through the top plate. In addition, it is assumed that the floors, which are schematized in standard widths of 2.4 metres, can be modelled as orthotropic floor plates that act as a whole over the entire span.

As the Kerto-Ripa plates that are used for the reference model consists of LVL ribs and plates, the Kerto-Ripa floors have different stiffness properties in both directions. As it is too intensive to model every floor beam in SCIA independently, it was chosen to model the Kerto-Ripa floor elements as orthotropic plates. In SCIA it is possible to manually adjust the membrane stiffness and the bending stiffness for both in x and y direction of the plate.

In Appendix C a hand calculation is displayed to model the stiffness values of the orthotropic plates. As the Kerto-Ripa ribs and the plates of the floor elements are glued together, full composite action can be assumed (Metsä, 2025). As floors are hollow, it is assumed that the Poisson ratio is equal to zero. Floors can be modelled as thin plates when the ratio between the span and the thickness of the plates is larger than 10 (Hendriks, 2021).

$$\frac{L_{span,min}}{t_{plate}} = \frac{3827}{290} = 13.2 > 10 \tag{5.1}$$

As the floors can be modelled as thin plates, the shear flexural stiffness is set to be infinite and modelled with a stiffness of 1 000 000 MNm^2/m. In Table 5.1, the stiffness properties of the Kerto-Ripa floors are summarized. In Figure 5.1, the stiffness properties are explained with drawings.

Stiffness Property	Description	Resulting value	Unity
D_{11}	Bending stiffness in x-direction	10,74	MNm^2/m
D_{22}	Bending stiffness in y-direction	2,11	MNm^2/m
D_{12}	Combined bending stiffness in x- and y-direction	0,00	MNm^2/m
D_{33}	Torsional stiffness	3,33	MNm^2/m
D_{44}	Shear flexural stiffness in x-direction	1 000 000	MNm^2/m
D_{55}	Shear flexural stiffness in y-direction	1 000 000	MNm^2/m
d_{11}	Axial stiffness in x-direction	835,5	MN/m
d_{22}	Axial stiffness in y-direction	120,0	MN/m
d_{33}	Shear membrane stiffness	158,3	MN/m
d_{12}	Combined axial stiffness in x- and y-direction	0,0	MN/m

Table 5.1: Overview stiffness properties orthotropic Kerto-Ripa floor elements.

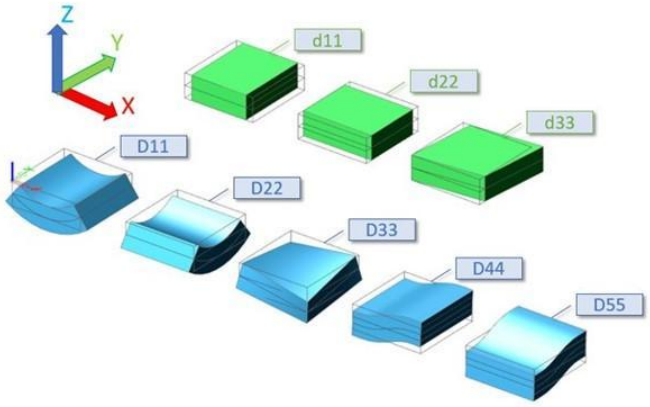

Figure 5.1: Stiffness properties orthotropic plates (SCIA Engineer, n.d.).

5.1.2 Schematisation and modelling of timber frame shear walls

The building concept that will be analysed in this thesis uses timber frame shear walls. A typical layout of a timber frame shear wall is displayed in Figure 5.2 (Hoekstra, 2012). A timber frame shear wall consists of vertical timber studs and horizontal rails. In between the studs insulation material is placed. The timber frames are finished with a board material. The board material is connected using fasteners on the studs of the frame. The slip of the fasteners along the panel perimeter contribute the most to the racking stiffness of the timber-frame shear-wall (Hoekstra, 2012). To control the moisture content inside the wall a vapour tight foil is placed on interior walls, and a watertight membrane is placed on exterior walls.

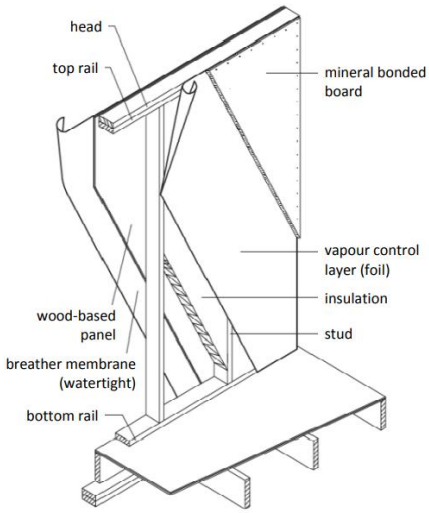

Figure 5.2: Layout of a timber-frame wall (Hoekstra, 2012).

When the building is subjected to a wind load, the floors of the building will generate a horizontal shear force on top of the timber frame shear walls. Three deformation mechanisms can be identified due to this shear force: sliding, tilting and racking of the shear wall (ISSO, 2020). These mechanisms are displayed in Figure 5.3. The stiffness of the timber frame shear walls influences the global stiffness of the building and is therefore a relevant parameter for the parametric model. The approach of Tunis Hoekstra neglects the sliding deformation. It is assumed that the sliding resistance is sufficiently resisted by the connectors of the timber walls and does not have a significant effect on the global lateral stiffness.

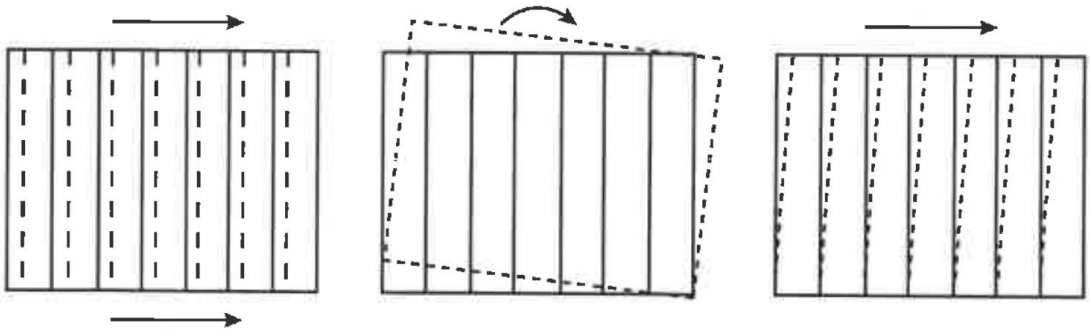

Figure 5.3: sliding (left), tilting (middle) and racking (right) of timber frame shear walls (ISSO, 2020).

A report of Hoekstra (Hoekstra, 2012) presents a method to combine the different stiffness parameters of timber-frame walls into one single parameter for the racking stiffness (R) to be able to model the racking stiffness using framework analysis software. The method considers the following stiffness parameters: fastener-slip of the nails of the panels, compression perpendicular to the grain of the bottom rail beneath the compressed stud and the hold-down stiffness. Horizontal slip of the shear wall is not considered. The model for the structural analysis of timber-frame shear-walls is displayed in Figure 5.4 (Hoekstra, 2012).

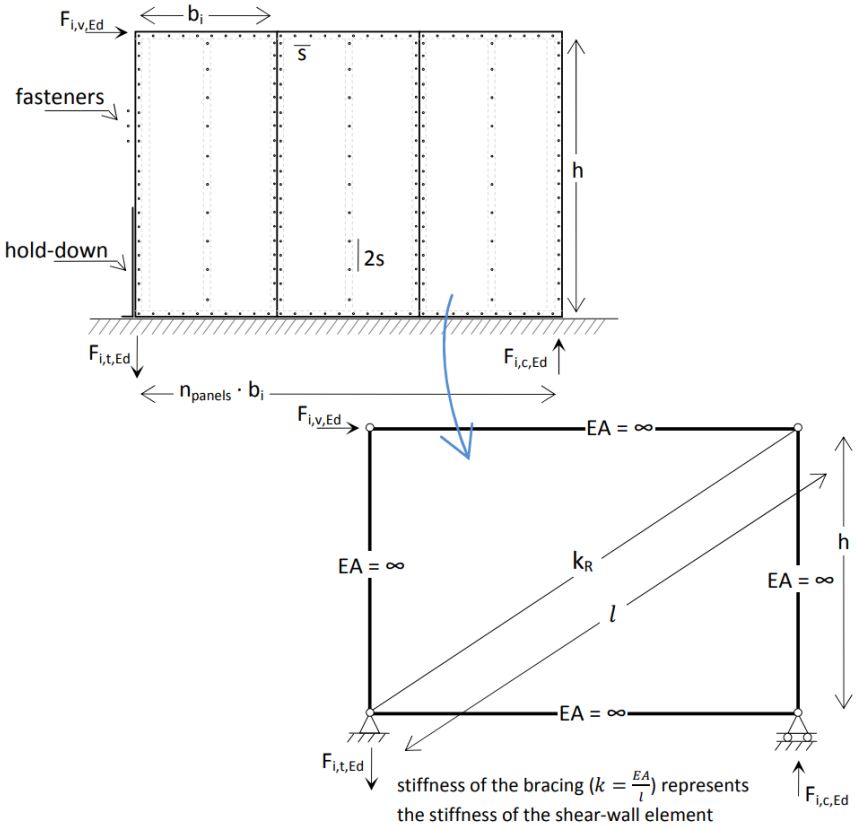

Figure 5.4: Model for the structural analysis of timber-frame shear-walls in a framework program (Hoekstra, 2012).

The stiffness of the equivalent diagonal (k_R) can be calculated using equation 5.2 (Hoekstra, 2012). In Appendix D, an example calculation of the racking stiffness and the equivalent diagonal stiffness is displayed

$$k_R = R * (1 + \frac{h^2}{b^2}) \quad (5.2)$$

Where:

R	[N/mm]	=	Racking stiffness of the timber-frame shear wall
h	[mm]	=	Total height of the shear wall
b	[mm]	=	Total width of the shear wall

Reference model:
In the reference model the timber frame wall properties from Table 5.2 are assumed. The reference values are based on standard materials and dimensions for timber frame walls (De Graaf & Banga, 2000). For the remaining properties of the reference model is referred to Section 3.2.2.

The stiffness of the timber frame walls is dependent on the sheeting material, the number of sheeted faces n_s (on one-side or both sides of the wall), the sheeting thickness t_s, the amount of studs in compression on the corner of the wall n_s, the diameter of the nails connecting the sheets with the timber frame d_n, the spacing between the nails s_n and the number of hold-downs per timber frame wall n_{hd}. All other timber frame dimensions were assumed to remain constant and can be found in the reference model as referred to in Section 3.2.2. The values are based on common materials and dimensions applied in timber-frame construction (De Graaf & Banga, 2000). The chosen upper-bound properties are displayed in table .

	Material [-]	**n_s** [-]	**t_s** [mm]	**G_{mean}** [MPa]	**$n_{s,corner}$** [-]	**d_n** [mm]	**s_n** [mm]	**n_{hd}** [-]	**$h_{eq,dia}$** [mm]
Reference properties	Triplex	1	8	500	2	2,5	60	2	**75**

Table 5.2: Properties of the timber frame shear walls in the baseline model.

The resulting equivalent diagonal which is used in the reference model is therefore a glulam GL24h beam member with dimensions of 75x75 mm^2. This equivalent diagonal was calculated for the timber frame walls in global x-direction of the building. Although the walls in y-directions have different dimensions, and therefore the dimensions of the equivalent diagonal would change, it was chosen to use the same equivalent diagonal dimensions as almost every variant is loaded in x-direction and therefore the result would hardly be influenced.

5.1.3 Schematisation and modelling of connections

To connect the beams, columns and diagonals in the exoskeleton and the braced core slotted-in steel-to-timber connections are used as described in Section 2.2. As the name suggests, slotted-in steel-to-timber connections uses steel-plates which are embedded in the timber element. The plates and timber element are connected using stainless steel dowels.

Locations of connections:

As the locations and total number of connections influence the stiffness of the building, the locations should be carefully considered. The connections are placed according to the principle that the columns in the exoskeleton and the braced core must not be interrupted. The reason for this is to prevent compression perpendicular to the grain in the beams and diagonals. Since it is assumed that the beams and diagonals lie in the same plane as the columns, this means that the beams and diagonals are interrupted at every column. A connection is placed at each end of the diagonals and beams.

In addition, the columns also have to be interrupted, because the maximum production and transport length is limited. It was decided to interrupt the columns every three stories. This length of three stories was chosen because it corresponds to the constant geometry, which changes every three stories. Moreover, fewer connections are required when the columns run continuously over several stories than when they are interrupted at every storey. With the choice to let the columns run continuously over three stories, the length of the columns becomes 9 metres. This length was also chosen because it can be transported by normal means of transport (PAO, 2021).

Schematization of connections:

Since the centre lines of the timber elements in the exoskeleton and the braced core intersect at a single point, the axial forces do not lead to moments in the nodes. For this reason, it is assumed that the rotational stiffness of the connections can be neglected. All connections are therefore modelled as hinges. The axial connection stiffness, however, is very important for timber connections. The axial connection stiffness is modelled by means of a spring in the extension of the beam, where the modelled spring stiffness is equal to the stiffness of the connection.

As a reference connection, a connection was chosen whose reference value lies at approximately one third of the selected parameter range, in line with the other parameters. The reference value of the connection is therefore equal to 100,000 N/mm. This connection stiffness is applied to every connection between the beams, diagonals, and columns in the exoskeleton and the braced core, which was chosen because it simplifies the parametric design. This stiffness corresponds to a connection with one steel plate, using three bolts in the parallel direction and two bolts in the perpendicular direction, with a diameter of 12 mm.

For the modelling in SCIA, however, the axial connection stiffness was not modelled at every end of every element where a connection is located. There are several reasons for this decision. First, it was decided not to place a spring in the columns. In the critical load combination for wind, there is no column in which tension develops. Since the columns are stacked with direct timber-to-timber contact, the forces are transferred directly through this timber-to-timber contact and not through the connection. As a result, the axial stiffness of the connection is not activated, and the springs in the columns were therefore removed to prevent the columns from intersecting one another in the FEM model.

In addition, it was decided to remove the connections in the beams. A manual sensitivity analysis showed that, like the dimensions of the beams, the springs in the beams have a negligible effect on the global stiffness. By varying the connection stiffness between its absolute lower and upper bound, a difference of only 0.2 mm was observed. To simplify the parametric model, the springs were therefore removed at the ends of the parametric model. The resulting implementation of the hinges is shown in Figure 5.5 for a connection at the edge of the building and at the centre of the building.

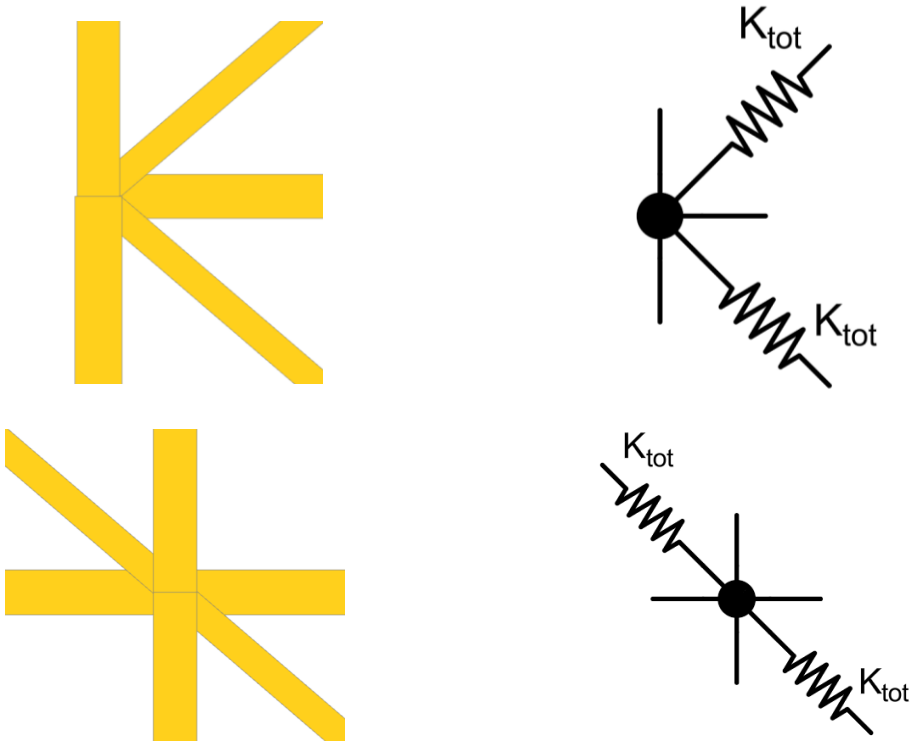

Figure 5.5: Overview of schematisation of connections. In the top two images the schematisation of connection at the edge of the exoskeleton and braced core is displayed. The bottom row connection can be found in the centre of the exoskeleton and braced core.

5.1.4 Schematisation of the foundation stiffness

The foundation stiffness is another parameter that influences the global displacement of the building. To account for this in the design of the model, it was decided not to fully fix the vertical translation of the supports of the building, but to assign them a vertical stiffness instead.

In the model, a support is placed under every column of the building. Since the forces in the columns differ, the supports would deform vertically by different amounts if the same vertical stiffness were assigned to all of them. For this reason, it was decided to scale the vertical stiffness of each support based on the forces in the reference model. A reference value of a vertical stiffness of 100 MN/m was chosen for a vertical reaction force of 2000 kN, using an average value of the column forces in the exoskeleton, the core, and the remaining columns. The choice of this specific factor is derived from engineering experience and the standard practices of Van Rossum, the engineering firm where this project was conducted.

This results in a stiffness of approximately 81 MN/m for the supports in the exoskeleton, a stiffness of 127 MN/m for the supports in the core, and a stiffness of 114 MN/m for the remaining columns. The influence of the choice of foundation stiffness was tested with a manual sensitivity analysis in Section 6.3.4.

5.1.5 Mesh setup

In addition to the modelling of the structural elements in the SCIA model, the choice of the mesh is also an important consideration. A trade-off has to be made between the accuracy of the results and the computational effort.

The dimensions of the mesh were chosen based on FEM guidelines. It is recommended to set the mesh of 2D elements equal to approximately one to two times the thickness of the plate. Since the floors are 290 mm thick, a 2D mesh of 500 mm was chosen (SCIA Engineer, n.d.). For the mesh of the 1D elements, a size equal to the height of the smallest elements in the reference model was chosen. This corresponds to a size of 200 mm.

To investigate to what extent the results are influenced by the mesh size, a mesh refinement was applied, in which the mesh size was halved and doubled. This showed that the global displacement was not affected, but that the bending moment diagrams were. For this reason, it was decided to use a finer mesh once for the dimensioning of the reference model, with 1D elements of 100 mm and 2D elements of 200 mm, while for the FEM iterations of the sensitivity analysis the 1D mesh was kept at 200 mm to reduce the duration per iteration.

5.2 Load definition

5.2.1 Applied loads

In this section the loads which are applied on the building are described and summarized in Table 5.3. A more detailed calculation of the load is described in Appendix A.

Loads	Load type	Value
Permanent:		
Facade	Line load applied on beams of exoskeleton	$G_{k,f}$ = 3,0 kN/m
Floating screed and ceiling installations	Surface load on the floors	$G_{k,sf}$ = 2,85 kN/m^2
Permanent load in core due to elevator, stairs, and floor	Line load on the beams of the braced core in global x- and y-direction	$G_{k,co,x}$ = 9,0 kN/m $G_{k,co,y}$ = 7,2 kN/m
Variable:		
Wind load in global x-direction	Line load applied on the beams of the exoskeleton divided in the lower part of the building, the upper part of the building and the top story.	$Q_{k,w,x,l}$ = 3,84 kN/m $Q_{k,w,x,u}$ = 4,65 kN/m $Q_{k,w,x,t}$ = 2,33 kN/m
Wind load in global y-direction	Line load applied on the beams of the exoskeleton divided in the lower part of the building, the upper part of the building and the top story.	$Q_{k,w,y,l}$ = 3,72 kN/m $Q_{k,w,y,u}$ = 4,62 kN/m $Q_{k,w,y,t}$ = 2,31 kN/m
Non-shared floors	Surface load on the floors	$Q_{k,sf}$ = 2,55 kN/m^2
Shared floor load	Line load on the beams of the core in global x- and y-direction	$Q_{k,co,x}$ = 5,9 kN/m $Q_{k,co,y}$ = 4,8 kN/m

Table 5.3: Overview considered loads on the building.

The self-weight of the elements modelled in SCIA, which comprise of the beams, columns, diagonals and floors of the building are calculated with the SCIA Engineer software. The façade is assumed to be made using prefab timber frame façade elements with a weight of 1,0 kN/m^2 (WEBO). In Figure 5.6 an indication of the façade element is displayed.

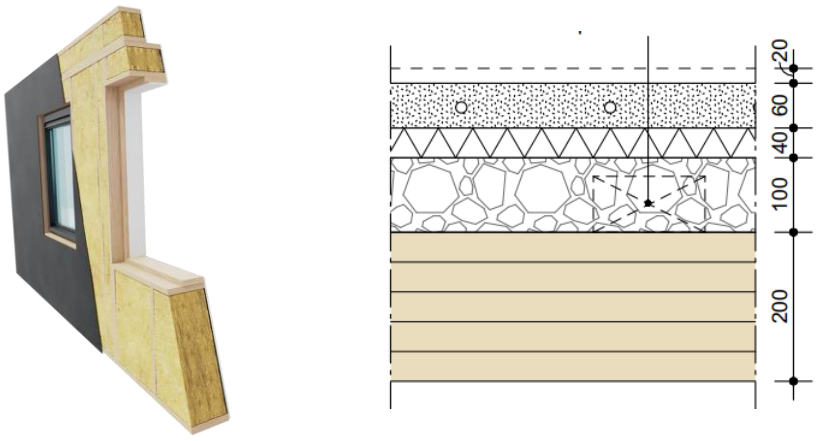

Figure 5.6: Facade element (WEBO) and floor element build-up (Urban Climate Architects, 2026).

The self-weight of the Kerto-Ripa floors is equal to approximately 0.90 kN/m². To reduce floor vibrations and acoustical noise a floating screed and insulation is applied. To determine the weight of the floating screed a CLT floor is used as reference (Urban Climate Architects, 2026). As the floating screed is applied to reduce floor vibrations and acoustical noise it is assumed the loads are similar for to Kerto-Ripa floor elements. In Figure 5.6 a detail of the floor build-up is displayed. A floating screed of 60 mm and a loose ballast layer of 150 mm is applied. The resulting weight of the floating screed and ballast layer is calculated in equation 5.3.

$$G_{screed} = 0{,}06 * 2000 + 150 = 270 \frac{kg}{m^3} = 2{,}7\ kN/m^2 \quad (5.3)$$

Including the self-weight of ceiling installation which is assumed to be equal to 0.15 kN/m^2 (Metsä, 2025) the total weight on the floors is equal to 2,85 kN/m^2.

To calculate the load which act from the core as a line load on the beams of the braced core a yield line load distribution is assumed. The total load inside the core is assumed to be evenly spread over this area. The permanent loads for the floors and stairs are assumed to be equal to the floor loads outside the core. To this load a load of 0,8 kN/m^2 is added to account for the walls and elevator in the core.

The wind load on the building is simplified so that it acts only on the direct façade of the building. Friction may be neglected for this building (NEN-EN 1991-1-4+A1+C2, 2011). The wind load depends on the number of stories of the building. Therefore, for the variants with varying heights, the wind load was recalculated and modelled in SCIA. In appendix A the calculation of the wind load is explained in more detail.

The variable floor loads inside the apartments and the core are determined according to Table 6.2 in the Dutch National Annex of Eurocode 1991 (NEN-EN 1991-1-1+C1/NB:2019 nl, 2019). The variable floor loads for the non-shared floors in the apartments is equal to 1,75 kN/m^2 and for shared floors inside the core is equal to 3,0 kN/m^2. A load of 0,8 kN/m^2 is added to the variable floor load to account for movable separating walls according to the guidelines of the Eurocode.

For the simplification reasons, it is assumed that the roof of the building carries the same loads as the load on the remaining floors. Since the reference building has 15 stories, this assumption is expected to have a small influence on the global deformation of the building.

5.2.2 Overview load cases and load combinations

With the load cases in Section 5.2.1, the critical load combinations for the design of the building and for determining the displacement of the building can be established. The load combinations are set up using the load factors, combination factors, and equations of NEN-EN 1990-NB (NEN-EN-1990-NB, 2019). An overview of the load combinations is presented in Table 5.4. For the meaning of the symbols, reference is made to Table 5.3.

Number	Governing load	Vertical loads favourable / unfavourable	Formula
C1 (ULS)	Permanent	Unfavourable	$1.35 * \sum G_k + 1{,}5 * 0{,}4 * Q_{k,sf} + 1{,}5 * 0{,}6 * Q_{k,co}$
C2 (ULS)	Variable floor	Unfavourable	$1.2 * \sum G_k + 1{,}5 * Q_{k,sf,p} + 1{,}5 * 0{,}4 * Q_{k,sf,s} + 1{,}5 * Q_{k,co,p} + 1{,}5 * 0{,}6 * Q_{k,co,s}$
C3 (ULS)	Wind x-direction	Unfavourable	$1.2 * \sum G_k + 1{,}5 * 0{,}4 * Q_{k,sf} + 1{,}5 * 0{,}6 * Q_{k,co} + 1{,}5 * Q_{k,w,x} + 1{,}5 * 0{,}4 * Q_{k,w,y}$
C4 (ULS)	Wind x-direction	Favourable	$0.9 * \sum G_k + 1{,}5 * Q_{k,w,x} + 1{,}5 * 0{,}4 * Q_{k,w,y}$
C5 (ULS)	Wind y-direction	Unfavourable	$1.2 * \sum G_k + 1{,}5 * 0{,}4 * Q_{k,sf} + 1{,}5 * 0{,}6 * Q_{k,co} + 1{,}5 * 0{,}4 * Q_{k,w,x} + 1{,}5 * Q_{k,w,y}$
C6 (ULS)	Wind y-direction	Favourable	$0.9 * \sum G_k + 1{,}5 * 0{,}4 * Q_{k,w,x} + 1{,}5 * Q_{k,w,y}$
C7 (SLS)	Wind x-direction	Unfavourable	$1.0 * \sum G_k + 0{,}4 * Q_{k,sf} + 0{,}6 * Q_{k,co} + 1{,}0 * Q_{k,w,x}$
C8 (SLS)	Wind x-direction	Favourable	$1.0 * \sum G_k + 1{,}0 * Q_{k,w,x}$
C9 (SLS)	Wind y-direction	Unfavourable	$1.0 * \sum G_k + 0{,}4 * Q_{k,sf} + 0{,}6 * Q_{k,co} + 1{,}0 * Q_{k,w,y}$
C10 (SLS)	Wind y-direction	Favourable	$1.0 * \sum G_k + 1{,}0 * Q_{k,w,y}$
C11 (SLS)	Floor deflection	Unfavourable	$1.0 * \sum G_k + 0{,}4 * Q_{k,sf} + 0{,}6 * Q_{k,co}$

Table 5.4: Overview considered load combinations.

Based on these load combinations for both the SLS and the ULS, it was found that load combination C7 is the critical combination for the global horizontal displacement of the building in the x-direction, and C8 for the displacement in the y-direction.

To account for wind loading which does not act perpendicular to the façade, for the ULS combinations, the wind in the non-governing direction was applied with a value of 40% of the design value. The choice of this specific factor is derived from engineering experience and the standard practices of Van Rossum, the engineering firm where this project was conducted.

In the SCIA model, it appeared that the diagonals in the building contribute to the vertical load transfer. These compressive forces can be explained by the fact that the ends of the diagonals must undergo the same deformation as the ends of the columns, since they are connected to one another through nodes. As a result, the diagonal must deform when the column deforms under the vertical load, which introduces a compressive force in the diagonal. This compressive force in the diagonal depends entirely on the relative axial stiffness of the diagonal with respect to the axial stiffness of the column. It is preferred that the vertical loads are transferred directly to the foundation through the columns. Since it is unclear to what extent this actually occurs in reality, and since the dimensions of the diagonals can vary considerably, it was decided to apply modification groups in SCIA Engineer. With modification groups, the stiffness of elements can be controlled for specific loads. For the reasons stated above, it was decided to reduce the axial stiffness of the diagonals of the exoskeleton, the braced core, and the equivalent diagonal of the walls by 99%, such that the remaining axial stiffness is 1% of the original stiffness.

5.3 Design of structural elements of the base-line model

This section provides an overview of the results of the ULS and SLS calculations for the dimensioning and design of the elements in the reference model. First, the results of the verifications of the columns are described, after which the same is repeated for the beams and floors of the building. The dimensioning of the diagonals in the exoskeleton is not included here. The forces in the diagonals depend strongly on the relative axial stiffness of the diagonals.

5.3.1 Design and verification of columns

The design on the columns in the building is based on the guidelines of NEN-EN-1995-1-1 (NEN-EN-1995-1-1, 2011). The verification resulted in the following dimensions of the columns in the exoskeleton, the braced core, and the remaining columns. The dimensions of the columns were determined every three stories. The resulting dimensions of the columns in the exoskeleton, the braced core, and the internal columns are summarized in Table 5.5.

Column Type	Dimensions Story 1-3 [mm]	Dimensions Story 4-6 [mm]	Dimensions Story 7-9 [mm]	Dimensions Story 10-12 [mm]	Dimensions Story 13-15 [mm]
Exoskeleton	320x320	290x290	250x250	210x210	170x170
Braced core	400x400	360x360	300x300	250x250	200x200
Internal	380x380	340x340	300x300	250x250	200x200

Table 5.5: Overview dimensions columns in the base-line model.

The critical loads in the columns were calculated with the finite element model based on the critical load combination. The resulting unity checks of the elements are summarized in Table 5.6.

Verification	UC exoskeleton	UC braced core	UC internal
Pure compression	0,95	0,96	0,95
Pure tension	0,00	0,00	0,00
Buckling	0,98	0,97	0,96

Table 5.6: Overview unity checks of columns in the base-line model.

For all columns, the governing failure mechanism was pure buckling of the columns. An example calculation of the buckling of the columns is presented in Appendix B.3.

5.3.2 Design and verification of beams

Since the vertical load is equal on every storey, the beams were given the same dimensions for every storey. Per storey, a distinction was made between four types of beams: beams in the exoskeleton, beams in the core, beams beneath the timber frame shear walls, and floor-supporting beams. Table 5.7 presents the resulting dimensions of the beams in the reference model.

Beam type	Beam dimensions (bxh) [mm]
Beams exoskeleton	150x300
Beams braced core	200x300
Wall supporting beams	250x350
Floor supporting beams	300x350

Table 5.7: Overview dimensions beams in the base-line model.

To ensure the architectural requirement of a minimum ceiling height of 2600 mm, with the stories being 3000 mm high, it was decided to keep the maximum height of the beams equal to 350 mm. Table 5.8 summarizes the verifications that were carried out for the dimensioning of the beams.

Verification	UC beams exoskeleton	UC beams braced core	UC wall beams	UC floor beams
Pure compression	0,38	0,32	0,38	0,30
Pure tension	0,44	0,37	0,43	0,34
Buckling	0,70	0,65	0,84	0,50

Table 5.8: Overview unity checks of beams in the base-line model.

The loads on the beams were determined by means of hand calculations. In these calculations, it was assumed that the Kerto-Ripa floors transfer all loads in the primary span direction (global x-direction), while accounting for a strip of 1 metre that is transferred in the secondary span direction (y-direction).

5.3.3 Design and verification of floors

For the design of the floors, the design tables of the floor manufacturer Metsä were initially used (Metsä, 2025). With the maximum span of 6.3 metres, this resulted in a Kerto-Ripa floor with a total height of 250 mm. In the design, the same floor type was used for the entire floor area.

Subsequently, the vertical deflection of the floors also needs to be verified for the instantaneous deflection w_{inst}, the final deflection after creep w_{fin}, and the total net deflection $w_{net,fin}$ according to Eurocode 5 (NEN-EN-1995-1-1, 2011). It is assumed that the floors don't have initial camber ($w_c = 0$). In Figure 5.7, an overview of the contributing deflections for beams is displayed.

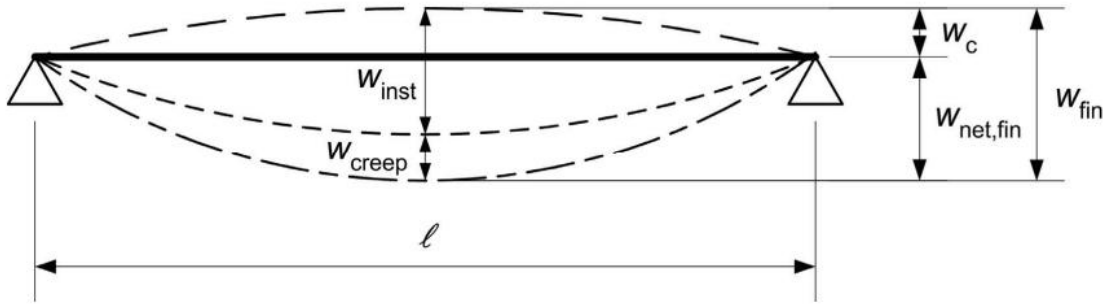

Figure 5.7: contributing deflections in beams in SLS (NEN-EN-1995-1-1, 2011).

The corresponding limits for the initial and final deflection are displayed in equation 5.4(5.4) to 5.6.

$$w_{inst} \leq \frac{l}{500} \tag{5.4}$$

$$w_{fin} \leq \frac{l}{300} \tag{5.5}$$

$$w_{net,fin} \leq \frac{l}{375} \tag{5.6}$$

Where:

l [mm] = The span between supports of the beam

The floors were subjected by the floor loads described in Section 5.2. From the deflection verification it was concluded that the floor height should be increased to 290 mm to fulfil the deflection criteria. The floors are composed of two 25 mm thick LVL plates which are connected using LVL ribs with a height of 190 mm and a thickness of 45 mm. In Table 5.9 the resulting UC are displayed.

Verification	w_{inst}	w_{fin}	$W_{net,fin}$
UC	0.93	0.80	0.70

Table 5.9: Overview unity checks of floors in the base-line model.

5.3.4 Design and verification of diagonals

The dimensions of the diagonals in the core were not determined based on the verification from NEN-EN 1995-1-1 but were chosen based on the reference value. As with the relative connection stiffness and the equivalent diagonal, it was decided to give the diagonals in the exoskeleton and the braced core a dimension that lies at approximately one third of the parameter range. The resulting dimensions of the diagonals are displayed in Table 5.10.

Diagonal type	Diagonal dimensions (bxh) [mm]
Diagonal exoskeleton	200x200
Diagonal braced core	200x200

Table 5.10: Overview of dimensions diagonals in the base-line model.

Although the diagonals in the exoskeleton and the braced core were not dimensioned based on the ULS calculation, the diagonals were nevertheless verified. Table 5.11 presents an overview of the verifications that were carried out.

Verification	UC diagonals exoskeleton x-direction	UC diagonals exoskeleton y-direction	UC diagonals braced core x-direction	UC diagonals braced core y-direction
Pure compression	0,38	0,32	0,38	0,30
Pure tension	0,44	0,37	0,43	0,34
Buckling	0,70	0,65	0,84	0,50

Table 5.11: Overview unity checks of diagonals in the base-line model.

For each diagonal, buckling is the governing failure mechanism. The forces in the diagonals were determined using the finite element model. Since the diagonals also take on dimensions smaller than 200x200 mm in the parameter study, it is likely that the diagonal can buckle, even though the forces in the diagonals are lower.

5.4 Validation of the finite-element model

To validate the finite-element model three verifications have been performed. First the sum of the reaction forces in the supports have been checked using hand calculations to check if the loads are correctly modelled. Secondly, to check if the connection stiffness was correctly modelled the deformation of a 1D member was verified using a hand calculation. Lastly the global deformation pattern of the building was observed to see if the deformation matches expectations.

5.4.1 Reaction Forces on the foundation:

To validate if the loads on the building are correctly implemented in the SCIA model, the resultant reaction forces on the foundation of the building are checked for every load case. First the reaction forces on the building for every load case were calculated using a hand calculation. After this the resulting loads on the foundation are determined using the SCIA model. The differences between the loads in the hand calculation and the results from SCIA for the load cases are displayed in Table 5.12. The results from the hand calculations and the results from SCIA are almost the same. Only the load-case of the self-weight shows a small difference between the results. In SCIA the self-weight is automatically calculated according to the dimensions of the elements. However, this difference remains very small and will therefore only have a limited effect on the results.

Type	Description	Load type	Result from hand calculation	Result from SCIA	Unity	Difference
LC1	Self-weight	Vertical	8943	8772	kN	1,9%
LC2	Permanent surface loads	Vertical	10581	10581	kN	0,0%
LC3	Permanent line loads	Vertical	6593	6593	kN	0,0%
LC4	Governing variable surface loads	Vertical	2180	2180	kN	0,0%
LC5	Non- governing variable surface loads	Vertical	14171	14172	kN	0,0%
LC6	Governing variable line loads	Vertical	322	322	kN	0,0%
LC7	Non- governing variable line loads	Vertical	2090	2090	kN	0,0%
LC8	Wind load	Horizontal	1471	1471	kN	0,0%
LC8	Bending	Bending	36873	36876	kNm	0,0%

Table 5.12: Overview verification of reaction forces for load cases.

5.4.2 Deformation of individual elements and use of modification factors

To verify whether the connection stiffness and the material and dimensions of the 1D members were modelled correctly, the deformation of a column in the exoskeleton was verified using a simple hand calculation. Since a linear analysis was carried out for the finite element model, so that the stiffness of the element is constant, the axial deformation of an element is directly linked to the axial force in the element.

The axial load in the diagonal and the column at the bottom storey for load case 1, which only contains the self-weight of the elements modelled in SCIA is equal to 263 kN, whereas in the column, a load of 1093 kN was observed. The vertical deformation of the node that connects the column and the diagonal is equal to 1.8 mm according to SCIA. As shown in Figure 5.8, for the schematization of the connections, springs are placed at both ends of the diagonals to represent the axial stiffness of the connections. Since the columns run continuously over several stories, and because it is assumed that the stiffness of the connections between the column and the foundation is included in the stiffness of the support, no springs were placed at the ends of the columns.

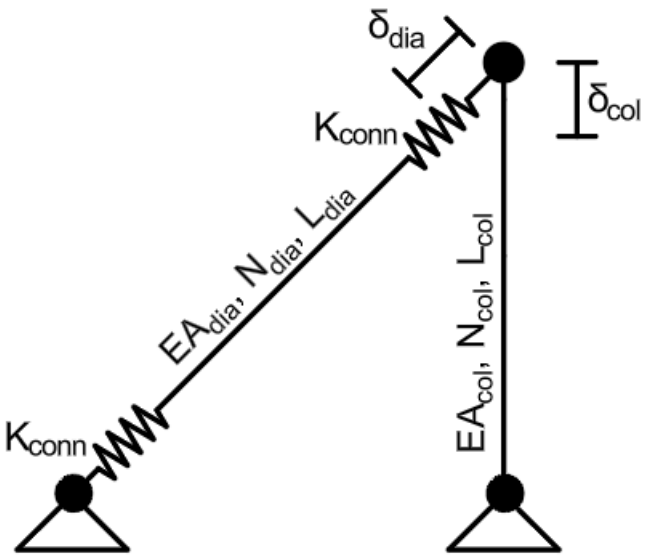

Figure 5.8: Schematisation verification axial deformation of individual elements.

The resulting axial deformation of the columns and diagonals can subsequently be calculated using equation 5.7 and 5.8.

$$\delta_{col} = \frac{N_{col} * L_{col}}{EA_{col}} = \frac{1093 * 10^3 * 4604}{11500 * 400^2} = 1.78\ mm \tag{5.7}$$

$$\delta_{dia} = \frac{N_{dia} * L_{dia}}{EA_{dia}} + 2 * \frac{N_{dia}}{K_{con}} = \frac{263 * 10^3 * 4604}{11500 * 400^2} + 2 * \frac{263 * 10^3}{575000} = 1.12\ mm \tag{2.8}$$

Where:

N_{col}, N_{dia}	[N]	=	The axial load in the column and diagonal
L_{col}, L_{dia}	[mm]	=	The length of the column and diagonal
A_{col}, A_{dia}	[mm]	=	The area of the column and diagonal
E	[N/mm^2]	=	The Young's modulus of glulam member with class GL24h
K_{conn}	[N/mm]	=	The axial connection stiffness of the steel-to-timber connection

Since the diagonal is connected to the column with a node in the FEM model, the displacement of the diagonal at this point must be equal to that of the column at this point. The vertical component of the axial deformation of the diagonal should therefore correspond to the vertical displacement of the column that was calculated and that is shown in SCIA. This vertical component can be calculated with equation 5.9.

$$\delta_{dia,v} = \frac{\delta_{dia}}{\cos(\alpha)} = \frac{1.12}{\cos(49{,}3)} = 1{,}72\ mm \tag{5.9}$$

Both the deformation of the diagonal and the deformation of the column correspond almost exactly to the deformation in SCIA Engineer of 1.8 mm, which shows that the connection stiffness and the material properties of the 1D elements were modelled correctly. Of course, this does not verify whether the elements are connected in the correct ways and whether the springs for the connection stiffnesses are placed at the correct locations.

In addition, another remark should be made regarding this verification. For this verification, only the loads due to the self-weight of the structure were considered. Since these loads all act vertically, this diagonal would normally not carry any axial force under a purely vertical load. However, because the diagonal has to deform together with the column, a compressive force develops in the diagonal, and the column itself is loaded less.

Because it is uncertain to what extent this compatibility would be present in reality, and because the forces should preferably be transferred directly through the columns, it was decided to model the SCIA model with modification factors. For the vertical loads, the axial stiffness of the diagonal was set to 1% of the original stiffness. For the horizontal loads, the diagonals remain fully active.

5.4.3 Global deformation pattern of the building

In addition to the deformation of the 1D elements, it is also examined whether the global deformation of the building is plausible. First, the horizontal displacement of the building is considered, after which the vertical settlement of the building is examined.

Horizontal deformation

In Figure 5.9, a side view of the building shows the horizontal displacement of the building due to the critical SLS load combination for the horizontal deflection, combination C7. The exoskeleton follows an expected deformation pattern. No unconnected elements are observed. The horizontal deformation gradually increases over the height. The maximum deformation of the reference model was found to be equal to 78.4 mm, which is within the limit of 90 mm.

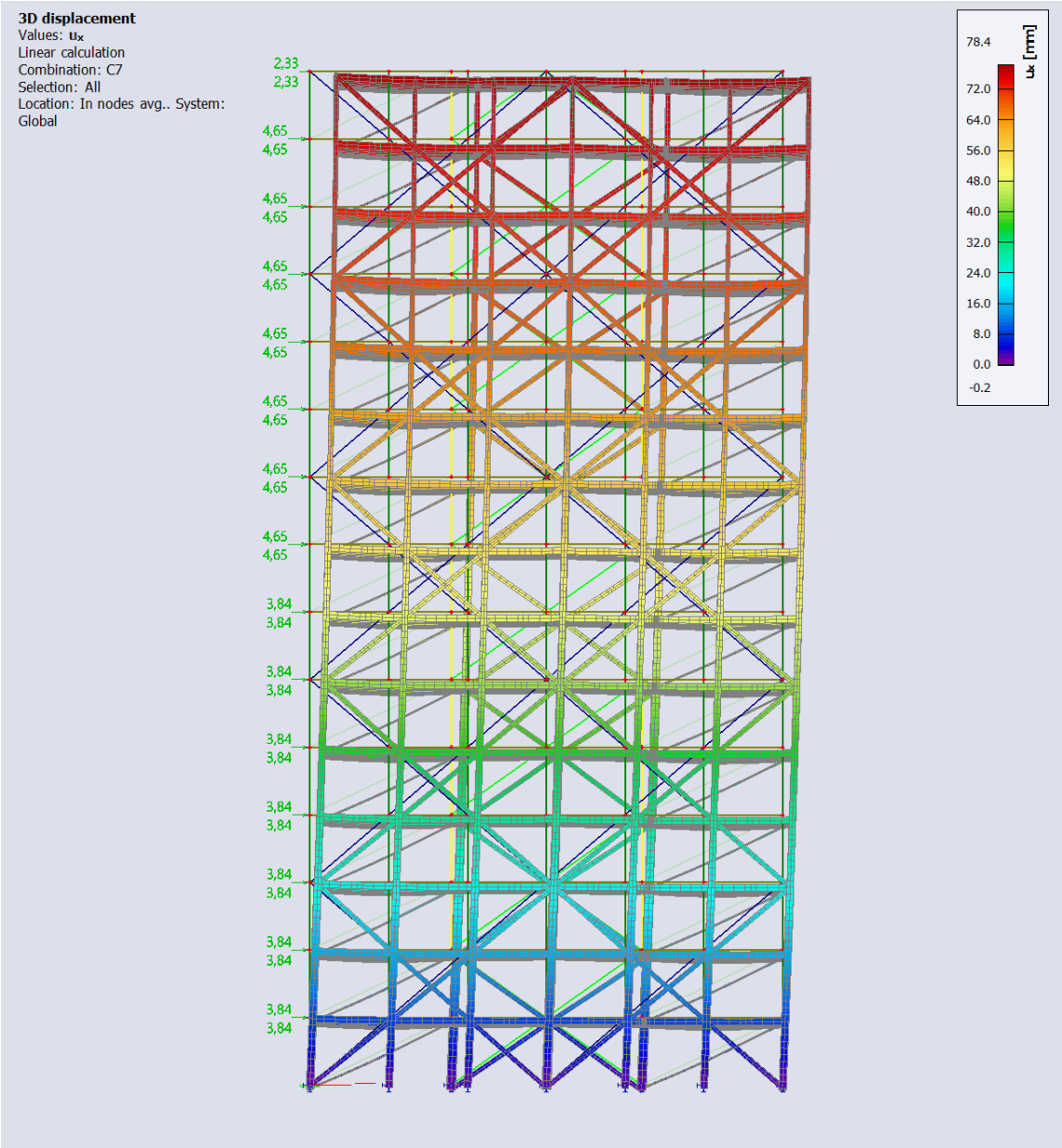

Figure 5.9: Horizontal deformation in x-direction of the baseline building due to the critical load combination C7.

In Figure 5.10, the horizontal deformation of the building due to the critical load combination is shown, where the plot is a top view of the top floor, storey 15. From the plot can be observed that a small amount of torsion is visible in the building. The horizontal displacement in the lower half of the figure is larger than that in the upper half, which is caused by the orientation of the diagonals in the core. This can be confirmed by comparing the result with the horizontal displacement of the floor on the 13th storey, displayed in Figure 5.11, where the diagonals of the core are oriented in the opposite direction and the torsion consequently acts in the opposite direction as well. When only the load case for the horizontal displacement is considered in isolation, this torsion is not visible.

Because the diagonals in the core change their orientation every two stories, the torsion does not have a large effect on the overall deformation of the building. The torsion is only equal to a few millimetres and is therefore relatively small compared to the total displacement of the building. This would, however, become a point of attention if the diagonals were oriented in the same direction over the entire height of the building. In that case, the torsion per storey would accumulate and could lead to a considerably larger total displacement.

Finally, a difference in deformation can be observed at the transition between the floor plates. This is explained by the fact that the floor plates are hinged to the intermediate beam. Since this top view shows the horizontal displacement of the top section, the deflection of the plates results in a difference in horizontal displacement between them.

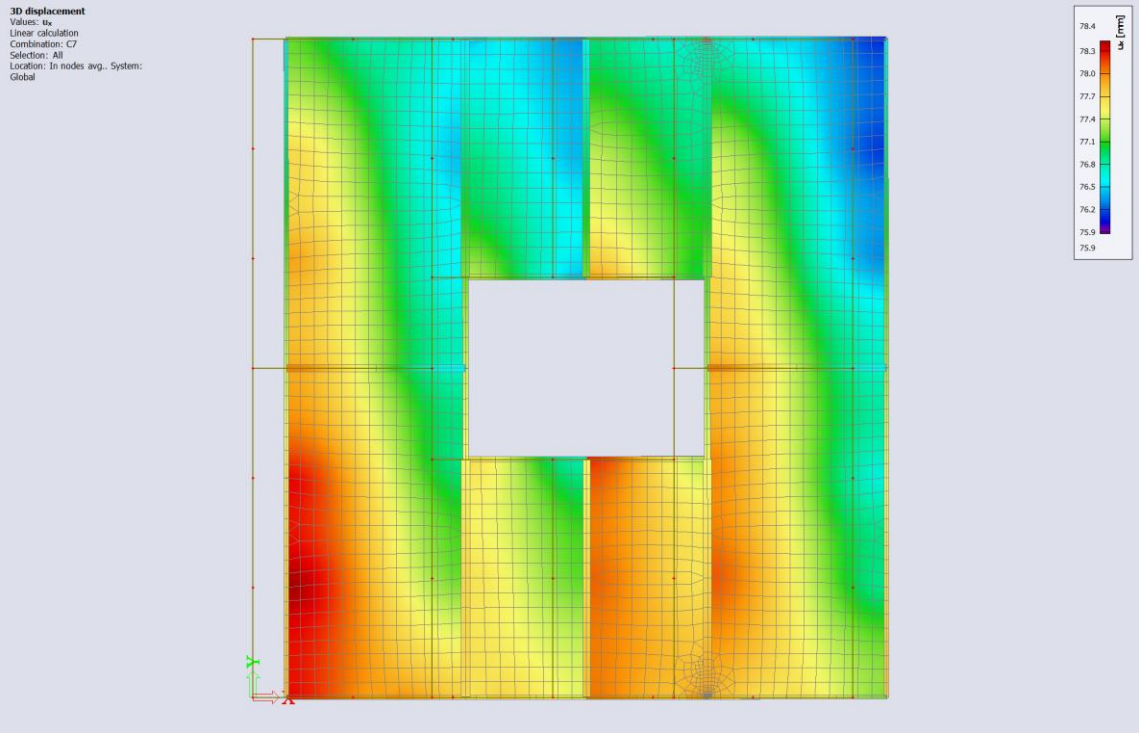

Figure 5.10: Horizontal deformation pattern of the top story due to the critical load combination C7.

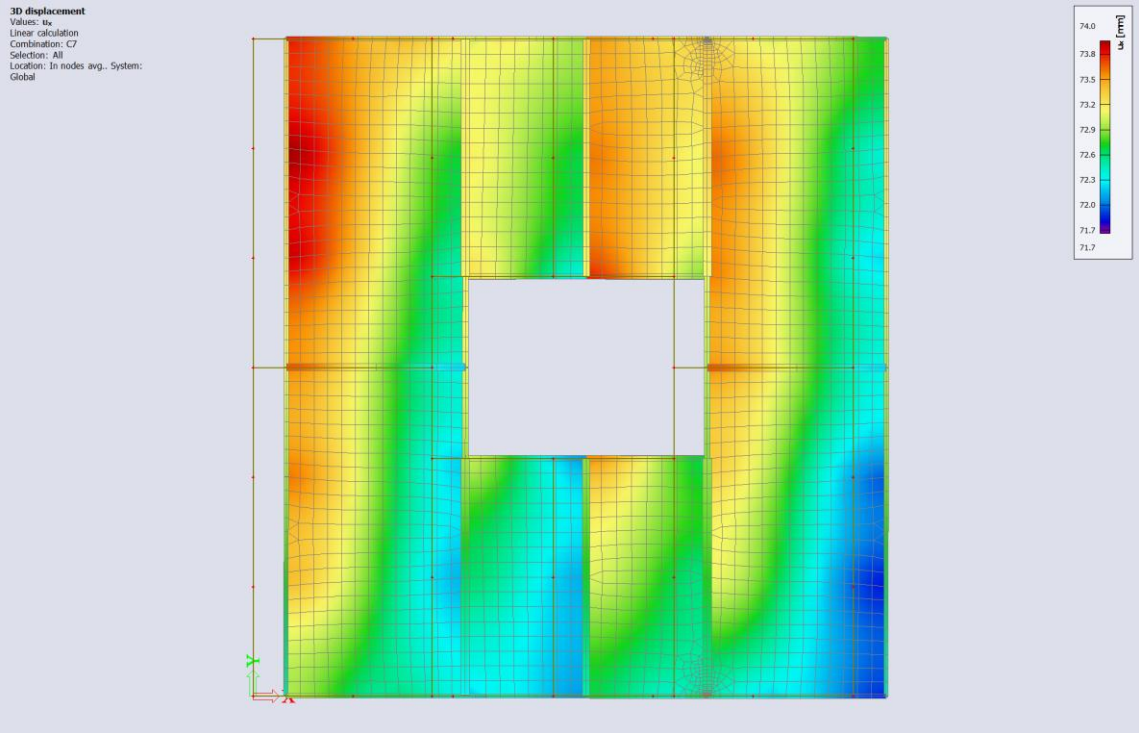

Figure 5.11: Horizontal deformation pattern of the 13th story due to the critical load combination C7.

Vertical deformation of the floors

In Figure 5.12, the vertical settlement of the building due to the SLS load combination for the deflection of the floors is shown. The figure shows that the vertical settlement of the building is symmetrical, which is expected given that the building itself is symmetrical.

In addition, it can be observed that the settlement in the middle of the building is larger than at the edges of the building. This is because the core carries a higher vertical load than the exoskeleton, and in addition the spacing between the internal columns is larger than that between the columns in the exoskeleton. The difference in deflection between the beams in the exoskeleton and the core is approximately 30 mm. This difference is not considered a problem as it could be levelled out with an anhydrite screed.

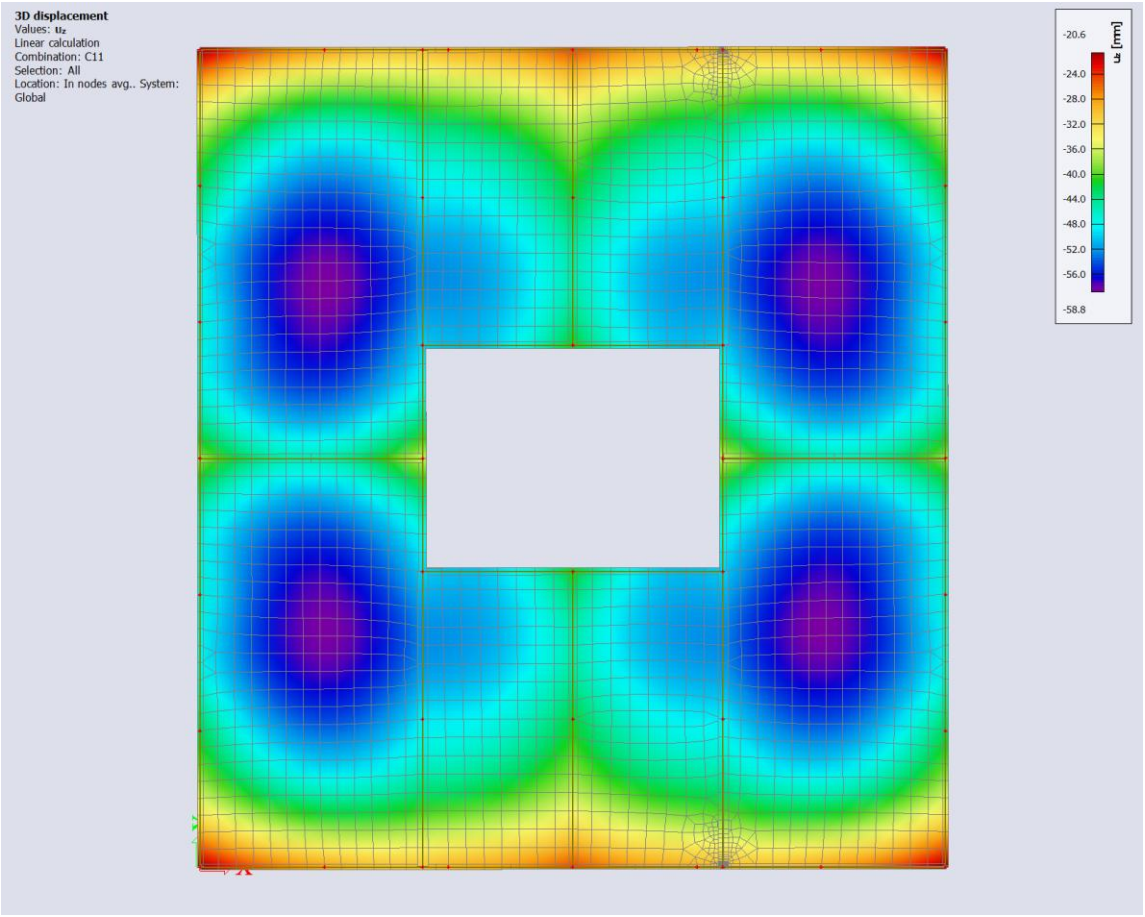

Figure 5.12: Vertical deformation pattern of the top story due to the vertical SLS load combination C11.

6 Sensitivity Analyses

A sensitivity analysis is the study of how uncertainty in the output of a model can be allocated to different sources of uncertainty in the model input (Saltelli & Tarantola, 2004). This aligns well with the objective of investigating to which extent the stability systems influence the lateral deflection of the building. In this study two sensitivity analyses have been performed for every design variant: a local sensitivity analysis using the One-At-a-Time method and a global sensitivity analysis using the variance-based Sobol-method. In Section 6.1 the difference between both analyses is explained. The definition of the parameter ranges are described in Section 6.2. The results of the local and global sensitivity analysis are presented and discussed in Section 6.3 and 6.4. In Section 6.5 the cost-effectiveness of the parameters is investigated.

6.1 Local vs Global Sensitivity Analysis

Methods to perform sensitivity analysis can be categorized in two main techniques: local sensitivity analysis (LSA) and global sensitivity analysis (GSA). In a local sensitivity analysis, the parameters of the model are varied around specific reference values to explore how different small changes in the input influence the output of the model. A local sensitivity analysis is easy to implement and requires little computational power. However, local sensitivity analysis also has limitations. The result of the analysis can be biased when the model is non-linear, as the result is strongly dependent on the location of the reference value of the parameter. In addition, local sensitivity analysis cannot account for interactions between different parameters (Reed & Hadjimichael, 2022).

In a global sensitivity analysis, the parameters of the model are not only changed with respect to reference value, but over the entire range of variables. Therefore, global sensitivity methods can deal with non-linear models, and the results are not dependent on the decision of the reference values (Sudret, 2007). However, global sensitivity methods also have disadvantages. In general, global methods are more computationally demanding. In addition, results are still dependent on the ranges over which the parameters are allowed to be varied.

In this research, both a local and global sensitivity analysis were performed for every structural variant. The local sensitivity analysis was initially conducted to gain a first understanding of each parameter's individual impact and to investigate the relationship between each parameter and the global horizontal behaviour of the building. Additionally, the results of the local sensitivity analysis are easy to interpret. However, because the relationship between the parameters and the output is non-linear and because interaction between the different stability systems was expected, also a global sensitivity analysis was performed to get a more complete overview of the influence of every parameter.

6.2 Definition parameter ranges

To investigate the influence of the parameters on the global horizontal deflection of the building, each parameter must be varied across a predefined range. As discussed in Section 6.1, the selection of the choice of the boundaries of these parameter ranges affect the results of the sensitivity analyses and should therefore be carefully formulated. The parameter ranges are selected such that every possible combination of parameters results in a feasible design. In this way, the sensitivity of each parameter is determined over a realistic and constructable domain.

This section describes the justification of the parameter boundaries, for the justification of the selection of the parameters is referred to Section 4.2. The section is structured as follows. Section 6.2.1 first provides an overview of the definition of the parameter bounds. The choice of the values of the lower and upper bounds for the diagonals, columns, shear walls and connection stiffnesses is explained in Sections 6.2.2 to 6.2.5. Finally, the resulting lower- and upper-bound values of the parameter ranges are summarized in Section 6.2.6.

6.2.1 Overview definition parameter ranges

The lower and upper bounds between which each parameter is allowed to vary are summarized in Table 6.1 and are briefly described below. The values which correspond to these definitions of the lower bounds are explained in Sections 6.2.2 to 6.2.5.

For the diagonals, columns and connections in the exoskeleton and the braced core, the lower bound is determined by a ULS verification. As the loads and the geometry of the building varies for each variant, the lower bounds of these parameters are redetermined for every variant. Since the equivalent diagonal of the shear walls is a modelling simplification and not a physical element, the shear walls are assumed to be completely absent in the lower-bound.

The upper bounds are determined by practical limitations. For the diagonals and columns, the upper-bound is determined by manufacturing limitations. For the shear walls, the upper bound corresponds to the maximum stiffness that can be achieved with common production material for timber frame walls. For the axial connection stiffness, the upper bound corresponds to the maximum stiffness that a connection ca achieve given the dimensions of the timber element in which the connection is located. This is limited by the requirement that the spacing between the dowels, and between the steel plates, must be sufficient.

Parameter	Lower bound	Upper bound
Cross-sectional dimensions of the exoskeleton columns	ULS verification	Manufacturing limitations
Cross-sectional dimensions of the exoskeleton diagonals	ULS verification	Manufacturing limitations
Cross-sectional dimensions of the braced core columns	ULS verification	Manufacturing limitations
Cross-sectional dimensions of the braced core diagonals	ULS verification	Manufacturing limitations
Cross-sectional dimensions of the equivalent diagonals for the timber frame shear walls	Completely absent	Maximum achievable stiffness with common production materials
Relative axial connection stiffness of the exoskeleton connections	ULS verification	Maximum achievable stiffness given the available space in the timber element
Relative axial connection stiffness of the braced core connections	ULS verification	Maximum achievable stiffness given the available space in the timber element

Table 6.1: Overview definition parameter ranges.

6.2.2 Lower- and upper bound of columns in the exoskeleton and braced core

The first parameter that is considered are the dimensions of the columns in the exoskeleton and the braced core. The main purpose of the columns is to transfer verticals load down to the foundation. To fulfil this requirement, the columns must satisfy the Ultimate Limit State (ULS) criteria for every parameter configuration. Therefore, the optimized cross-sections from the baseline model design in Section 5.3 are used as the absolute lower-bound for the column dimensions.

Since the column dimensions are optimized every three stories, it would be inefficient to change all columns over the entire height of the building with the same dimension. Therefore, a proportional scaling method is used where all columns with different dimensions are multiplied by a uniform scaling factor instead of changing every column with a fixed dimension. Consequently, the lower-bound column factor is set to 1, which corresponds to the cross-section dimensions of the columns on the bottom three stories. For the variants with varying number of stories, the lowest stories are removed, such that the columns of the original fourth story become the bottom columns. The cross-sectional dimensions of the columns for each variant are presented in Section 5.3.1.

The upper-bound of the exoskeleton column scaling factor is determined by the maximum dimensions which can be achieved for glulam element using standard manufacturing processes. Stora Enso, a prominent manufacturer of glulam member, specifies a maximum width of 600 mm for block-glued glulam elements (Stora Enso, n.d.). Although a height up to 1200 mm can be produced the limit was set to 600 mm as for this study all elements are assumed to be square. From an architectural standpoint large dimensions of the exoskeleton are also not preferred. Large cross-sections reduce the available floor area, can obstruct the view and reduce the amount of daylight inside the building.

As the columns in the exoskeleton and braced core cannot exceed this maximum dimension of 600x600mm, the maximum factor at which the dimensions of the columns can be scaled can be calculated with equation 6.1 and 6.2.

$$F_{col,exo,upper} = \frac{h_{max}}{h_{col,exo,bottom}} = \frac{600}{320} = 1.875 \quad (6.1)$$

$$F_{col,core,upper} = \frac{h_{max}}{h_{col,core,bottom}} = \frac{600}{400} = 1.5 \quad (6.2)$$

Where:

h_{max}	[mm]	=	Maximum dimensions of the glulam cross-section
$h_{col,exo,bottom}$	[mm]	=	Dimension of the bottom exoskeleton column in the base-line model
$h_{col,core,bottom}$	[mm]	=	Dimension of the bottom braced core column in the base-line model

Since the columns of at the bottom story experience the highest axial forces and therefore have the largest dimensions, these columns are critical for determining the upper-bound of the column factor. These specific upper-bounds of the column scale factor apply for the base-line model. For the lower variants with 6, 9 and 12 stories, the dimensions of the bottom columns are smaller. Consequently, the upper-bound of the column scale factor is therefore higher.

6.2.3 Lower- and upper bound of diagonals in the exoskeleton and braced core

The main purpose of the diagonals in the exoskeleton and the braced core is to provide lateral stability to the building against horizontal loads. However, as the building is statically indeterminate, the axial load in the diagonals of the exoskeleton and braced core strongly depends on their axial stiffness.

The lower bound of the diagonals is determined by a ULS verification, in which the smallest cross-section was determined by the largest force that can occur in the diagonal for every possible parameter combination. The maximum force in the diagonals of the exoskeleton occurs when the dimensions and the connection stiffness in these diagonals are set to their upper-bound, while the other parameters are set to their lower-bound. With this approach it is ensured that every parameter combination results in a feasible design. However, the dimensions of the diagonals in the exoskeleton and the braced core could be reduced while still meeting the ULS requirement when the stiffness of the complementary lateral stability systems is increased. This contribution is not accounted for in the lower-bound, which makes the lower-bound conservative. To study the influence of this lower-bound, additional variants have been investigated with varying lower-bounds as described in Section 4.3.

The upper bound of the diagonals in the exoskeleton and the braced core is determined using the same principles as the upper bound of the columns as described in Section 6.2.2. Therefore, the upper bound dimensions of the diagonals in the exoskeleton and braced core is equal to 600x600mm.

The resulting lower- and upper-bound of the diagonals in the exoskeleton and braced core of every variant are displayed in Table 6.2. As the lower-bound of the diagonals is determined using the ULS verification the lower-bound is changing for every variant. The variant where the wind-load is applied in y-direction has the same design as the baseline model.

Variant	Maximum load in the exoskeleton diagonals	Lower-bound cross-sectional dimension of the exoskeleton diagonals	Maximum load in the braced core diagonals	Lower-bound cross-sectional dimension of the braced core diagonals
	[kN]	[mm]	[kN]	[mm]
15 stories, baseline	485	220	690	250
15 stories, y-direction	485	220	690	250
15 stories, open diagonal	550	230	850	270
12 stories	280	190	395	220
9 stories	200	170	250	210
6 stories	120	150	265	200

Table 6.2: Overview of lower bounds dimensions of diagonals for considered variants.

6.2.4 Lower- and upper bound dimensions equivalent diagonal shear walls

To model the shear stiffness of the timber frame walls in the building concept, the timber frame wall is modelled using the equivalent diagonal method as described in section 5.1.2. Consequently, the parameter representing the shear stiffness of the timber frame wall is the cross-sectional dimension of the equivalent diagonal.

As the equivalent diagonal is only a model simplification and not a physical element, and as it is assumed that the timber frame walls do not contribute to the vertical load distribution, the lower-bound of the equivalent cannot be determined using a ULS verification. Therefore, for the lower-bound a scenario is chosen where the timber-frame wall is completely absent and gives zero shear stiffness. While this corresponds to an equivalent diagonal dimension of 0 mm, a minimal cross-section of 1x1 mm is applied to prevent problems when running the finite-element analysis.

The upper bound is determined by calculating the equivalent diagonal dimension of a timber-frame shear wall which is configured to provide the maximum achievable shear stiffness, using standard construction materials and dimensions. To maximize the shear stiffness of the timber frame shear wall, several properties were optimized: the sheeting material, the number of sheeted faces n_s (on one-side or both sides of the wall), the sheeting thickness t_s, the amount of studs in compression on the corner of the wall n_s, the diameter of the nails connecting the sheets with the timber frame d_n, the spacing between the nails s_n and the number of hold-downs per timber frame wall n_{hd}. All other timber frame dimensions were assumed to remain constant. The values are based on common materials and dimensions applied in timber-frame construction (De Graaf & Banga, 2000). The chosen upper-bound properties are displayed in Table 6.3.

	Material [-]	n_s [-]	t_s [mm]	G_{mean} [MPa]	$n_{s,corner}$ [-]	d_n [mm]	s_n [mm]	n_{hd} [-]	$h_{eq,dia}$ [mm]
Upper-bound properties	OSB/4	2	22	2380	2	3,1	20	2	**225**

Table 6.3: Timber frame shear wall properties of the upper-bound.

The resulting upper-bound of the equivalent diagonal corresponds therefore of a glulam GL24h cross-section of 225x225 mm. In Appendix D, an example calculation is displayed on how the equivalent diagonal is calculated.

As the shear stiffness of the timber frame shear walls is dependent on the total width and height of the wall, the resulting upper-bound of the equivalent diagonal for the variant where the wind-load is applied in y-direction should be adjusted. Using the same wall properties, the resulting upper-bound value of the timber frame shear walls in y-direction is equal to 146 mm.

6.2.5 Lower- and upper bound relative connection stiffness of connections in exoskeleton and braced core

The definition of the parameter ranges for the axial stiffness of the connections in the diagonals of the exoskeleton and the braced core is the least straightforward as the axial stiffness that a slotted-in steel-to-timber connection can achieve is dependent on the size of the timber elements in which the connection is located. A larger timber cross-section provides room for more dowels and steel plates while maintaining sufficient spacing and can therefore achieve a higher axial stiffness than a smaller cross-section. For the sensitivity analysis and the optimization, it is important that every parameter configuration is possible to achieve the most realistic results.

To ensure this, instead of an absolute axial connection stiffness, a relative connection stiffness parameter κ was chosen. The relative axial connection stiffness parameter functions as a utilization ratio, varying between a lower-bound of 0 to an upper-bound of 1, where 0 corresponds to the stiffness of the connection when it can just satisfy the ULS verification, and 1 corresponds to the strongest connection that can be realized within the given timber element.

However, as the finite-element analysis requires an absolute stiffness value, a relationship between the cross-sectional dimensions of the timber element and the absolute lower- and upper-bound of the connection stiffness needs to be formulated. The relative connection stiffness parameter is subsequently linear interpolated between these two absolute bounds.

Lower-bound of the absolute axial connection stiffness:
The lower-bound of the absolute axial stiffness of the connection, corresponding to a relative stiffness of zero, is determined using the same governing loads as the lower bound of the diagonals as described in Section 6.2.3. This force indicates the largest axial force that can occur in the diagonal for all possible parameter combinations. Based on this force, a slotted-in steel-to-timber connection is designed that just satisfies the ULS requirement. The axial stiffness of this connection is taken as the lower-bound.

As the critical forces in the connections vary for each variant, the lower-bound of the absolute axial connection stiffness is determined for every variant. In addition, the critical load in the diagonals of the core vary from the critical load in the diagonals of the exoskeleton. In Table 6.4, for every variant the critical load and the resulting lower-bound of the axial connection stiffness are displayed which is used for the local and global sensitivity analyses. It should be noted that there are multiple connection configurations that could just resist the same forces but result into different connection stiffness values. Therefore, the lower bounds of the connection stiffness were determined by using similar connection configurations across the different variants.

Variant	Maximum load in the exoskeleton connections	Lower-bound axial connection stiffness of the exoskeleton connections	Maximum load in the braced core connections	Lower-bound axial connection stiffness of the braced core connections
	[kN]	[MN/m]	[kN]	[MN/m]
15 stories, baseline	485	120	690	144
15 stories, y-direction	485	120	690	144
15 stories, open diagonal	550	120	850	180
12 stories	280	90	395	120
9 stories	200	72	250	120
6 stories	120	60	265	72

Table 6.4: Overview of lower bounds dimensions of axial connection stiffness for considered variants.

Upper-bound absolute connection stiffness:
The upper-bound of the absolute connection-stiffness, corresponding to a relative stiffness equal to 1, is defined as a function of the dimensions of the element in which the connection is located. This maximum stiffness was determined manually be altering the number of steel plates, the diameter of the dowels, the number of dowels in parallel direction and in perpendicular direction.

To prevent brittle failure, the dowels and steel plates should fulfil the spacing requirements from EuroCode 5 (NEN-EN-1995-1-1, 2025). To exclude brittle failure modes, the bolt spacings a_1, a_2, and end distance $a_{3,t}$ are multiplied with factor k_{br} as described in Section 2.2.3. The minimum spacing between the steel plates was determined to guarantee the formation of plastic hinges in the dowels. The number of dowels perpendicular to the grain is limited by the height of the cross-sections. While the number of dowels parallel to the grain could theoretically extend over the entire length of the timber element, the efficiency of the connection reduces when the length over which the dowels are placed is longer. Therefore, it was chosen to limit the maximum connection length to twice the height of the timber element, with a maximum of 1000 mm.

The parameters that were varied to determine the upper bound of the axial connection stiffness are the number of steel plates n_p (between 1-4), the number of dowels parallel to the grain $n_{b,0}$, the number of dowels perpendicular to the grain $n_{b,90}$ and the diameter of the dowels dd (between 8-14 mm). The thickness of the steel plates was kept constant with a thickness of 10 mm. In Table 6.5, the resulting upper-bound connection stiffness is determined for varying dimensions of the timber cross-section. The connection stiffness is determined both using the method provided in EuroCode 5 (NEN-EN-1995-1-1, 2025) and using the method provided by Malo (Malo, 2023) as described in Section 2.2.6. The axial connection stiffness which will determine the upper-bound, has been chosen to be the minimum of both calculation methods for a safe approximation.

dimension	n_p	d_d	$n_{d,0}$	$n_{d,90}$	$K_{EC,max}$	$K_{Malo,max}$	$K_{critical}$ (min)
[mm]	[-]	[mm]	[-]	[-]	[N/mm]	[N/mm]	[MN/m]
0	-	-	-	-	0	0	1
100	1	8	9	1	80	95	80
200	2	12	6	2	431	326	326
300	3	10	4	4	719	517	517
400	4	10	5	5	1497	824	824
500	4	14	5	5	2096	1153	1153
600	4	14	5	5	2096	1153	1153

Table 6.5: Connection configuration for determining upper-bound connection stiffness.

To define a relation between the dimensions of the timber element and the maximum achievable stiffness, a 3rd degree polynomial was fitted through the data point. The decision for the 3rd degree polynomial was chosen as it showed to best fit of the available datapoints and because the 3rd degree polynomial can account for the flattening of the curve at the maximum cross-sections. However, it should be noted that the exact relationship between the diagonal dimensions is unknown. The relation between the dimensions of the timber elements and the axial connection stiffness is displayed in Figure 6.1.

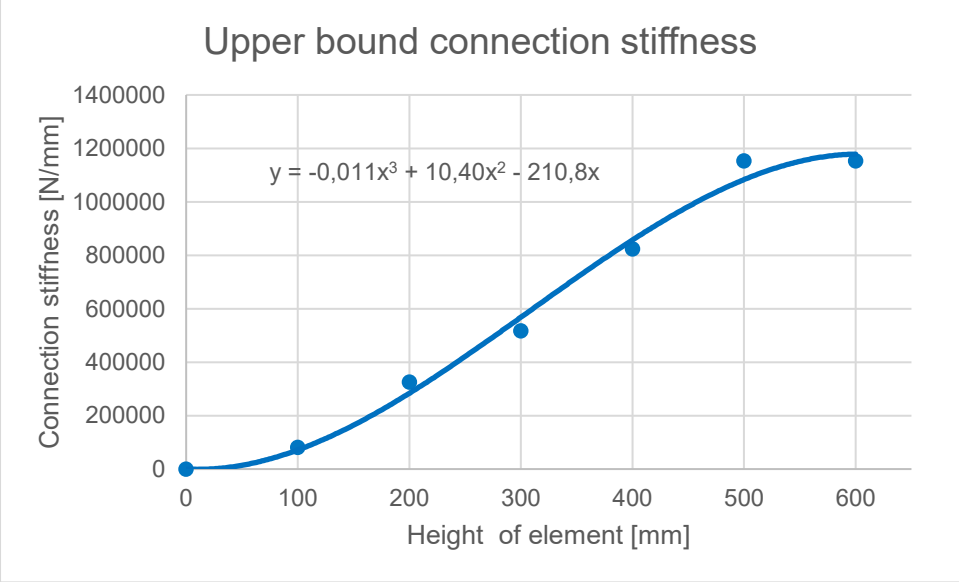

Figure 6.1: Relationship between the maximum achievable connection stiffness in N/mm as function of the height of the timber element in mm.

The resulting upper-bound connection stiffness K_{upper} in N/mm as function of the dimension of the timber element is displayed in equation 6.3. As the upper-bound of the connection stiffness is based on geometry, the same upper-bound function for the connections in the exoskeleton and the connection in the braced core is used.

$$K_{upper}(h) = -0.011 * h^3 + 10.40 * h^2 - 210.8 * h \quad (6.3)$$

Where:

h [mm] = the height of the timber element in which the connection is located

Relation between absolute and relative connection stiffness:
In between the lower-bound and the upper-bound the connection stiffness varies linearly dependent on the value of the relative stiffness factor (κ). The resulting relation between the relative stiffness and the absolute connection stiffness is displayed in equation 6.4.

$$K_{exo} = K_{lower} + \kappa * (K_{upper}(h) - K_{lower}) \quad (6.4)$$

Where:

κ	[-]	=	The relative stiffness factor
K_{lower}	[N/mm]	=	The lower-bound formula of the axial connection stiffness
K_{upper}	[N/mm]	=	The upper-bound formula of the axial connection stiffness

6.2.6 Resulting lower- and upper-bound values of the baseline model

The resulting lower- and upper bound values for every parameter in the baseline model are displayed in Table 6.6. In between brackets the corresponding absolute values of the lower-bound and upper-bound for the diagonals and connection stiffness are displayed for the baseline model.

Parameter	Lower bound	Upper bound
Scale factor for dimensions of columns in the exoskeleton	1.0 (320 mm)	1.88 (600 mm)
Dimensions of diagonals in the exoskeleton	220 mm	220 mm
Scale factor for dimensions of columns in the braced core	1.0 (400 mm)	1.5 (600 mm)
Dimensions of diagonals in the braced core	250 mm	250 mm
Dimensions of equivalent diagonal of timber frame shear walls	1 mm	225 mm
Relative connection stiffness of diagonals in exoskeleton	0.0 (120 MN/m)	1.0 (1240 MN/m)
Relative connection stiffness of diagonals in braced core	0.0 (144 MN/m)	1.0 (1240 MN/m)

Table 6.6: Overview resulting lower- and upper-bounds of the base-line model.

6.3 Local sensitivity analysis: One-At-a-Time method

6.3.1 Description of OAT method

The first sensitivity analysis performed in this study is a local sensitivity analysis using the One-At-a-Time (OAT) method. As the name suggests, in the OAT-method, one parameter is changed at a time while all others are kept constant to the reference values (Reed & Hadjimichael, 2022). The OAT-method was applied on the case-study for several reasons The method is easy to implement and requires a limited amount of data points, making the model computationally efficient. In addition, result of the analysis intuitive allows for straightforward interpretation of how individual parameters affect the building's global response.

Despite these advantages, the OAT-method has also clear limitations. As the relationship between the parameters and the horizontal deflection of the building is non-linear, the results of the OAT method are dependent on the chosen reference values and parameter ranges. Furthermore, since only one parameter is changed at a time, interactions between different parameters cannot be measured. In the case-study interaction between stability systems is expected. Nevertheless, the local sensitivity analysis serves as a valuable initial tool to gain a first understanding of the influence of every parameter. In addition, the local sensitivity analysis provides insight into the relationship between the parameter and the global horizontal deflection of the building.

.

6.3.2 Results of the OAT-method for the base-line variant

In this paragraph, the results of the local sensitivity analysis using the OAT-method for the base-line variant with 15 stories, a dense diagonal configuration and a wind load applied in x-direction are displayed. In Figure 6.2, the parameter range for every parameter is plotted on the x-axis with the horizontal global deflection of the building on the y-axis. As described in section 6.3.1, only one parameter is changed at the time, while the other parameters are kept constant to their base-line value. For the columns in the exoskeleton and braced core both the plots with on the x-axis the column scale factor and the actual dimension of the bottom column is displayed. For the axial connection stiffness in the OAT-method the relative connection stiffness was varied between 0 and 1 as described in Section 6.2.5. However, as dimensions of the diagonals in the exoskeleton and core are kept constant, the relative connection stiffness can directly be related to the absolute connection stiffness. Therefore, it was chosen to plot the absolute connection stiffness on the y-axis as this allows for an easier interpretation.

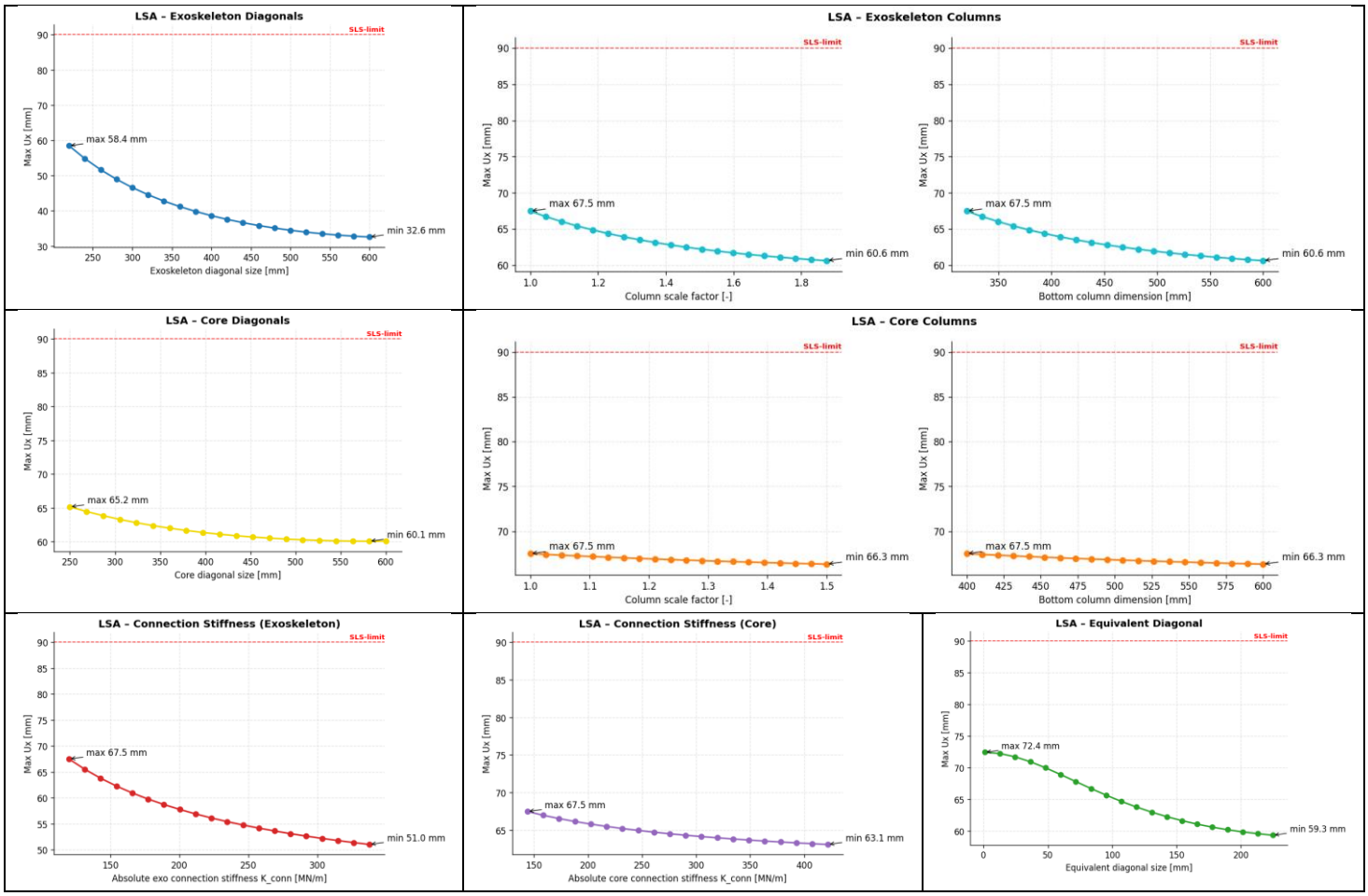

Figure 6.2: Horizontal displacement of the building by varying each individual parameter over their respective parameter range.

The results of the OAT-method are summarized using a Tornado-Chart indicating the difference between the maximum and maximum obtained value in the chosen parameter range. This difference gives an indication on how much changing the parameter within the chosen range can influence the global horizontal deformation of the building. The parameters in the tornado-chart are ranked by influence.

In addition to the absolute influence on the deformation of the building of each parameter, the percentual influence of each parameter is calculated and displayed in a pie-chart in Figure 6.4. The percentual influence of each parameter calculated by dividing the difference between the maximum and minimum value of the parameter range with the sum of all differences between the maximum and the minimum value as described in equation 6.5.

$$I_i = \frac{(U_{i,max} - U_{min,i})}{\sum_{i=1}^{n}(U_{i,max} - U_{min,i})} \tag{6.5}$$

Where:

$U_{i,max}$	[mm]	=	The maximum obtained horizontal displacement of parameter i
$U_{i,min}$	[mm]	=	The minimum obtained horizontal displacement of parameter i

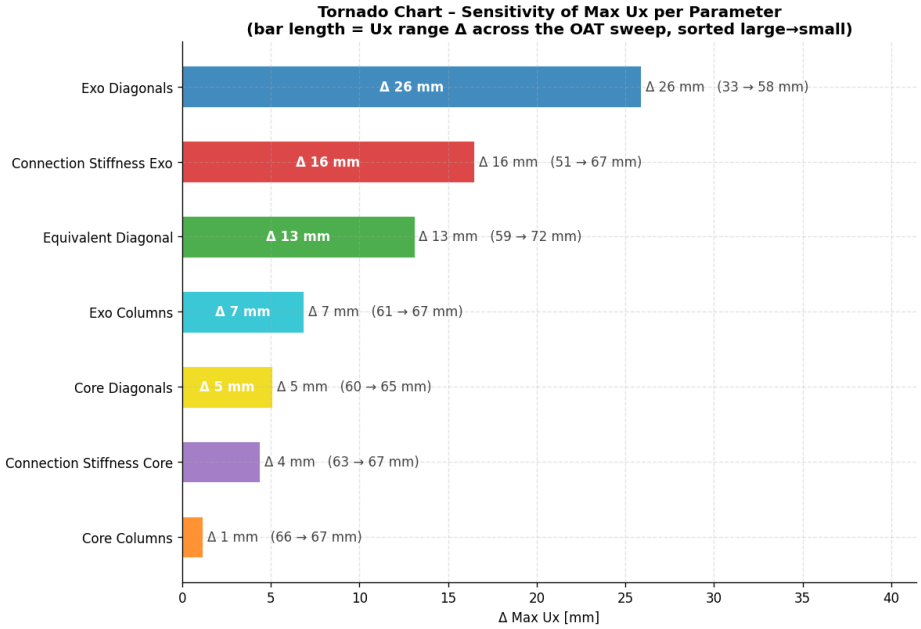

Figure 6.3: Tornado-chart indicating the difference between the maximum and minimum horizontal displacement over the parameter range of each parameter.

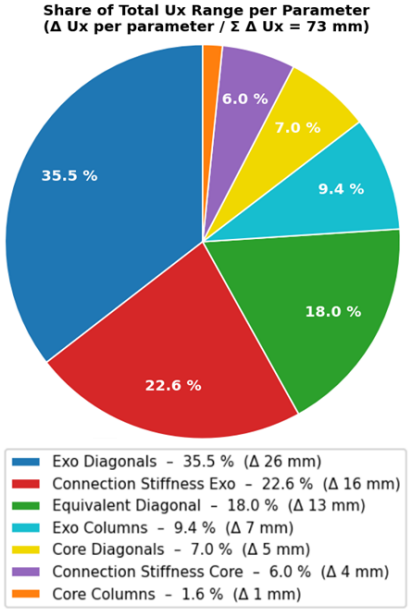

Figure 6.4: Pie-chart indicating the share of displacement difference of each parameter over the total found displacement difference.

From the plots in Figure 6.3 and Figure 6.4, the following observations can be made:

- The exoskeleton dominates the bending stiffness of the building. The diagonals, columns and connections in the exoskeleton have a significant larger influence on the deflection that the diagonals, columns and connections in the braced core. Together, the parameters of the exoskeleton account for 67.5% of the total influence, compared to only 14.6% for the parameters of the braced core.
- The dimensions of the diagonals are the most influential parameter. By increasing the dimensions of the diagonals in the exoskeleton, the deflection of the building can be reduced by almost half. The share of the total deflection of the exoskeleton is equal to 35.5%
- The stiffness of the connections has the second largest influence on the deflection. Varying the axial connection stiffness has an influence of 22.6% of the total deflection.
- The shear stiffness of the timber frame shear walls has a significant influence on the bending stiffness of the building. With a share of 18.0% the influence of the timber frame walls is larger than the influence of the braced core.
- The columns have a lower influence on the bending stiffness of the building than the diagonals. The total influence of the columns on the deflection is equal to 11.0% whereas the diagonals have a total influence of 42.5%.
- All parameter configurations satisfy the SLS-requirement for the horizontal deformation of the building. The maximum found displacement of the building is equal to 72.4 mm.

For the interpretation and discussion of the results of the OAT-method for the base-line method and the additional variants is referred to Section 6.3.5.

6.3.3 Results of the OAT-method for main additional variants

In addition to the base-line variant, the OAT-method has also been applied to the additional variants described in Section 4.3 to investigate how the results are influenced by a varying number of stories, varying building geometries and varying lower-bounds of the parameter ranges. This section first displays the displacement graphs for every parameter and every variant. Subsequently, a comparison is made of the results of the OAT-method for the variants with varying number of stories. After this, a plot is displayed to compare the results for the varying geometries. Lastly, the results of the OAT-method are displayed for varying lower-bounds of the parameter.

First, the displacement graphs for every parameter and every variant are shown in Figure 6.5. The parameter range is plotted on the x-axis and the global horizontal displacement of the building on the y-axis, where the different variants are indicated by different shapes of the data point. This figure provides a first visual impression of whether the trends observed for the baseline variant are consistent for all the other variants. As described in Section 6.2.2, the parameter range is not equal for every variant, since the lower bound is determined by ULS verifications

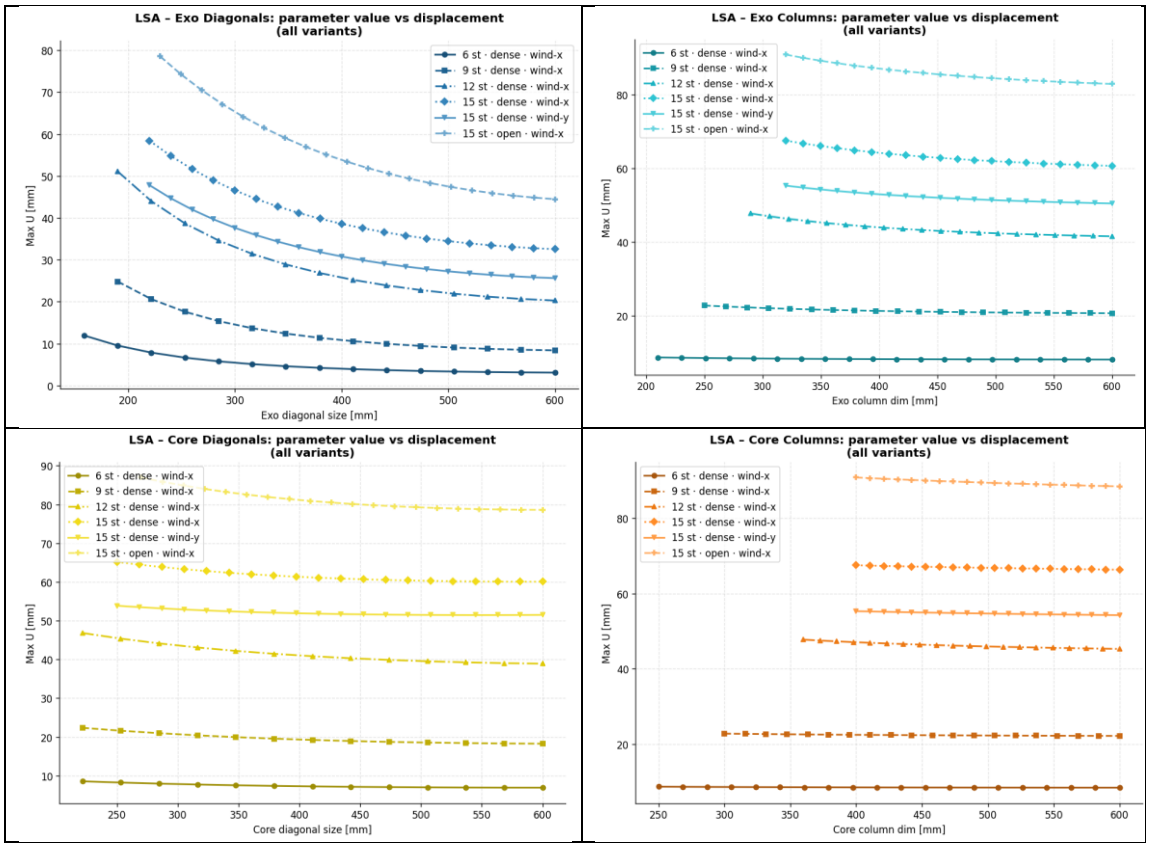

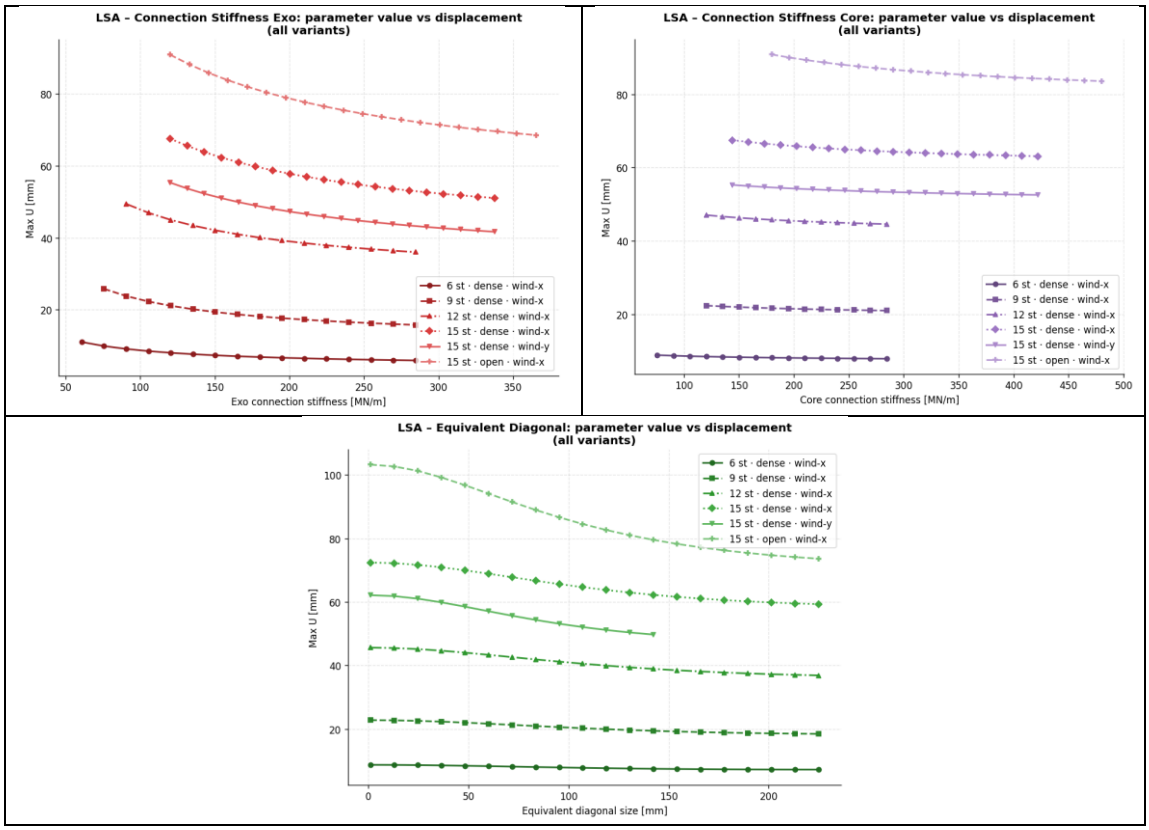

Figure 6.5: Horizontal displacement in the local sensitivity analysis of every parameter over their respective parameter range for every considered variant.

From Figure 6.5, the following observations can be made:

- The trend of the parameters is consistent across the different variants. Although the magnitude of the deflection for every variant is different, the shape of the curve is similar for every variant.
- The same non-linear behaviour of the parameters is visible across every variant. Although this behaviour is not clearly visible for the parameters with limited influence on the horizontal deflection of the building, the non-linear behaviour was also found for every parameter.
- For every parameter the ranking of the variants remains consistent, when the parameter is varied between the lower- and upper-bound.

Influence of varying number of stories:

To study the influence of the parameters on the global horizontal deformation of the building for varying studies, the influence of every parameter according to the Local Sensitivity Analysis is plotted in Figure 6.6. In the Figure on the left the influence of every parameter is plotted with the lower-bounds according to the ULS-verification as described in Section 6.2. As the loads on the building decrease when the building height decreases, the lower bounds of every variant with a varying number of stories is different. To make an equal comparison of the influence of the parameters, the results of the LSA for the variants with varying has also been displayed where the lower-bound of the diagonals and connection stiffness is equal to zero, for which the lower-bounds are equal for every variant.

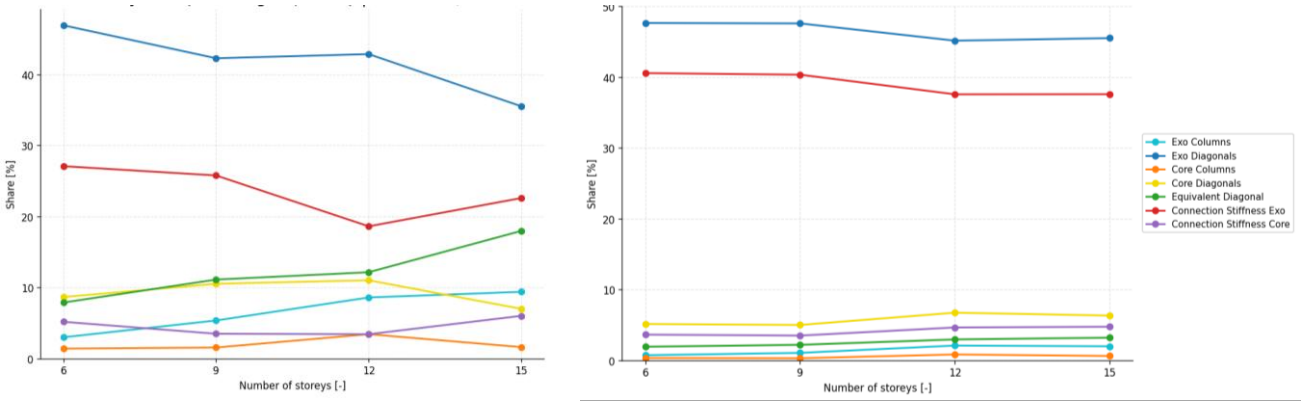

Figure 6.6: Parameter shares on the horizontal displacement for variants with varying number of stories. On the left diagram the results for variants with lower-bounds based on ULS-verification is displayed. On the right diagram constant lower-bound and parameter ranges are applied across the variants with varying number of stories.

From the results in Figure 6.6 the following observations can be made:

- In the plot where the lower bounds are determined using a ULS verification for every variant, the influence of the diagonals in the exoskeleton decreases when the number of stories of the building increases.
- In the plot where the lower bounds are determined using a ULS verification for every variant, the influence of the timber frame shear walls in the exoskeleton increases when the number of stories of the building increases.
- In the plot where the lower bounds are equal for every variant, the influence of every parameter remains roughly constant when the number of stories of the building is varied. Only a slight decrease in the influence of diagonals and connections in the exoskeleton can be observed, while the other parameters show a slight increase in influence.

For the interpretation and discussion of the results of the OAT-method for the base-line method and the additional variants is referred to Section 6.3.5.

Influence of varying geometries:
The local sensitivity analysis (LSA) was also performed on variants with a varying structural geometry to study how the chosen geometry affects the sensitivity of the parameters. To study this influence, two additional variants were considered and compared to the baseline model. In the first variant, the baseline model is used, but the wind is applied in y-direction. In this direction the braced core of the building is relatively slender, and the width of the exoskeleton is slightly larger. In the second variant, half of the diagonals in the exoskeleton have been removed to obtain a more open diagonal structure.

In Figure 6.7, the results of the LSA are displayed for both the ULS lower-bounds and the zero lower-bound. The result of the near-zero lower-bounds is included because for these variants the lower bounds for every variant in this model are equal, due to which a more consistent comparison between the variants can be made.

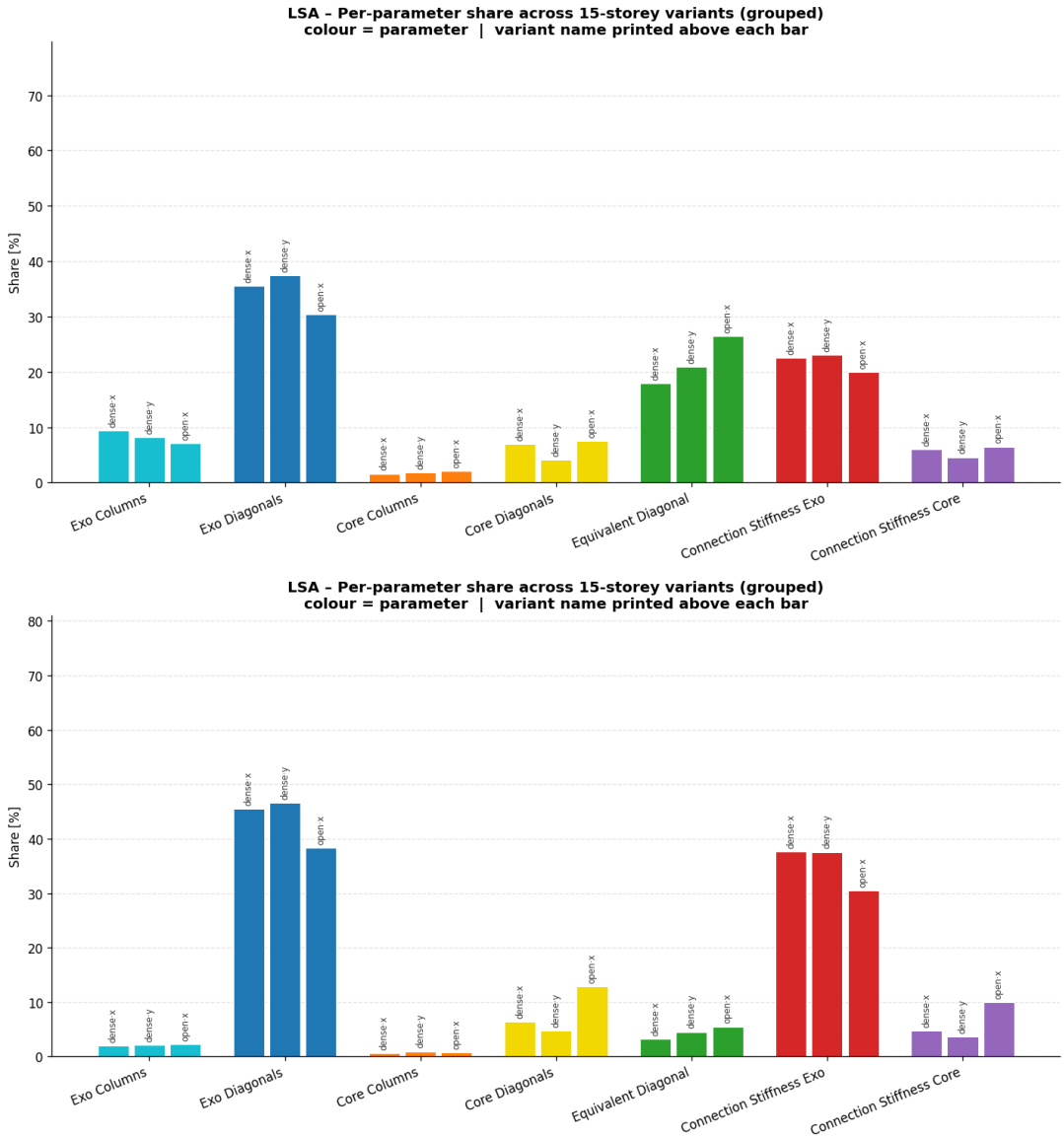

Figure 6.7: Influence of parameters on the horizontal displacement for varying structural geometries. The top diagram indicates the influence of parameters with ULS lower bounds is displayed. In the bottom diagram the influence of parameters with an equal zero-lower bound for every parameter is displayed.

From Figure 6.7 the following observations can be made:

- Independent of the structural geometry, the diagonals and connections in the exoskeleton have the strongest influence on the global horizontal behaviour of the building.
- In the variant with the open diagonal structure, the influence of the diagonals in the exoskeleton decreases, whereas the influence of the braced core and timber frame shear walls increases.
- Although the influence of the diagonals decreases for the variant with open diagonal structure, but still the diagonals of the exoskeleton have the highest influence on the global horizontal deformation of the building.
- In the variant where the wind load is applied in y-direction, the influence of the core reduces.
- The influence of the columns in the exoskeleton and braced core remains mostly constant when equal lower bounds are used for every variant.

Influence of varying lower bounds:

To study how the influence of the parameters on the global horizontal deflection of the building is dependent on the choice of the lower bounds. The local sensitivity analysis was performed for the baseline model with three different parameter ranges. In the first variant the lower bounds of the diagonals and the connection stiffness in the exoskeleton and braced core was determined according to ULS verifications, which corresponds to the approach which is used for the baseline model. In the second variant the lower-bounds of the diagonals and connection stiffness was set to a near-zero value to account for complete absence of these parameters. Lastly, an average lower-bound was considered where the lower-bound was determined to guarantee ductile failure of the connections when the diameter of the dowels is equal or larger than 8 mm. The corresponding lower-bound dimension of the diagonals in this variant is equal to 100 mm. The lower-bound values of the columns and the equivalent diagonal remain constant across these variants. In Figure 6.8, the influence of every parameter is displayed for every variant with varying lower bounds.

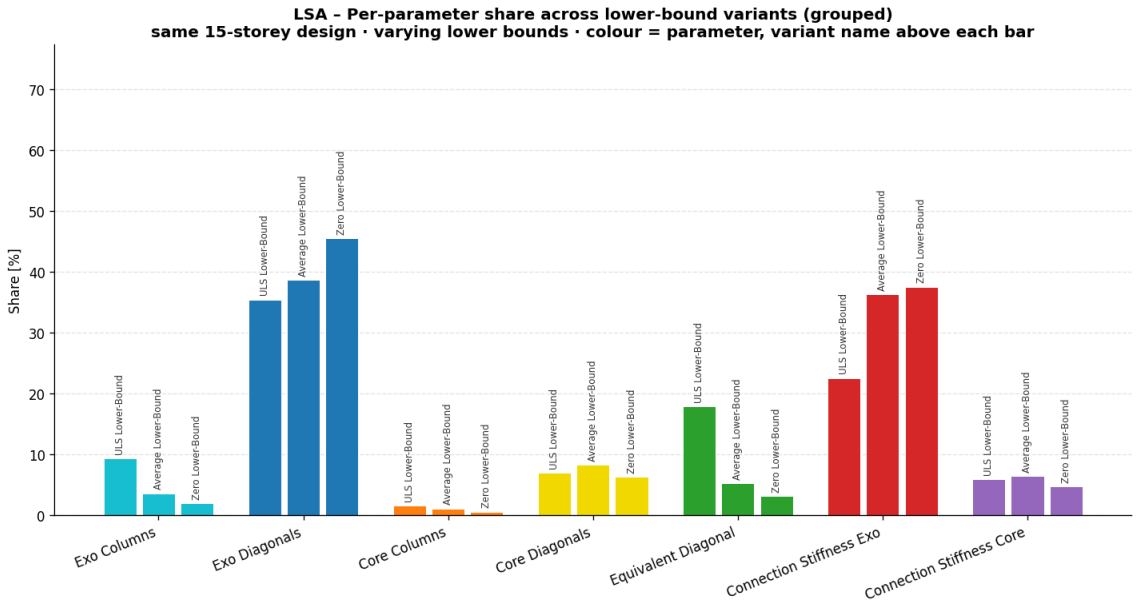

Figure 6.8: Influence of parameters on the horizontal displacement for varying lower bounds.

From the results in Figure 6.8, the following observations can be made:

- The decision of the lower-bound has a significant influence on the share that every parameter contributes to the horizontal deflection of the building.
- The influence of the diagonals and connection stiffness of the exoskeleton increases when the value of the lower-bound of these parameter decreases.
- The influence of the timber frame shear wall and the columns in the exoskeleton and braced core decrease when the lower-bound of the diagonals and the connection stiffness decreases.
- The influence of the diagonals and connection stiffness of the core is dominant on the deflection of the building, independent of the decision of the lower-bound.
- The relative influence of the diagonals and connection stiffness of the braced core does not increase when the lower bounds of the diagonals and the connection stiffness decrease.

For the interpretation of the results of the OAT-method for the base-line method and the additional variants is referred to Section 6.3.5.

6.3.4 Exploratory studies of the building

In addition to the main additional variants, a number of exploratory variants were considered to investigate the influence of the foundation stiffness and to study whether each individual stability systems could satisfy the horizontal displacement limit when the stability system is the only system in the building.

Variant to study the influence of the foundation stiffness:
In the first exploratory variant, the influence of the foundation stiffness on the horizontal displacement of the building is studied. As described in Section 5.1.4, the foundation stiffness is modelled by assigning a flexible vertical stiffness to every hinged support of the building. The foundation stiffness was varied by multiplying (upper-bound) and dividing (lower-bound) the baseline value by a factor of $\sqrt{2}$. The choice for these specific factors is based on engineering experience and standard practices of Van Rossum, the engineering firm where this project was conducted. For a consistent comparison, the foundation stiffness was kept equal for every variant.

To study the influence of the foundation stiffness, the variants with varying number of stories are considered. As the influence of the foundation stiffness is independent of the stiffness of the building when second order effects are neglected, the influence of the foundation stiffness was not studied for the additional variants with 15 stories. The share of the total displacement in the results of the LSA could be slightly different for these additional variants of 15 stories, but it is assumed that this only marginally affects the results.

Number of stories	$U_{x,lower\text{-}bound}$ [mm]	$U_{x,upper\text{-}bound}$ [mm]	$U_{x,lower\text{-}bound} - U_{x,upper\text{-}bound}$ [mm]	Share of total Ux in OAT-method [%]
15	81,9	74,6	7,3	1,4%
12	47,9	44,1	3,8	1,3%
9	23,7	22,1	1,6	0,8%
6	9	8,5	0,5	0,6%

Table 6.7: Overview of the influence of the foundation stiffness on the horizontal deformation of the building.

From Table 6.7, it can be concluded that the influence of the foundation stiffness on the global horizontal deformation of the building is relatively low, independent of the height of the building. In addition, it can be observed that the influence of the foundation stiffness decreases when the height of the building decreases. As the foundation stiffness only has a limited effect on the horizontal deformation and as the foundation stiffness could not be parametrically modelled using the chosen parametric workflow, the influence of the foundation stiffness was not considered in the remaining part of this report.

Variants with only one stability mechanism:
To study if every independent stability system could satisfy the SLS requirement alone, multiple variants have been created from the baseline model for which only one stability system remains. First, the displacement of the building was determined when the reference values of the remaining stability system are used. Subsequently, the model was run for which the parameters of the remaining stability system where increased to the upper bounds. The same approach was performed for the variant with 6 stories to study if the individual stability systems could give sufficient stiffness when the height of the building decreases.

The maximum allowed horizontal displacement for the variants with 15 stories is equal to 90 mm, whereas the maximum horizontal displacement of the variant with 6 stories is equal to 36 mm. The dimensions of the reference model are described in Section 5.3. The upper-bound dimensions of the parameters are described in Section 6.2.

Variant	**Displacement at the baseline dimensions [mm]**	**Displacement at the upper-bound value [mm]**
15 story variant with exoskeleton diagonals only	103	28
15 story variant with braced core diagonals only	389	204
15 story variant with timber frame shear walls only	797	442
15 story variant with braced core diagonals and timber frame shear walls	260	103
6 story variant with braced core diagonals only	40	16
6 story variant with timber frame shear walls only	29	19

Table 6.8: Overview of the horizontal deformation of the building for variants with only one or two stability mechanisms.

From the results in Table 6.8, the following observations can be made:

- In the 15-story variant, the braced core and the timber frame shear walls cannot individually or together give sufficient stiffness to the building to meet the SLS-requirement for the horizontal displacement.
- The exoskeleton can satisfy the SLS-requirement when the exoskeleton is the only stability mechanism in the building.
- For the 6-story variant, when only the braced core or the timber frame shear walls, the SLS-requirement for the horizontal deformation can be met.

6.3.5 Interpretation of the results of the OAT-method

In this paragraph, the main observations and conclusions from the results of the Local Sensitivity Analysis (LSA) using the OAT-method are discussed, explained and interpreted.

The relation between the parameters and the horizontal deflection of the building is non-linear and shows asymptotic behaviour:

The Figures in Section 6.3.2, shows that an non-linear semi-asymptotic behaviour of the output when the parameter is varied between the lower- and upper-bound. First the deflection of the building decreases rapidly. When the dimension of the cross-section increases the change in deflection decreases.

This behaviour is expected. If the building is modelled as a cantilever beam, the horizontal deflection due to a distributed load can be determined using the equation 6.6. By substituting the expression for the moment of inertia as a function of the exoskeleton dimensions into this formula and keeping the other variables constant the relation between the dimensions of the exoskeleton and deformation can be found. This relation corresponds to asymptotic behaviour.

$$w_H = \frac{qL^4}{8EI} = \frac{qL^4}{8E * (\frac{1}{12} * h_{exo,tot}^4)} = \frac{1}{h_{exo,tot}^4} \tag{6.6}$$

The asymptotic behaviour between the dimension of the exoskeleton and the horizontal deflection can also be explained by the fact that at a certain point further increasing a single parameter has negligible impact, as the global deformation is also dependent on the stiffness of the other parameters. This explains why the asymptote does not lie on the x-axis at zero deflection but instead converges to a specific value.

Due to the asymptotic behaviour of the parameters, the decision of the lower-bound should be carefully determined as this decision can strongly affect the influence of the parameter on the total deflection, whereas the decision of the upper-bound affects the influence on the deflection of the building less.

The exoskeleton has stronger influence on the horizontal deflection of the building than the braced core.

The larger influence of the exoskeleton can be explained due two main reasons. First of all, the amount of material used in the exoskeleton is significantly higher than the amount of material used in the braced core. Therefore, varying the dimensions of the diagonals and columns in the exoskeleton with the same dimensions as the diagonals and columns in the braced core, result in a higher increase in the used material for the exoskeleton. Therefore, the stiffness of the exoskeleton is increased more compared to the stiffness of the braced core when the dimensions of the diagonals and columns are varied with the same dimensions resulting in a stronger influence on the deflection of the building

In addition, the bending stiffness of the exoskeleton is higher due the fact that lever arm of the columns in the exoskeleton is higher. In equation 6.7, Steiner's displacement rule is displayed.

$$I_{tot} = \sum(I_0 + a^2 * A) \quad (6.73)$$

Where:

I_0	[mm^4]	=	The moment of inertia of a single column
a^2	[mm]	=	The lever-arm between the centre of the building and the centre of the column
$h_{col,core,bottom}$	[mm]	=	The cross-sectional are of the column

As the lever-arm a of the columns in the exoskeleton is higher than the columns in the core, the contribution to the bending stiffness of the columns is much higher than the contribution of the columns, resulting in stronger influence on the horizontal behaviour.

Lastly, in the baseline variant the lower-bounds of the sensitivity analysis is higher for the diagonals, columns and connections in the braced core compared to the lower-bounds of the exoskeleton. Therefore, the parameters are allowed to very less due to which the parameters have a lower influence on the deformation of the building.

The columns in both the exoskeleton and braced core have a lower effect on the global horizontal deflection of the building than the diagonals and connections:

As the axial stiffness of the diagonals and the axial stiffness of the connections, both influence the total axial stiffness of the diagonal, and therefore have a similar effect, these parameters are considered to have the same effect. This observation could be explained due to two reasons. First of all, the building considered in this study is not very slender with a slenderness ratio of approximately 1:2. Therefore in general, the shear deformation of the building is relatively large compared to the bending deformation of the building. The diagonals and the connection stiffness in the core contribute the strongest to the shear deformation and have therefore a stronger influence on the global horizontal deformation of the building.

In addition, the dimensions of the diagonals and connection stiffness do not only influence the shear deformation of the building, they also mechanically connect the columns to each other. Therefore, the moment of inertia is not just the sum of the separate columns, but instead the columns act together increasing the moment of inertia and therefore bending stiffness of the building.

The influence of the varying number of stories on the parameters:

In Figure 6.6, where the influence of every parameter is plotted for a varying number of stories, the influence of the parameters varies for the different stories when the lower-bound is determined using the ULS-verification. This variation is therefore explained by the decision of the lower-bound. As the lower bounds change for the variants with varying stories no clear comparison can be made between the parameters.

Therefore, the influence of varying number of stories has also been investigated when the lower bounds of all parameters are equal across every variant. In this Figure, it can be concluded that the influence of every parameter remains mostly constant. Only a small decrease in the influence of the diagonals and connection stiffness in the exoskeleton and small increase in influence of the remaining parameters is visible. Although this change in parameter is very small and could therefore be caused by uncertainty in the results, the decrease of the diagonals and connections and the increase of the influence of the columns could be explained using beam deflection formulas due to the bending stiffness and shear stiffness of a cantilever beam:

$$w_{bending,max} = \frac{1}{8} * \frac{q * L^4}{EI} \quad (6.8)$$

$$w_{shear,max} = \frac{1}{2} * \frac{q * L^2}{GA_s} \quad (6.9)$$

From these formulas it can be concluded that the bending deformation of the building increases with the power 4 when the height of the building increases, whereas the shear deformation increases with the power 2. Therefore, when the height of the building L increases, the bending deformation becomes more dominant on the total deflection of the building. As the diagonals contribute most to the shear stiffness of the building and the columns contribute most to the bending stiffness of the building, the influence of the columns in the building is expected to increase when the height of the building increases.

The influence of different geometrical variants:

From the results of the variants with varying structural geometries in Section 6.3.3 to main observations can be made. In the variant where the wind load is applied in y-direction, the influence on the deflection of the core decreases and the influence of the exoskeleton increases. This can simply be explained by the fact that core is more slender in y-direction of the building than in x-direction. In addition, the exoskeleton is 1 meter wider in y-direction.

Another observation is that for the variant with the open diagonal structure the influence on the deflection of the exoskeleton decreases and the influence of the other parameters increases. This is a logical outcome. As this variant uses less material in the exoskeleton, the stiffness of the exoskeleton and therefore the influence on the deflection decreases, due to which the influence of the other parameters increases.

Influence of different lower bounds for the parameter ranges for the sensitivity analysis:

From the results of the variants with varying lower-bounds for the parameter ranges in Section 6.3.3, it can be concluded that the influence of the parameters is strongly dependent on the decision of the lower-bound. For the different variants the lower bounds of the columns and timber frame shear walls remained constant. However, the lower-bounds of the diagonals and connections vary between a near-zero value to the lower-bound according to the ULS verifications.

When the lower bounds of the diagonals and connections decreases, the range in which the parameters can vary increases. Therefore, the influence of these parameters on the total deflection of the building increases. The relative influence of the columns and the timber frame shear walls therefore decreases. Although the influence of the parameters changes, for every lower-bound the diagonals and connections in the exoskeleton dominate the horizontal deflection of the building.

6.3.6 Conclusion local sensitivity analysis

In summary, the following conclusions can be made from the local sensitivity analysis.

- The relation between the parameters and the horizontal deflection of the building is non-linear and shows asymptotic behaviour.
- The exoskeleton has stronger influence on the horizontal deflection of the building than the braced core, independent of the number of stories, considered structural geometries and chosen lower bounds.
- The columns in both the exoskeleton and braced core have a lower effect on the global horizontal deflection of the building than the diagonals and connections.
- The influence of the timber frame shear wall is strongly dependent on the chosen parameter ranges.
- The influence of the different parameters remain mostly constant for the varying building height
- Varying the structural geometry of the building affects the influence of the parameters, but the exoskeleton still has a dominant influence on the deflection of the building for the considered variants.
- The influence of the foundation stiffness on the deflection of the building is relatively small compared to the other parameters.
- The braced core and timber frame shear walls are not able to satisfy the horizontal deflection limited when applied alone or together for the variant with 15 stories. The exoskeleton is able to satisfy the horizontal deflection limit alone.
- For the variant with 6 stories both the braced core and timber frame shear walls could satisfy the horizontal deflection limit alone.

6.4 Global sensitivity analysis: Sobol-method

In the Local Sensitivity Analysis (LSA) of Section 6.3, a first indication is given on the influence of the differ parameters on the horizontal deflection of the building. However, as in the LSA only one parameter is changed at the time and because the parameters show a non-linear relation with the deformation of the building. The influence of every parameter is dependent on the used reference model. Therefore, also a Global Sensitivity Analysis (GSA) is performed using the Sobol-method. First in Section 6.4.1 a description of the Sobol-method is given. Subsequently, the used surrogate model is explained and validated in Section 6.4.2. The results of the GSA for both the baseline as additional variants are displayed in Section 6.4.3 and 6.4.4. In Section 6.4.5 the results of the analysis are interpreted, and the main conclusions are summarised in Section 6.4.6.

6.4.1 Description of the Sobol-method

For the global sensitivity analysis of the parameters, the Sobol-method is used. The Sobol-method is a Variance-Based method. Instead of changing one parameter at a time, it changes all parameter at once. Every configuration is a random combination of the parameter values within the parameter ranges. In the Sobol-method the total variation in the output can be decomposed in the variance which is caused by each individual parameter. The percentage every parameter contributes to the variance of the output can directly be interpreted as a measure of sensitivity (Reed & Hadjimichael, 2022).

To apply the Sobol-method a number of conditions must be met. First of all, the input variables must be independent of each other, meaning that the value of one parameter cannot be related to the value another parameter. For this reason, it was chosen to implement a relative connection stiffness parameter, as the upper-bound for the connection stiffness is dependent on the dimensions of the timber element in which the connection is located. Another condition that needs to be met, is that a minimum number of configurations are needed to compute the Sobol Indices accurately. The minimum amount of datapoints which are needed to quantify the sensitivity of each parameter can be calculated using the rule of thumb that $N_{sobol} > 1000*d$, where d is the number of parameters (Reed & Hadjimichael, 2022). As for this study 7 different parameters are considered, at least 7000 datapoints are needed. As the number of configurations can easily be extended using the surrogate model, in this study the Sobol Indices were computed using 1,000,000 different configurations.

With the Sobol-method it is not only possible to quantify the effect for each individual parameter using the first-order Sobol-index, but also to quantify the effect of two or more parameters at the same time using higher-order Sobol-indices. The first order index indicates what percentage of the variance of the output is caused by that specific parameter only. In equation 6.10 the conceptual formula for calculating the first order Sobol-index are displayed.

$$S_i^1 = \frac{V_1}{V(Y)} \tag{6.10}$$

$$V_1 = V_{X_i}(E_{X_{\sim i}}[(Y|X_i)]) \tag{6.11}$$

Where:

X_i	[-]	=	The dataset with input values of parameter i
$X_{\sim i}$	[-]	=	The dataset with input values of all parameters except parameter X_i
Y	[-]	=	The dataset with the output of the model: the displacement
V_1	[-]	=	The output variance after eliminating the uncertainty of parameter X_i
E	[-]	=	The expected or average value of the data set
V	[-]	=	The variance of the data set

The first-order Sobol index indicates which fraction of the total variation in the output can be assigned to only parameter X_i. To determine the first-order Sobol index, a large dataset of configurations, in which the values of all parameters are randomly chosen, with each a certain output Y. To determine the influence of parameter X_i only, a number of steps are taken. First, parameter X_i is fixed at one value, while all other parameters are allowed to vary. The average output over all these configurations is then computed. This average value represents the expected output for that particular value from the X_i dataset (Saltelli A. , 2008).

This step is repeated for every value within the dataset of X_i. This results in a new dataset with the average output for every value within the dataset X_i. From this new dataset the variance V_1 is determined. Since only X_i was kept fixed and all other parameters are averaged, this variance represent the variation in output that was caused by X_i. For example, if the parameter has a small influence on the output, the averaged value of the remaining output will hardly change and therefore the variation of the data set with averaged values will be small. By dividing this variance by the total variance of the output V(Y), the first order Sobol index is described as the fraction that the specific parameter contributes to the total variance of the output (Saltelli A. , 2008).

In addition to the influence of one single parameter, it is also possible to measure the interaction between multiple parameters using the second order Sobol index. The second order Sobol index is calculated using a similar approach, but here two parameters are fixed at the same time. The second order index is calculated using equation 6.12.

$$S_{ij}^2 = \frac{V_2}{V(Y)} \tag{6.124}$$

$$V_2 = V_{X_{ij}}(E_{X_{\sim ij}}[(Y|X_i)]) - V_i - V_j \tag{6.13}$$

Where:

X_i	[-]	=	The dataset with input values of parameter i
$X_{\sim i}$	[-]	=	The dataset with input values of all parameters except parameter X_i
Y	[-]	=	The dataset with the output of the model: the displacement
E	[-]	=	The expected or average value of the data set
V	[-]	=	The variance of the data set

By subtracting Second order Sobol index of parameter i and parameter j with their individual first order Sobol Indices, it can be determined if the parameters amplify each other. When the second order Sobol index is equal to the sum of the first other index of both parameters, the influence on the output of parameter i is independent of the value of parameter j. On the other hand, when this is not the case, the influence of parameter i on the output is dependent on the value of parameter j and the other way around.

6.4.2 Description and validation of the Gaussian Processing surrogate model

As described in Section 6.4.1, the computation of the Sobol indices requires thousands of FEM configurations. For the baseline model, running a single configuration takes approximately 2.5 minutes. Consequently, running the thousands of configurations needed to compute the Sobol indices of only a single variant would take several weeks. As multiple variants are computed, using FEM configurations for computing the Sobol-Indices is not feasible for this thesis.

For this reason, the surrogate model is used. A surrogate model is a mathematical model that is trained to mimic a computationally expensive model (Gramacy, 2020). The surrogate model predicts the expected output, in this case the global horizontal displacement of the building, from the combination of parameters, without running a computationally expensive FEM solver. Using the model, the expected output of millions of different configurations can be evaluated in seconds.

Latin Hypercube Sampling:

To generate the parameter combinations for each configuration on which the surrogate model will be trained, Latin Hypercube Sampling (LHS) is used. LHS is a stratified sampling method, where the range of each parameter is divided into equal intervals (Diwekar, 1997). The number of intervals equals the number of FEM iterations to be computed. In every interval one value of the parameter is randomly chosen. Subsequently, the intervals are paired with a random interval of another parameter, but one interval cannot be paired with the same interval of another parameter twice. Using this method a more uniform distribution of the random combinations is obtained, compared to when a purely random Monte Carlo sampling would be used, which prevents cluster formation. With LHS it is therefore possible to create a dataset with relatively few FEM runs.

Description of the surrogate model:

There are several different techniques to predict the output mathematically using a surrogate model. Polynomial Chaos Expansion (PCE) is a surrogate model that is commonly used in combination with the Sobol method. In PCE, a multidimensional polynomial is fitted though the data points of the FEM configurations. The main advantage of PCE in combination with the Sobol-method is that the Sobol indices can be derived analytically from the PCE coefficients (Sudret, 2007). However, for this model PCE was not used. The surrogate model using PCE was not able to fit the asymptotic behaviour of the output when the parameters were varied.

For this reason, a Kriging surrogate model was chosen, which is also known as Gaussian Process (GP) Regression. Kriging is an interpolation method which is based on the principle that points that lie close together in the parameter space will also produce a similar output. The method interpolates between the FEM-configurations which are deterministic. Instead of fitting a polynomial response through the entire dataset, the Kriging model predicts a new point by focusing on the datapoints which are surrounded closely. In Figure 6.9, an illustration of the Gaussian Process method is displayed (SciKit, n.d.).

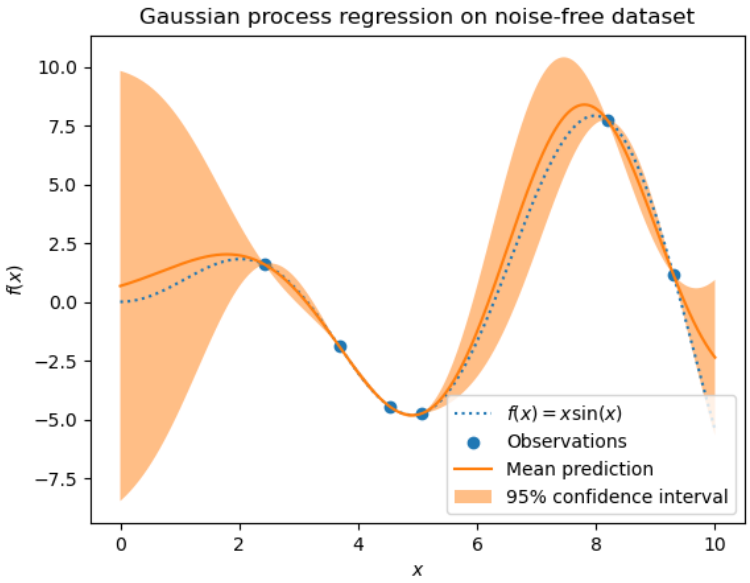

Figure 6.9: Illustration of Gaussian Process Regression (SciKit, n.d.).

By adjusting the kernel or covariance function it can be controlled how strongly the outputs of configurations are related as function of their distance in the parameter space (SciKit, n.d.). In this study, an anisotropic Matérn kernel with smoothness parameter v = 2.5 is used. This parameter indicates how smoothly the predicted function fits between the data-points. This value was chosen because it provided a good fit and accurate predictions of the output.

The Kriging surrogate model is therefore able to predict the asymptotic behaviour of the output more accurately. Another advantage of Kriging compared to PCE is that Kriging is more cost-efficient, requiring fewer data points. For this study, the surrogate model was trained using varying number of FEM configurations, ranging from 100 to 360. A rule-of-thumb states that the minimum number of data points should equal 10 times the number of parameters (J.L. Loeppky, 2013). Since this study considers 7 parameters, at least 70 FEM configurations are required. A disadvantage of Kriging compared to PCE is that the Sobol-Indices cannot be determined analytically. However, using the surrogate-model the computation of the Sobol-Indices still takes only approximately takes 20 seconds.

Validation of the surrogate-model

To ensure that the results of the sensitivity analyses are reliable, the accuracy of the surrogate model must be validated. To validate the Gaussian Process Regression model, the predictive squared correlation coefficient Q^2 is used. The Q^2-factor is determined using the Leave-One-Out Cross Validation (LOODCV) techniques. In this technique, one iteration is removed from the FEM configurations training set, and a new Kriging surrogate model is fitted on the remaining data points. The removed configuration is subsequently precited using this new model. The error is equal to the difference between the real FEM result and the blind predicted value from the model. This procedure is repeated for every configuration in the training set. The Q^2-factor can be calculated using equation 6.14.

$$Q^2 = 1 - \frac{\sum\left(Y_{FEM} - Y_{blind,prediction}\right)^2}{\sum(Y_{FEM} - \mu_{FEM})^2} \tag{6.14}$$

Where:

Y_{FEM}	[-]	=	The real output from a specific FE iteration
$Y_{blind,prediction}$	[-]	=	The blind predicted output from the surrogate model at the location of the specific iteration
μ_{FEM}	[-]	=	The average output of all FE iterations

A Q^2-value close to 1 indicates that the surrogate model predicts the blind configurations accurately. For the baseline model a Q^2-value of 0.994 was obtained, which shows that the surrogate model is able to replicate the output with high accuracy. In Figure 6.10, the predictions of the surrogate model are illustrated. On the x-axis the output of every FEM configuration is displayed, while the y-axis displays the output of the surrogate model for the same parameter configurations. When the data-points lie close to the red dashed line, the prediction of the surrogate model closely matches the real FEM output. The plot shows that in general the output of the surrogate model corresponds closely with the output of the FEM configurations.

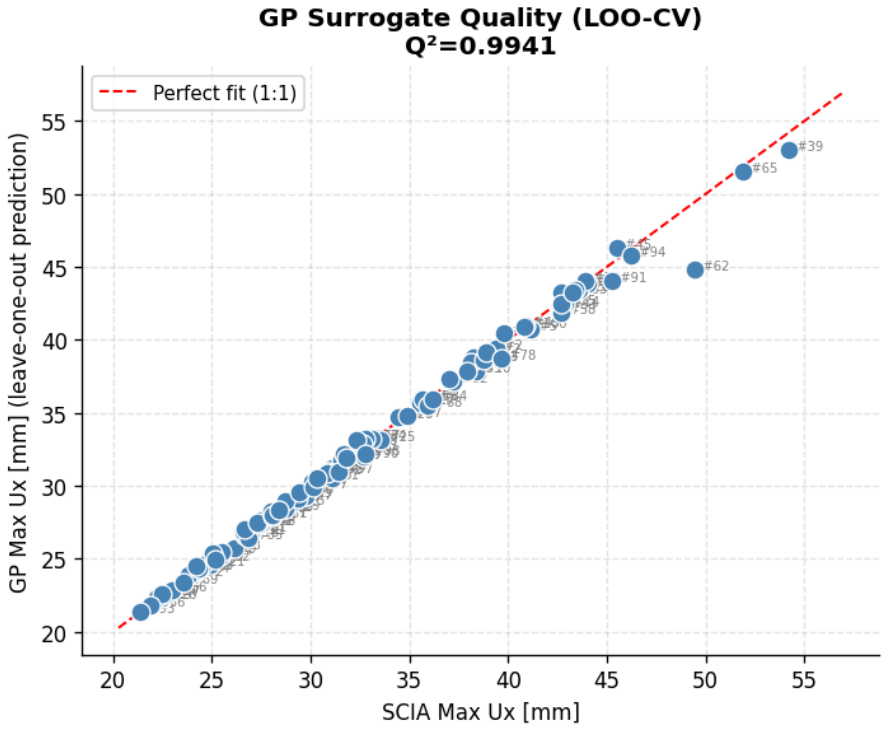

Figure 6.10: Gaussian Process Regression surrogate quality plot.

6.4.3 Global sensitivity analysis of the base-line variant

In this paragraph, the results of the global sensitivity analysis using the variance-based Sobol-method for the base-line variant with 15 stories, a dense diagonal configuration and a wind load applied in x-direction are displayed. The interpretation of the result will be described in Section 6.4.5. As described in Section 6.4.1, the Sobol-Indices can directly be interpreted as the influence of every parameter on the deformation of the building. In Figure 6.11, the results of the global sensitivity analysis are displayed. The dark bar indicates the first order Sobol-index, which indicates the independent effect of the parameter on the output. The light bar indicates the total effect of the parameter which is the summation of the independent effect and all the interaction with other parameters.

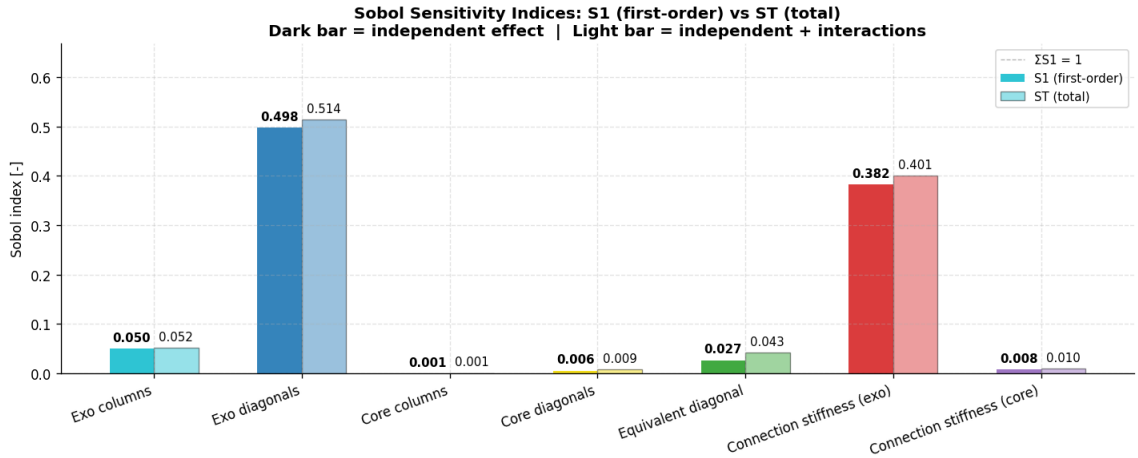

Figure 6.11: Results of global sensitivity analysis for the base-line variant. The left bar for every parameter indicates the first order Sobol-index and the right bar of every parameter indicates the total Sobol-index.

In the Pie-Chart in Figure 6.12, the first order Sobol indices are expressed in percentages, the total influence of the interactions of the parameters is also indicated in the pie-chart. In addition, a heat map is displayed in Figure 6.13, presenting the 2nd order Sobol shows the interactions between two parameters. The darkness of the squares shows the magnitude of the 2nd order Sobol index which is displayed with the number in the square. A 2nd order index of 0.008 can be interpreted that 0.8% of the total influence on the horizontal global displacement is caused by interactions of the parameters. In Figure E.1 and Figure E.2 in Appendix E.1, the 2nd-order interactions for the average lower-bound variant is displayed. In this plot the interaction between the parameters become more apparent as the lower-bound influence of the core is slightly higher.

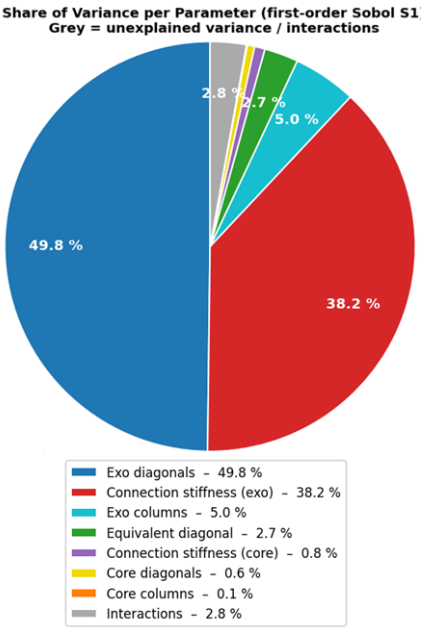

Figure 6.12: Pie-chart indicating the percentual first order index of every parameter.

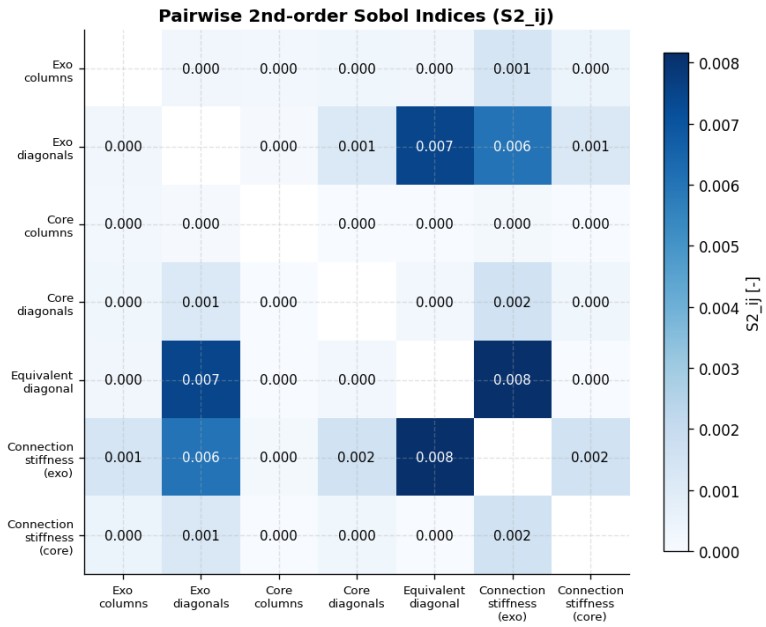

Figure 6.13: Interaction diagram of every parameter with each other. The darker the colour of the square, the stronger the interaction.

From the results in Figure 6.12 and Figure 6.13 the following observations can be made:

- Similar to the results of the Local Sensitivity Analysis (LSA) the exoskeleton dominates the influence on the deflection of the building. The influence of the exoskeleton diagonals, the exoskeleton connection stiffness and the exoskeleton columns including their interactions, together account for 93% of the variance, whereas the effect of the remaining parameters of both the braced core and the timber frame shear walls is equal to approximately 4%.
- The influence of the diagonals and connection stiffness in the exoskeleton in the results of the Global Sensitivity Analysis (GSA) has increased compared to the results of LSA. The influence of the diagonals in the exoskeleton increased from 38% to 50% and the influence of the connection stiffness in the exoskeleton increased from 23% to 36%
- The influence of the timber frame shear walls has reduced most compared to the results of the LSA. In the GSA the influence of the equivalent diagonal is 2.7% whereas the influence of the timber frame shear wall in the LSA was equal to 18%.
- The influence of the equivalent diagonal is mainly caused by the interaction with the exoskeleton. From Figure 6.12, it can be observed that the two highest 2nd order indices are containing the timber frame shear walls. In addition, from Figure 6.11 can be derived that of the total influence of the parameter 37% is caused by interactions with other parameters.
- The diagonals in the exoskeleton and the connection stiffness in the exoskeleton show almost no interaction. Although the interaction between these parameters is the 3rd largest, the relative interaction of the parameter compared to their total influence is very low.
- The interaction between the diagonals and connection stiffness of the braced core and the diagonals and connection stiffness in the exoskeleton is low but relatively speaking significant. For the core approximately 30% of the total influence is caused by interactions.
- The influence of varying the columns is significantly lower than the influence of varying the diagonals and connection stiffness for both the exoskeleton and the core.

6.4.4 Global sensitivity analysis of additional variants

Similar to the Local Sensitivity Analysis the influence of varying variants have also been investigated by with varying number of stories, a varying diagonal structure and where the wind-load is applied on y-direction. In addition, the influence of the decision for the lower-bound of the parameter ranges was investigated.

Result of varying stories

To study the influence of the parameters on the global horizontal deformation of the building for varying studies, the influence of every parameter according to the Global Sensitivity Analysis is plotted in Figure 6.14. In the diagram on the left the influence of every parameter is plotted with the lower-bounds according to the ULS-verification as described in Section 6.2. As the loads on the building decrease when the building height decreases, the lower bounds of every variant with a varying number of stories is different. To make an equal comparison of the influence of the parameters, the results of the GSA for the variants with varying has also been displayed where the lower-bound of the diagonals and connection stiffness is equal to zero, for which the lower-bounds are equal for every variant.

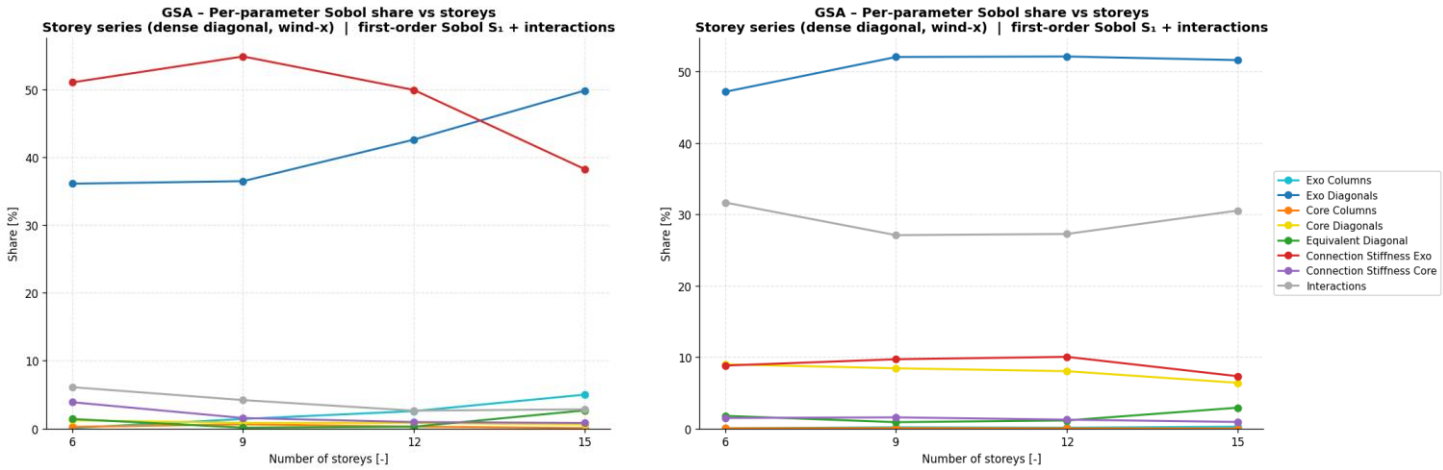

Figure 6.14: Parameter shares on the horizontal displacement for variants with varying number of stories. On the left diagram the results for variants with lower-bounds based on ULS-verification is displayed. On the right diagram constant lower-bound and parameter ranges are applied across the variants with varying number of stories.

From the results in Figure 6.14 the following observations can be made:

- For the ULS lower bound plot on the left Figure, the influence of the diagonals in the exoskeleton seems to increase when the number of stories of the building increases and the influence of the connection stiffness in the exoskeleton seems to decrease. However, with equal lower-bounds the influence of every parameter remains roughly constant when equal lower-bounds are used as was found in the results of the LSA. Therefore, it is concluded that the influence of the parameters remains constant when the number of stories is varied.
- Independent of the number of stories, the dimensions of the diagonals and the connection stiffness in the exoskeleton dominate the influence on the global horizontal deformation of the building.
- The influence of the connection stiffness in the exoskeleton is strongly dependent on the decision of the lower-bound. The influence of different lower bounds will be discussed further in the next paragraph.

Results of varying geometry

The global sensitivity analysis (GSA) was also performed on variants with a varying structural geometry to study how the chosen geometry affects the sensitivity of the parameters. To study this influence, two additional variants were considered and compared to the baseline model. In the first variant, the baseline model is used, but the wind is applied in y-direction. In this direction the braced core of the building is relatively slender, and the width of the exoskeleton is slightly larger. In the second variant, half of the diagonals in the exoskeleton have been removed to obtain a more open diagonal structure.

In Figure 6.15, the results of the GSA are displayed for both the ULS lower-bounds and the zero lower-bound. The result of the near-zero lower-bounds is included because for these variants the lower bounds for every variant in this model are equal, due to which a more consistent comparison between the variants can be made.

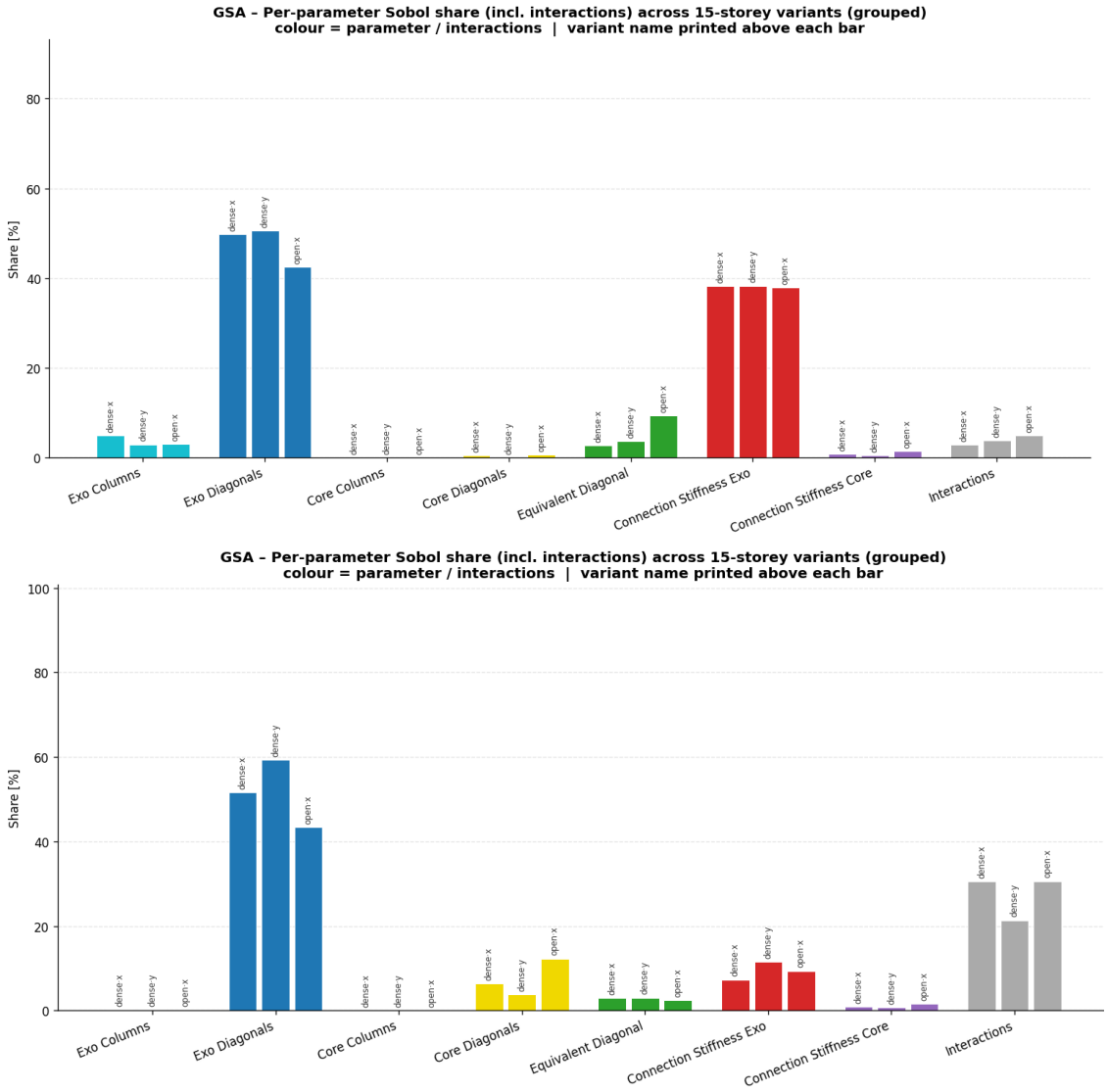

Figure 6.15: Influence of parameters on the horizontal displacement for varying structural geometries. The top diagram indicates the influence of parameters with ULS lower bounds is displayed. In the bottom diagram the influence of parameters with an equal zero-lower bound for every parameter is displayed.

From Figure 6.15 the following observations can be made:

- Independent of the structural geometry, the diagonals and connections in the exoskeleton have the strongest influence on the global horizontal behaviour of the building as was observed in the results of the LSA.
- In the variant with the open diagonal structure, the influence of the diagonals in the exoskeleton decreases, whereas the influence of the braced core and timber frame shear walls increases.
- Although the influence of the diagonals decreases for the variant with open diagonal structure, the dimension of the exoskeleton still has the highest influence on the global horizontal deformation of the building.
- In the variant where the wind load is applied in y-direction, the influence of the braced core reduces.
- The comparison between the variants with different geometries shows similar results as the comparison of these variants for the LSA.

Results of varying lower bounds

To study how the influence of the parameters on the global horizontal deflection of the building is dependent on the choice of the lower bounds. The global sensitivity analysis was performed for the baseline model with three different parameter ranges. In the first variant the lower bounds of the diagonals and the connection stiffness in the exoskeleton and braced core was determined according to ULS verifications, which corresponds to the approach which is used for the baseline model. In the second variant the lower-bounds of the diagonals and connection stiffness was set to a near-zero value to account for complete absence of these parameters. Lastly, an average lower-bound was considered where the lower-bound was determined to guarantee ductile failure of the connections when the diameter of the dowels is equal or larger than 8 mm. The corresponding lower-bound dimension of the diagonals in this variant is equal to 100 mm. The lower-bound values of the columns and the equivalent diagonal remain constant across these variants. In Figure 6.16, the first order indices of every parameter and the total interactions are displayed for every variant.

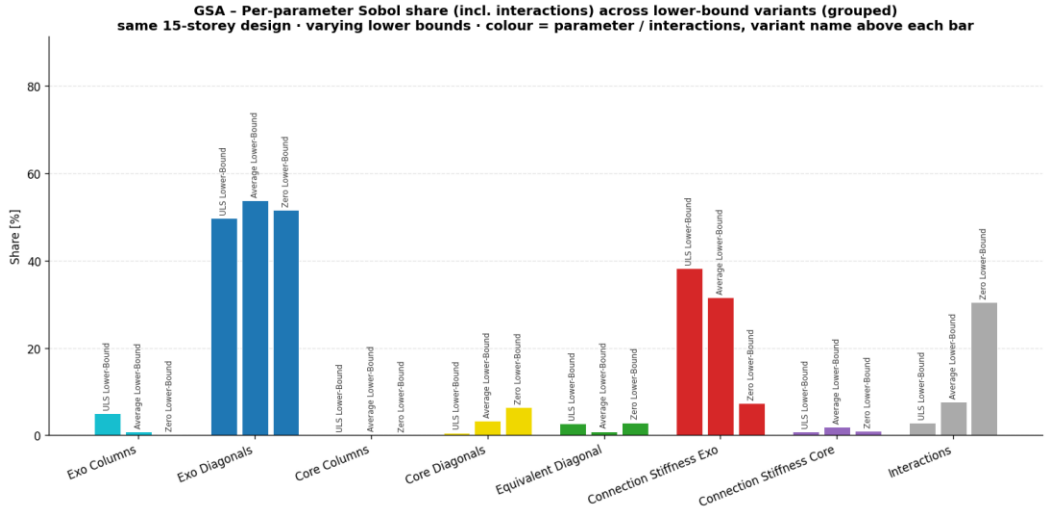

Figure 6.16: Influence of parameters on the horizontal displacement for varying lower bounds.

From the results in Figure 6.16, the following observations can be made:

- The influence of the connection stiffness in the exoskeleton is strongly dependent on the decision of the lower-bound value. The influence of the connection stiffness with the ULS lower-bound is equal to approximately 38%, whereas the influence with the near-zero lower-bound is equal to approximately 8%. This strong decrease in influence of the connections in the exoskeleton is not visible for the LSA.
- The interaction between the parameters strongly increases when the lower-bounds of the dimensions of the diagonals and connection stiffness decrease to a near-zero value.
- The influence of the diagonals in the exoskeleton remains dominant and stable across the three variants.
- The influence of the core diagonals increases when the near-zero lower-bound is used, but the influence of the core is still significantly lower than the influence of the diagonals in the exoskeleton.
- The influence of the columns of the columns in the exoskeleton decreases when the lower bounds of the diagonals and connection stiffnesses are reduced.

For the interpretation of the results of the Sobol-method for the base-line method and the additional variants is referred to Section 6.4.5.

6.4.5 Interpretation of the results of the global sensitivity analysis

In this paragraph, the main observations and conclusions from the results of the Global Sensitivity Analysis (GSA) using the Sobol-method are discussed, explained and interpreted. As many results of the local and global sensitivity analysis are similar, only the observations that are different from the Local Sensitivity Analysis (LSA) are discussed in the paragraph.

The influence of the diagonals and connection stiffness in the exoskeleton has increased compared to the local sensitivity analysis:

When the results of the GSA are compared to the results of the LSA it can be observed that the influence of the diagonals and connections has increased. It should be noted that for the LSA all parameters are changed one at a time compared to the reference model, where the reference model is equal to the lower-bound of every parameter. As in the GSA all parameters are changed at the same time over the same range, the average dimensions of the model in the GSA are higher compared to the reference model. From this can be concluded that the diagonals and connections in the exoskeleton have the most dominant influence on the horizontal deformation of the building. In addition, can be concluded that the influence of the remaining parameters is strongly dependent on the dimensions of the diagonals and the stiffness of the connections. Which shows that the different parameters interact with each other, and which confirms that the relation between the parameters and the deflection is non-linear. As the parameters interact with each other, the choice of the reference model influences the results of the local sensitivity analysis.

The interaction between the diagonals and the connection stiffness is relatively small, whereas the interaction between the exoskeleton, the timber frame shear walls and braced core are relatively higher.

From the bar diagrams and the heat map in Section 6.4.3, it can be concluded that the absolute percentage of interactions between the parameters is very small. This was not expected at prior. The reason why the global sensitivity analysis was performed in the first place was due to the suspicion that the choice for the reference model could influence the parameter sensitivity. For example, if the dimensions of the exoskeleton in the reference would be very high, changing the dimensions of the core should have limited effect and therefore there should be an interaction between the parameters.

However, the fact that the total absolute percentage of interactions is very small, does not directly mean that there is no interaction between the parameters at all. From the bar diagrams it can be found that although the absolute percentage of interactions of the core skeleton is small (0.3%), 33% of the total effect of the core skeleton is due to interactions with other parameters. For the equivalent diagonal approximately 63% of the total index is caused by the interaction with other parameters.

The interaction between the exoskeleton, the core skeleton and the equivalent diagonal is therefore ‘hidden’, but present since the Sobol indices of the connection stiffness and the exoskeleton are dominating the deflection of the building.

These results could be explained using an analogy with serial and parallel springs. In the axial connection stiffness of the connections is modelled using a spring at the end of the timber elements. The timber elements itself can also act as a spring as they can contract or expand. These two springs of the connection and timber element are connected in serial. Therefore, the derivation in equation 6.15.

$$
\begin{aligned}
u_{tot} &= u_{exo} + u_{conn} \\
u_{tot} &= \frac{F_{exo}}{k_{exo}} + \frac{F_{conn}}{k_{conn}} \\
F_{exo} &= F_{conn} = F \\
u_{tot} &= \frac{F}{k_{exo}} + \frac{F}{k_{conn}}
\end{aligned}
\tag{6.15}
$$

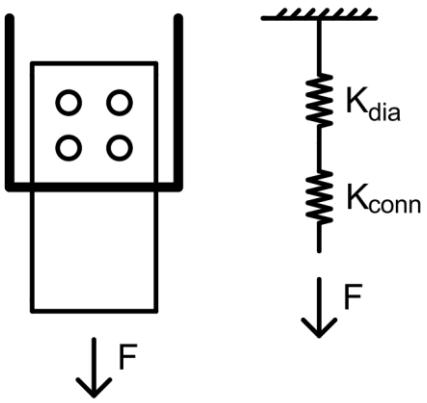

Figure 6.17: Schematisation for analogy of serial connected springs.

From the resulting formula it can be concluded that there is no interaction between the stiffness of the connections and the stiffness of the exoskeleton: a change of the connection stiffness would always lead to the same change in total deformation independent of the stiffness of the exoskeleton. Therefore, no interaction between the exoskeleton dimensions and the connection stiffness is expected which is corresponds with the results of the GSA.

The timber frame shear walls and the braced core show relatively the strongest interactions with exoskeleton. These interactions could be explained with the theory of springs in parallel. In Figure 6.18, this analogy is sketched. If it is assumed that the floors between the exoskeleton and the core skeleton are infinitely stiff in-plane, the horizontal deformation of the exoskeleton should be equal to the horizontal deformation of the core. Therefore, the system could be simplified using equation 6.16.

$$
\begin{aligned}
F_{tot} &= F_{exo} + F_{conn} \\
F_{tot} &= k_{exo} * u_{exo} + k_{core} * u_{core} \\
u_{exo} &= u_{core} = u_{tot} \\
F_{tot} &= (k_{exo} + k_{core}) * u_{tot} \\
u_{tot} &= \frac{F_{tot}}{k_{exo} + k_{core}}
\end{aligned}
\tag{5}
$$

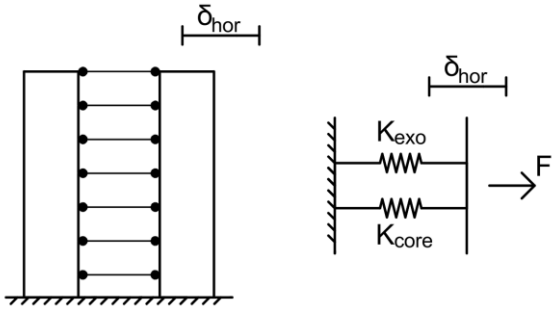

Figure 6.18: Schematisation for analogy of parallel connected springs.

From this formula it can be concluded that there is an interaction between the stiffness of the core and the stiffness of the exoskeleton: if the dimensions of the exoskeleton are very high, corresponding to a high stiffness of the exoskeleton, a change of the stiffness of the core will have limited effect on the horizontal deformation. Whereas if the same change of stiffness is applied to the core while the stiffness of the exoskeleton is very low, the horizontal deformation would have a large effect.

The influence of the connection stiffness in the diagonals strongly decreases when the lower bounds of the diagonals and the connections decrease:
In Section 6.4.5, it can be observed that the influence of the connection stiffness of the connections in the exoskeleton strongly decreases when the lower bounds of the diagonals and the connections decrease. This phenomenon is not visible in the results of the LSA. In addition. this is result is at first unexpected as, when the lower-bound of the connection decrease, the axial stiffness of the connection could be varied over a wider range, for which it would be expected that the influence on the displacement of the building would increase.

However, this observation can be explained due to the fact that not an absolute, but a relative connection stiffness parameter is used. Therefore, the upper-bound of the connection stiffness is dependent on the dimensions of the timber element in which the connection is located. The parameter configuration that cause the strongest variation in the output are on the located close to the lower-bound of the dimensions of the diagonals in the exoskeleton. However, when the in dimensions of the timber element are low, the maximum value which the connection stiffness can achieve is very low. Therefore, varying the relative connection stiffness has a small influence on the absolute connection stiffness and therefore a small influence on the output. In addition, when the dimensions of the diagonals in the exoskeleton are close to the lower-bound, the axial stiffness of the connections will be low by definition. Due to this the influence of the diagonals is overestimated in the sensitivity analysis.

6.4.6 Conclusion global sensitivity analysis

In summary, the following conclusions can be made from the global sensitivity analysis.

- The main conclusions of the local sensitivity analysis apply for the results of the local sensitivity analysis
- The surrogate model using Gaussian Process Regression can accurately simulate the results of the finite element model.
- In the results of the GSA the influence on the deflection of the diagonals and connections in the exoskeleton increases compared to the results of the LSA, which confirms that there is interaction between different parameters and that in the LSA the influence of every parameter is dependent on the choice of the reference model.
- The relative interactions between the diagonals and the connection stiffness is low, whereas the interactions between the parallel stability systems - the exoskeleton, timber frame shear walls and the core – is relatively high.
- Not only does the choice of the lower bounds, but also the definition of the parameters strongly influences the results of the parameters.

6.5 Costs-effectiveness analysis

The local sensitivity analysis using the OAT method and the global sensitivity analysis have provided insight into the influence of the different parameters on the horizontal displacement of the building. However, in these analyses, the cost of adjusting each parameter was not taken into account. A parameter with a large influence on the displacement is therefore not necessarily an efficient parameter to increase, as changing the parameter comes at a high cost. To account for the costs of changing every parameter, this section presents an approach to estimate the cost of adjusting each parameter and to relate this cost to its influence on the displacement.

The section is structured as follows. First, Section 6.5.1 explains the calculation of the material costs and the shadow costs. Subsequently, Section 6.5.2 compares the influence of each parameter on the horizontal displacement of the building with its share in the total cost. Finally, in Section 6.5.3, the costs are computed per variant from the surrogate model, to investigate what the most cost-efficient design looks like. This is done for both the material costs and the environmental costs.

6.5.1 Material and shadow costs calculation framework

In this section a summary of the material and shadow costs calculation is given. For the calculations of the economic and shadow costs of every variant only the costs of the load bearing structure is considered. The load bearing structure consists of the glulam beams, columns and diagonals, the Kerto-Ripa floors, the timber frame shear walls and the slotted-in steel-to-timber connections. In addition, for the calculation only the material costs are considered. The costs for labour and transport are not considered as these costs are difficult to estimate as these costs vary strongly for each construction project. The calculation of the costs should not be interpreted as a detailed value, but more as an indicative value to compare different configurations.

In Table 6.9, the reference values which are used to estimate the material and shadow costs for every configuration are displayed. The reference values for the material costs are obtained from recent quotations provided by Koopmanschap Bouwkosten Advies, from reference studies, and from the websites of product suppliers. The shadow costs are calculated using reference values from the Milieudatabase. The shadow costs represent the costs required to compensate for the environmental impact of the materials.

Element Type	Material Costs	Shadow Costs	Unit
Glulam Gl24h (1D elements)	1300	95	€/m^3
Kerto-Ripa (Floors)	55000	1300	€/storey
Timber frame shear walls (Equivalent diagonal)	39	8	€/mm
Slotted-in steel connections (Steel plates and stainless-steel dowels)	88	11	€/MN/m

Table 6.9: Reference values for calculating material and shadow costs.

The material costs of the diagonals and columns in both the exoskeleton and the braced core are therefore calculated as a function of the material volume. The costs of the Kerto-Ripa floors are expressed as a function of the number of stories, since each storey has a constant floor area of

approximately 480 m^2. The costs of the timber frame shear walls are expressed in terms of the dimensions of the equivalent diagonal, and the costs of the connections are expressed as a function of the connection stiffness.

6.5.2 Costs versus influence comparison

To account for the cost of adjusting each parameter, the share of the total costs for adjusting each parameter is calculated for each variant using the reference values as described in Table 6.9. The cost shares are not based on the total cost of the parameter within the variant, but only on the additional cost required to increase that parameter. In this way, the analysis reflects the cost of improving the stiffness of the building through each parameter, which gives a better indication if increasing the parameter is cost-efficient.

This additional cost of varying the parameters is determined for the 50% configurations with the cheapest additional costs that satisfy the SLS requirement. This selection was made such that the costs are evaluated on the most relevant optimal variants, without only considering the cost hare of the most optimal variant which could be a local optimum.

In Figure 6.19 for every parameter influence on the displacement and the share in the costs is displayed for every variant for both the results of the GSA (left) and the LSA (right). The grey dashed line separates two regions: above the line, a parameter contributes more to the cost than to the displacement, while below the line the parameter contributes more to the displacement than to the cost.

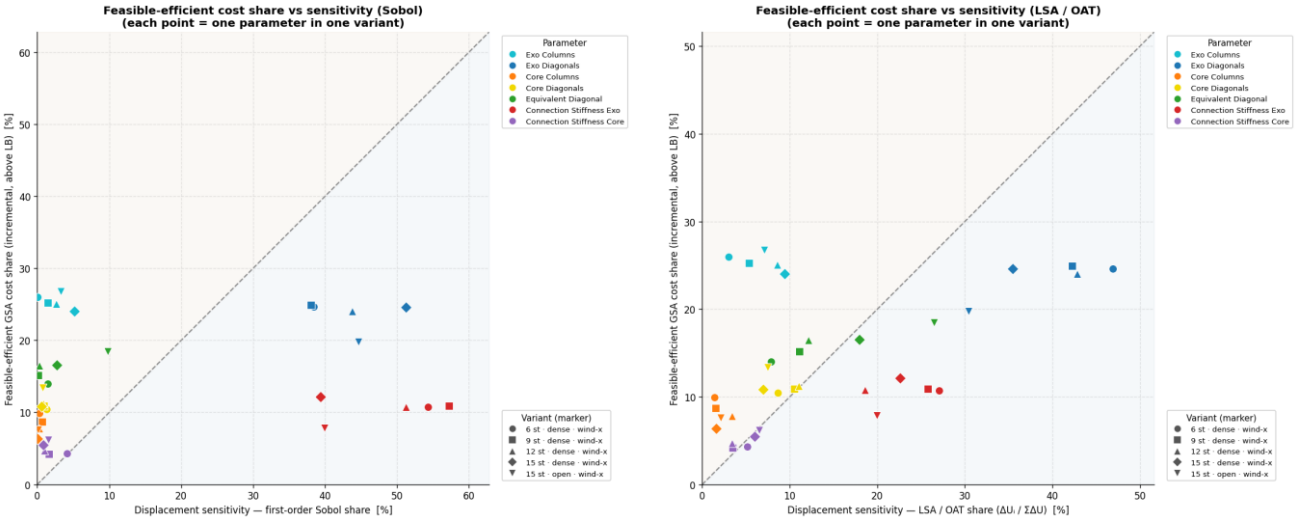

Figure 6.19: Material cost-effectiveness diagrams for the results of the GSA (left) and the LSA (right). On the x-axis the percentual influence on the deformation is displayed, on the y-axis the percentual influence on the costs is displayed. Parameters in the bottom-right are therefore cost-effective, whereas parameters in the top-left are not cost-effective.

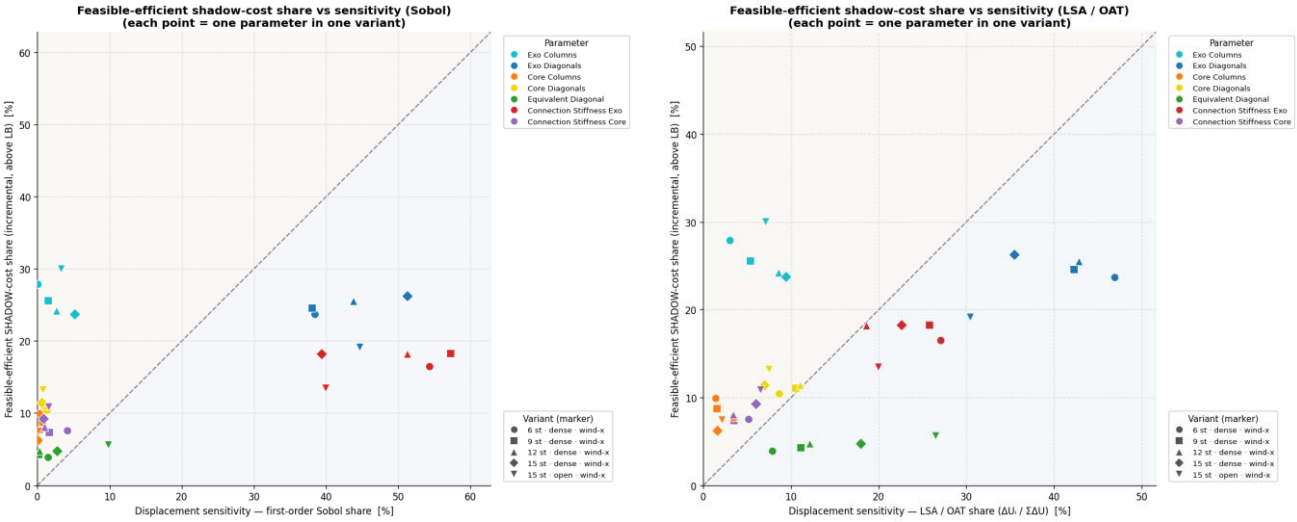

Figure 6.20: Shadow cost-effectiveness diagrams for the results of the GSA (left) and the LSA (right). On the x-axis the percentual influence on the deformation is displayed, on the y-axis the percentual influence on the costs is displayed. Parameters in the bottom-right are therefore cost-effective, whereas parameters in the top-left are not cost-effective.

From Figure 6.19 and Figure 6.20 the following observations can be made:

- Increasing the dimensions of the diagonals is both for the material costs and shadow costs an effective measure to increase the stiffness of the building. For all variants the datapoints representing the exoskeleton diagonals lie below the grey line.
- Increasing the stiffness of the connections is both for the material costs and shadow costs an effective measure to increase the stiffness of the building. Similar to the diagonals in the exoskeleton the datapoints for the connection stiffness of the diagonals lie below the grey line.
- The connection stiffness has a larger share in the shadow costs than in the material costs. On average the share in the shadow costs is twice the share in the material costs for the connection in the exoskeleton.
- Increasing the dimensions of the columns in the exoskeleton is not cost-efficient.
- The diagonals, columns and connection in the braced core have a low influence on both the horizontal displacement as the material and shadow costs.
- The diagonals, columns and connection in the braced core are not cost efficient
- The timber frame shear walls are relatively more expensive in material costs than in shadow costs.

6.5.3 Costs optimalisation of the base-line model

In this paragraph, the cost-effectiveness of the parameters is determined by using the configurations of the surrogate model are used to determine the most optimal combination of parameters for both the material costs and the shadow costs.

Since the lower bounds for the baseline variants were determined such the ULS requirements are fulfilled for every parameter combination, the lower bounds are conservative. As can be seen displacement plots of the OAT analysis show that every configuration fulfils the SLS requirement. Consequently, the optimal model would simply correspond to the model in which every parameter is set to its lower bound. For this reason, it was decided to let the lower bounds of the diagonals and the connection stiffnesses vary down to zero for the optimization. The most optimal model was subsequently verified manually against the ULS requirement.'

To determine what the optimal configuration looks like, the 20 cheapest configurations are considered. Since parameters that have little influence on both the displacement and the cost show a large spread among these top 20 variants, the optimal variant is taken as the average of the top 20 variants. In addition, the average value of each parameter, the spread of the parameters across these cheapest variants is also determined as indication of the influence on the displacement and the costs of the parameter.

If the standard deviation of the parameter is low, the parameter either or both a large influence on the costs of the building or a large influence on the displacement of the building. If the standard deviation of the parameter is high, the parameter has a small influence on both the costs as the displacement of the building. In Table 6.10 the results of the optimal configurations with the lowest material costs for the different variants are displayed. In Table 6.11 the results of the optimal configurations with the lowest shadow costs is displayed.

	Exo Columns [mm]	Exo Diagonals [mm]	Core Columns [mm]	Core Diagonals [mm]	Equivalent Diagonal [mm]	Connection Stiffness Exo [MN/m]	Connection Stiffness Core [MN/m]
Applied range:	210 – 600	1 – 600	250 – 600	1 – 600	1 – 225	1.0 – 1178	1.0 – 1178
6 st · dense · wind-x	222 ± 9	63 ± 18	277 ± 17	103 ± 57	14 ± 10	19.6 ± 15.1	48.1 ± 56.5
9 st · dense · wind-x	261 ± 9	93 ± 23	322 ± 17	119 ± 61	15 ± 9	42.2 ± 17.5	57.0 ± 40.5
12 st · dense · wind-x	304 ± 12	123 ± 21	382 ± 20	163 ± 75	13 ± 12	74.8 ± 28.8	136.5 ± 104.0
15 st · dense · wind-x	332 ± 11	179 ± 19	422 ± 16	139 ± 63	12 ± 11	156.3 ± 27.3	104.6 ± 90.0
15 st · open · wind-x	331 ± 7	254 ± 24	420 ± 14	134 ± 50	12 ± 10	295.3 ± 45.8	81.3 ± 62.6

Table 6.10: Resulting parameter values after optimizing material costs for every considered variant. The first value indicates the average value of the 20 parameter configurations with the lowest material costs that fullfill the SLS requirement. The second number in the table indicates the standard deviation of these 20 most optimal configurations.

	Exo Columns [mm]	Exo Diagonals [mm]	Core Columns [mm]	Core Diagonals [mm]	Equivalent Diagonal [mm]	Connection Stiffness Exo [MN/m]	Connection Stiffness Core [MN/m]
Applied range:	210 – 600	1 – 600	250 – 600	1 – 600	1 – 225	1.0 – 1178	1.0 – 1178
6 st · dense · wind-x	219 ± 8	42 ± 18	273 ± 20	82 ± 46	53 ± 35	9 ± 8	32 ± 38
9 st · dense · wind-x	256 ± 4	78 ± 20	319 ± 12	110 ± 27	69 ± 46	27 ± 13	55 ± 35
12 st · dense · wind-x	299 ± 6	99 ± 23	372 ± 13	158 ± 45	125 ± 67	46 ± 24	109 ± 58
15 st · dense · wind-x	327 ± 6	149 ± 22	420 ± 14	162 ± 53	118 ± 64	112 ± 31	106 ± 59
15 st · open · wind-x	329 ± 5	189 ± 36	420 ± 13	175 ± 40	156 ± 66	169 ± 55	137 ± 63

Table 6.11: Resulting parameter values after optimizing shadow costs for every considered variant. The first value indicates the average value of the 20 parameter configurations with the lowest shadow costs that fullfill the SLS requirement. The second number in the table indicates the standard deviation of these 20 most optimal configurations.

From Table 6.10 and Table 6.11 the following observations can be made:

- The results confirm the findings of Section 6.5.2, where parameter which have limited influence on both the costs and displacement show a large variation in values for the optimal variants.
- In the variants for optimizing the shadow costs, the connection stiffness in the exoskeleton and braced core is in general lower than for the optimization of the material costs. This can be explained by the fact that ratio between the costs of the connection stiffness with costs of glulam is relatively higher for the shadow costs than for the material costs.
- In the variants for optimizing the shadow costs, the stiffness of the timber frame shear walls is higher than for the optimization of the material costs although a large variation is visible. This aligns with the plots in Section 6.5.2.
- The dimensions of the columns in the exoskeleton and braced core approach the lower-bound and show little variation. This confirms the results of Section 6.5.2, where the influence on the costs of the columns is relatively high, whereas the influence on the displacement of the columns is low.
- Although the dimensions of the diagonals in the braced core show a high variation, the optimal variants the dimensions of the diagonals in the braced core is very similar to the dimensions of the diagonals in the exoskeleton. For the variants with 6, 9 and 12 stories the average dimensions of the diagonals in the braced core are in general higher than the dimensions of the diagonals in the exoskeleton.

The observation that the dimensions of the diagonals in the braced core are similar to the dimensions of the diagonals in the exoskeleton, while the results of the LSA and GSA show that the diagonals in the core have a relatively small influence on the horizontal deformation of the building could be explained as follows. The main purpose of the diagonals in the braced core is to prevent shear deformation between the stories of the building. The shear stiffness of the diagonal can be derived using equation 6.17. The parameters for the derivation are illustrated in Figure 6.21.

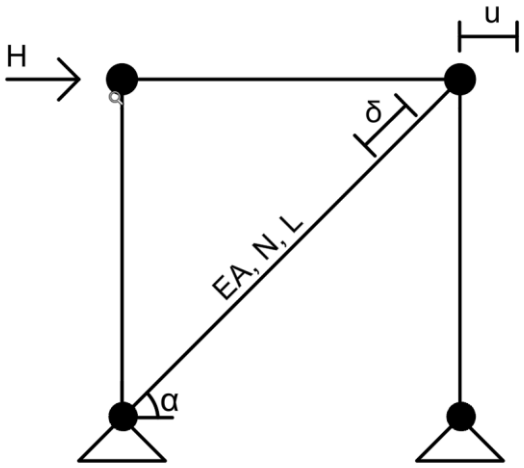

Figure 6.21: Schematisation for the derivation of the formula for the shear stiffness influence of the diagonals.

$$\begin{aligned} \delta &= u * \cos(\alpha) \\ N &= \frac{EA}{L} * \delta \\ N &= \frac{EA}{L} * \ u * \cos(\alpha) \\ H &= N * \cos(\alpha) \\ H &= \frac{EA}{L} * \ u * \cos^2(\alpha) \\ k_{dia,shear} &= \frac{H}{u} = \frac{EA}{L} * \cos^2(\alpha) \end{aligned} \tag{6.17}$$

Where:

δ	[mm]	=	The axial deformation of the diagonal
u	[mm]	=	The horizontal deformation of the frame
EA	[Nmm^2]	=	The axial stiffness of the diagonal
N	[N]	=	The normal force in the diagonal
L	[mm]	=	The length of the diagonal
H	[N]	=	The horizontal force acting on the frame
α	[rad]	=	The angle of the diagonal

Therefore, the contribution to the shear stiffness of the diagonals is independent of the width of the building. When it is assumed that axial stiffness of the floors is infinite and full diaphragm action can occur and as both the diagonals in the exoskeleton and braced core are made of the same materials. It can be concluded that placing the diagonals in the core has the same cost-efficiency as placing the diagonals in the exoskeleton to increase the shear stiffness of the building. However, it should be noted that the diagonals not only influence the shear stiffness of the building but also contribute to the bending stiffness of the building.

6.5.4 Conclusion cost-effectiveness analysis

In summary, the following conclusions can be made from the cost-effectiveness analysis.

- Increasing the dimensions of the diagonals and the stiffness of the connections in the exoskeleton are for both the material and the shadow costs an effective measure to reduce the deflection of the building.
- Increasing the dimensions of the columns in the exoskeleton and braced core are for both the material and the shadow costs not an effective measure to reduce the deflection of the building.
- Increasing the shear stiffness of the timber frame walls is for the shadow costs an effective measure to reduce the deflection of the building but for the material costs.
- The axial connection stiffness of the connection stiffness has a stronger influence on the shadow costs than on the material costs.
- Although the dimensions of the diagonals of the core have limited influence on the deflection of the building, the cost-effectiveness of the diagonals in the core seems similar to the cost-effectiveness of the exoskeleton.

7 Discussion

In this chapter, the limitations and constraints of the study are discussed critically. The detailed interpretation of the results of the local sensitivity analysis, the global sensitivity analysis and the cost-effectiveness analysis is provided in Sections 6.3.5, 6.4.5 and 6.5.4, respectively. This chapter mainly reflects on the assumptions, limitations and modelling choices that are made which could influence the results and their conclusions.

The results of the local and global sensitivity analysis are dependent on the choice of the definition of the parameters:
A limitation of this study is that the outcome of the sensitivity analyses is strongly dependent on how the parameters are defined. In particular, the connection stiffness was implemented as a relative parameter instead of an absolute parameter. Because the maximum axial stiffness that a slotted-in connection can achieve is governed by the cross-sectional dimensions of the timber element in which it is located the decision of the relative parameter causes that the absolute connection stiffness increases when the relative connection stiffness is constant and the diagonal cross-section increases. Therefore, the influence of the connections is potentially underestimated while the influence of the diagonals is correspondingly overestimated. However, it should be noted that this does not reflect a modelling error but a compromise, since a suitable parameter range had to be selected. Defining the connection stiffness in absolute terms would either restrict the parameter to an unrealistically narrow parameter range or to the inclusion of unrealistic configurations. The relative definition was therefore adopted as the most reasonable trade-off, while acknowledging that it has influence on the relative influence of the diagonals and the connections.

The results of the local and global sensitivity analysis are dependent on the chosen parameter range:
In addition to the choice of the definition of the parameters, the results of the of the sensitivity analyses are strongly dependent to the choice of the parameter ranges and in particular to the lower bounds. In this study the lower bounds of the baseline variant were derived from conservative ULS verifications, makes sure that every parameter configuration is feasible. However, many feasible parameter combinations have been excluded due to this lower-bound. The strong influence of the lower bound could be explained by the non-linear, semi-asymptotic relationship between the parameters and the horizontal deflection: near the lower bound the deflection changes rapidly with the parameter, whereas near the upper bound the response has largely flattened. In the interpretation of the result for varying variants, it should be accounted for that the lower bounds vary between different variants.

Choice of the baseline variant:
In this study, the variant with the dense-diagonal configuration was used as baseline. The analyses indicate, however, that the variant with the more open diagonal structure is also able to satisfy the horizontal-displacement requirement, while using less material in the exoskeleton. This suggests that the open-diagonal variant could in fact be a more optimal design than the baseline variant and that the baseline choice was too conservative. However, it should be noted that the exoskeleton remains the governing stability system in both configurations.

The results of the analyses were determined for a small number of varying structural geometries:
The study was restricted to a single structural geometry, with the exception of the number of storeys and the density of the diagonals in the exoskeleton. The sensitivity of the stability systems is, however, dependent on the chosen geometry. It is consequently possible that the results could change for buildings with a significant different aspect ratio or diagonal layout.

Limitations of the local sensitivity analysis (LSA):
There are several limitations of the local sensitivity analysis which is performed in Section 6.3. First, the method is mainly meant for parameters whose relationship with the output is linear. In this study the relationship between the parameters and the output was found to be the non-linear. Therefore, the results are dependent on the choice of the reference model around which the parameters are varied. In addition, interactions between the parameters cannot be measured in the local sensitivity analysis. However, it should be noted that as the used reference model is equal to the lower-bound value of every parameter with exception of the timber frame walls. And this lower-bound reference model satisfy the horizontal displacement requirement, the configurations in the LSA are on average closer to the optimal design of the building compared to the GSA.

Limitations of the global sensitivity analysis (GSA):
The variance-based Sobol method was introduced specifically to remove the dependence on a reference model, since it varies all parameters simultaneously across their entire ranges. However, it is important to note that this does not eliminate the dependence on the parameter ranges themselves. The global analysis therefore gives therefore a more equal comparison over the entire range of the parameters but is still dependent on the choice of the lower bounds that also affects the local analysis.

Limitations of the material and shadow costs estimation:
The cost-effectiveness analysis should be interpreted with care, as the cost calculation is a rough approximation. Only the material and shadow costs of the load-bearing structure were considered, whereas labour and transport costs were excluded because they vary strongly between construction projects and are difficult to estimate. Since connections in particular are labour-intensive to fabricate and install, the inclusion of these costs could possibly change the relative cost-efficiency of the parameters. The cost results should therefore be interpreted as indicative values for comparing configurations rather than as an accurate approximation of the total costs.

8 Conclusions and recommendations

8.1 Conclusions

In this section, the main findings of the study are summarized. First, the main objective of the research is addressed. Subsequently, the sub-questions are answered one by one. Finally, the additional conclusions that followed from the research are discussed.

Main objective:
The objective of this report is to investigate, through a parametric study, the extent to which the various stability systems of a timber building concept, comprising an exoskeleton, a braced core and timber frame shear walls influence the horizontal deflection of the building and how these systems can be optimized.

The parametric study shows that the three stability systems have a varying contribution to the lateral stiffness of the building. The exoskeleton is governing for the horizontal displacement. In the local sensitivity analysis, the exoskeleton accounts 67% of the total observed deflection, whereas the timber frame shear walls and braced core respectively contribute for 18% and 15% of the total observed deflection According to the global sensitivity analysis, the exoskeleton diagonals, the exoskeleton connection stiffness and the exoskeleton columns, including their interactions, together account for approximately 93% of the variance in the horizontal displacement, whereas the braced core and the timber frame shear walls together account for only about 4%. Within the exoskeleton, the cross-sectional dimensions of the diagonals and the axial stiffness of the slotted-in connections are dominant with approximately 50% and 36% of the variance in the global analysis, respectively, while the columns have a comparatively minor effect.

The building concept is optimised most effectively by prioritising the diagonal dimensions and the connection stiffness of the exoskeleton, as these are the only measures that improve the lateral stiffness cost-efficiently for both material and environmental shadow costs. However, in the optimal design configurations the dimensions of the diagonals in the core were similar to the dimensions of the diagonals in the exoskeleton.

Sub-questions:
What is the current state of technology of timber buildings?
From The literature review it can be concluded that the achievable height of a timber building is governed by its lateral stability system. Buildings that rely on light-weight timber frame shear walls for their lateral stability are limited to approximately six storeys. Greater heights can be achieved by introducing a concrete core or cross-laminated timber (CLT) cores, reaching heights of roughly 73 m. The tallest timber building uses a large-scale glulam truss system, reaching a height of 85.4 m. The conclusions from the state of the art motivate the investigated core–exoskeleton concept, which aims to reach mid-rise height without a concrete or CLT core, provided the timber frame walls are not overloaded in the vertical and horizontal directions.

How can a parametric workflow be developed to study the horizontal deflection of the timber building concept?

For this study a parametric workflow was developed that couples SCIA Engineer to a Python script through the SCIA OpenAPI and XML editing. The workflow consists of three stages. In the set-up stage, the reference model is built in SCIA Engineer, exported as an XML file and read into Python, where the parameter ranges are defined. In the computation stage, Python generates a new XML file for each parameter configuration, updates the model through the OpenAPI, performs a linear finite-element analysis and stores the resulting horizontal deformation. In the post-processing stage, the results are used to train a surrogate model, to compute the Sobol indices and to visualise the sensitivity results. Because a full finite-element evaluation of every configuration is computationally expensive, a Gaussian Process (Kriging) surrogate model was used. As shown in the global sensitivity analysis, the surrogate model is able to reproduce the finite-element results accurately, which validates the workflow to study the influence of the parameters on the horizontal deflection. This parametric approach is recommended as the XML-files can be easily interpreted and edited using coding tools supported by Artificial Intelligence.

Which stabilizing system contributes most to the lateral stiffness of the building?

The exoskeleton contributes most to the lateral stiffness, this conclusion was found for both the local and the global sensitivity analyses. Its dominance has two main causes: the exoskeleton contains considerably more material than the braced core, and the columns have a larger lever arm, resulting in a higher bending stiffness. The diagonals and connections in the exoskeleton have a stronger influence on the deflection than the columns. This behavior can be explained by the fact that the building has a relatively low slenderness ratio. Consequently, the horizontal displacement of the building is expected to be governed by shear deformation rather than bending deformation. In addition, the diagonals enable the truss action between the columns The beams of the exoskeleton and braced were found to have a near zero influence on the deflection of the building and were therefore not considered as parameter. The influence of the timber frame shear wall is generally higher than the influence of the core but is strongly dependent on the parameter values of the other stability systems. In additional exploratory studies it was found that foundation stiffness only has a small influence on the horizontal deformation of the building. The stiffness of every individual stability system was also determined. In contrast to the fifteen-storey variant, both the braced core alone and the timber frame shear walls alone were able to satisfy the SLS horizontal-displacement limit for the variant with 6 stories.

How does the influence of the stability systems change when varying the number of storeys or the structural geometry?

When equal lower bounds are applied across the variants, the relative influence of each parameter remains almost constant for the variant of 6, 9, 12 and 15 storeys in both sensitivity analyses, with the exoskeleton diagonals and connections remaining dominant for every variant. Varying the structural geometry changes the individual contributions but not the overall ranking. Applying the wind load in the y-direction reduces the influence of the braced core, which is more slender in y-direction. The variant with a more open diagonal structure the influence of the exoskeleton diagonals reduces and the influence of the braced core and the timber frame shear walls increases. However, in every geometry considered for this study, the exoskeleton remains the dominant system.

How can the stability systems be optimized to minimize material costs and environmental impact?
The cost-effectiveness analysis, which relates the influence of each parameter on the displacement to its share in the material and shadow costs, shows that increasing the cross-sectional dimensions of the exoskeleton diagonals and the axial stiffness of the exoskeleton connections is an effective measure to reduce the deflection for both material and shadow costs. Increasing the dimensions of the columns in either the exoskeleton or the braced core is not cost-efficient; in the optimal configurations the columns consistently approach their lower bound. The axial connection stiffness has a larger effect on the shadow costs than on the material costs. Therefore, the optimal configurations for the shadow-cost have a lower connection stiffness than the optimal variants for the material costs. The timber frame shear walls are relatively more expensive in material costs than in shadow costs. A notable observation is that, although the diagonals of the braced core have limited influence on the horizontal deformation, their cost-efficiency in providing shear stiffness is comparable to that of the exoskeleton diagonals, because the shear contribution of a diagonal is independent of the width of the building.

Additional conclusions:
In addition to the answers to the research questions, the following observations followed from the study:

- The relationship between the parameters and the horizontal deflection is non-linear and shows asymptotic behaviour: increasing the parameter first reduces the deflection rapidly after which the deflection curve flattens. Therefore, the choice of the lower bound of a parameter range strongly affects influence of the parameter, whereas the choice of the upper bound has a relative low effect.
- The results depend strongly on the definition of the parameter ranges and on the definition of the parameters themselves. In particular, the use of a relative connection-stiffness parameter, whose absolute value depends on the dimensions of the timber element in which the connection is located, causes the influence of the connections to be relatively underestimated and that of the diagonals to be relatively overestimated.
- The local sensitivity analysis is affected by the choice of the reference model. The global sensitivity analysis removes this dependency, but its results still depend on the ranges over which the parameters are varied.
- The interactions between the diagonals and the connection stiffness are small, which is explained with the analogy of springs acting in series, whereas the interactions between the parallel stability systems, the exoskeleton, the braced core and the timber frame shear walls, are relatively larger, consistent with the analogy of springs in parallel.
- The Gaussian Process (Kriging) surrogate model reproduces the finite-element results accurately and captures the asymptotic behaviour better than a Polynomial Chaos Expansion, making it a suitable basis for the variance-based sensitivity analysis and the cost optimisation.

8.2 Recommendations

In this section the main conclusions and findings of this report are translated into practical design recommendations and recommendations for future research.

8.2.1 Practical design recommendations

Use the exoskeleton as the primary lateral stability system:
It is advisable to use the exoskeleton as the primary stability system to improve lateral stiffness. From the results, it was found that the exoskeleton has the strongest influence on the stiffness of the building. Variants without the exoskeleton, relying only on the timber braced core and timber frame shear walls, are not able to provide sufficient stiffness for the baseline model of 15 stories.

From the global sensitivity analysis and the local sensitivity analyses with comparable lower-bound values, it was found that the braced core and timber frame shear walls only have a marginal effect on the displacement of the building. Therefore, it is advised not to implement these systems when the exoskeleton system is applied. Although the braced core has a marginal effect, the cost-effectiveness of the braced core was found to be similar to that of the exoskeleton. This is because the shear deformation of the building dominates the overall displacement, as the slenderness ratio of the building is relatively low.

Focus on the diagonals and axial connection stiffness to improve the lateral stability system:
It is advised to focus on the diagonals and axial connection stiffness to improve the lateral stability system. From every sensitivity analysis, it was found that the diagonals and axial connection stiffness have a much larger effect on the horizontal deformation of the building than the columns and beams. In addition, the cost-effectiveness analysis showed that increasing the dimensions of the columns is a cost-intensive measure. The optimization of the parameters confirmed these results. In the optimal models, the dimensions of the columns in the exoskeleton and core are minimized to their lower-bound.

Use the results of the local sensitivity analyses to analyze the influence of a parameter on a fixed base design, and use the results of the global sensitivity analysis for a comprehensive overview of parameter sensitivity:
The results of the local sensitivity analysis (LSA) and the global sensitivity analysis (GSA) show some differences. The influence of the diagonals and axial connection stiffnesses increases [in the GSA]. This demonstrates that the parameters interact with each other and that their influence depends on the baseline model. Because the GSA evaluates the entire parameter range, sensitivity is also measured across areas that may be less relevant. In contrast, the LSA utilizes a realistic baseline variant from which individual parameters are varied. Therefore, it is recommended to use the LSA when determining the influence of a single parameter around an existing, semi-fixed design, while the GSA is recommended for determining the actual influence of parameters across their full parameter ranges.

Combine SCIA Engineer with Python using SCIA OpenAPI modules and XML-formatting for parametric modelling:
In this study, a parametric workflow was used which combines the powerful finite element software SCIA Engineer with the extensive possibilities of Python. By exporting the SCIA model to an XML file, the model parameters can easily be adjusted using a Python script. Combining SCIA Engineer with Python opens up many opportunities. Not only can model parameters be adjusted, but the SCIA model can also be run in the background.

The use of Python is recommended over other parametric approaches using Rhino and Grasshopper, as Python offers more freedom and is not dependent on pre-coded modules. In addition, in recent years we have seen a strong increase in the capabilities of artificial intelligence, which has become very powerful and fast in coding with Python. These AI capabilities can be utilized to create complex parametric models using the powerful finite element software of SCIA Engineer.

The use of a surrogate model is advised when performing sensitivity analysis or investigating a single result:
In this research, a surrogate model was used to increase the number of configurations on which the global sensitivity and optimization were performed. The surrogate model was able to accurately mimic the outcomes of the FEM analyses. Therefore, significant computational time was saved and many iterations could be run, which opened up new opportunities. Therefore, the use of a surrogate model is advised when one single output parameter is researched for a combination of input parameters.

8.2.2 Recommendations for future research

Implement geometric parameters into the parametric model:
For this study, it was chosen to keep the geometry of the building constant and only implement cross-section and stiffness parameters. This decision was made because a standard geometry was provided as part of the WoodCore project, and at the beginning of the study, it was assumed to be too difficult to implement geometric parameters inside the Python script. In hindsight, it should be doable to implement geometric parameters inside the Python script. In addition, this could be an interesting expansion of this study, as the variants with different geometries, with the exception of the number of stories, show that the results are dependent on the geometry. Geometric parameters that are interesting to investigate are the density and locations of diagonals in the exoskeleton, and the spacing between columns, and therefore the angles of the diagonals, in the exoskeleton.

Implement ULS verification inside the parametric script:
For this parametric model, it was decided to ensure that every configuration fulfills the ULS verification by adjusting the boundary conditions. However, due to this decision, not every parameter combination that fulfills the ULS verification is included in the model. The lower-bound is determined by setting all other parameters to their lower-bound and adjusting the critical parameter to a value such that it fulfills the ULS requirement. By implementing the ULS verification inside the parametric script, all possible parameter combinations can be computed. The configurations that do not fulfill the verification can simply be removed from the dataset.

Investigate the maximum achievable height using the building concept:
In this study, a maximum height of 15 stories was considered. This decision was made as this is the maximum goal as part of the WoodCore project. However, it would be interesting to see the maximum height which can be reached using this full-timber building concept, and to see if the parameter influences change if the slenderness ratio of the building varies more.

Investigate fire safety of the building:
In this study, fire safety was not considered in the design calculations of the building. However, building a full-timber building does not only present structural challenges, but also challenges related to fire safety. For timber structures, fire safety can be critical when designing timber cross-sections.

Bibliography

Abrahamsen, & Malo. (2014). *STRUCTURAL DESIGN AND ASSEMBLY OF “TREET” - A 14 STOREY TIMBER RESIDENTIAL BUILDING IN NORWAY.* Quebec City, Canada: World Conference on Timber Engineering.

Abrahamsen, R. (2017). *Mjøstårnet - Construction of an 81 m.* Moelv, NorwayMoelv, Norway: Moelven Limtre AS.

Blaß, H., & Sandhaas, C. (2017). *Timber Engineering - Principles of Design.* Karlsruhe: KIT Scientific Publishing.

BOB. (2015). *Treet, Bergen.* Retrieved from Skyscraper Center: https://www.skyscrapercenter.com/building/treet/16540

Buehler. (2019). *First of its Kind – 1430 Q Street Mixed-Use.* Retrieved from buehlerengineering.com: https://buehlerengineering.com/news/first-of-its-kind-1430-q-street-mixed-use

CBS. (2024, 12 11). *2. Hoe hangen materiaalstromen samen binnen de Nederlandse economie?* Retrieved 11 17, 2025, from https://www.cbs.nl/nl-nl/longread/rapportages/2024/groeiend-naar-een-groene-economie-/2-hoe-hangen-materiaalstromen-samen-binnen-de-nederlandse-economie-?utm_source=chatgpt.com

CBS. (2024, juni 11). *Woningmarkt*. (CBS) Retrieved november 14, 2025, from https://www.cbs.nl/nl-nl/visualisaties/dashboard-economie/woningmarkt#:~:text=In%20oktober%202022%20waren%20bestaande,bedraagt%20428%2C1%20duizend%20euro.

CLT Rezult. (2024). *Sara Kulturhus Center, Sweden*. Retrieved from clt-rezult.com: https://clt-rezult.com/en/portfolio-item/shvetsiia-sara-kulturhus-center-white-arkitekter/

Copper8, et al. (2024). *Bouwen binnen planetaire grenzen: CO2-impact van de Nederlandse bouw.*

Crocetti, R. (2016). *Timber Structures for Large-Span Structures.* Retrieved from ResearchGate: https://www.researchgate.net/publication/309293735_Timber_Structures_for_Large-Span_Structures

CWC. (n.d., 12 12). *Mid-Rise Buildings*. (Canadian Wood Council) Retrieved 11 20, 2025, from https://cwc.ca/articles/mid-rise-buildings-2/

De Graaf, P., & Banga, J. (2000). *Handboek Houtskeletbouw.* Rotterdam: stichting bouwresearch, centrum hout.

Diwekar, U. a. (1997). *Efficient Sampling Technique for Optimization under Uncertainty.* AIChE Journal.

EN 14080. (2013). *Timber structures - Glued laminated timber and glued solid timber - Requirements.* Nederlands Normalisatie-instituut.

F. Barbosa, e. a. (2017). *Reinventing construction: A route to higher productivity.* New York: McKinsey.com.

Finnish Forest Industries Federation. (n.d.). *Handbook of Finnish Handbook.*

Folkins, G. (n.d.). *1430 Q.* D&S Development, Sacramento.

Gaaij, J. d. (2021). *Multidisciplinary Design Optimization of Timber High-Rise.* Delft: TU Delft repository.

Gramacy, R. B. (2020). *Surrogates: Gaussian process modeling, design and optimization for the applied sciences.* CRC Press.

Hendriks, M. A. (2021). *Plate analysis, theory and applications.* Delft: TU Delft.

Hoekstra, T. (2012). *MULTI-STOREY TIMBER-FRAME BUILDING - modelling the racking stiffness of timber-frame shear-walls.* Delft: TU Delft Repository.

ISSO. (2020). *ISSO-handboek HBhsb - Houtskeletbouw - Ontwerp, techniek en uitvoering.* Rotterdam: ISSO.

J. Porteus, A. K. (2007). *Structural Timber Design to Eurocode 5.* Edinburgh: Blackwell Publishing.

J.L. Loeppky, J. S. (2013). *Choosing the Sample Size of a Computer Experiment: A Practical Guide.* London: Taylor & Francis.

Leur, S. v. (2023). *Material efficiency.* Delft: TU Delft repository.

Malo, A. (2023). *SERVICEABILITY STIFFNESS OF TIMBER CONNECTIONS WITH DOWELS AND SLOTTED-IN STEEL PLATES.* Oslo: World Conference on Timber Engineering.

Marelli, S., & Lüthen, N. (2026, 01 26). *The Framework for Uncertainty Quantification*. Retrieved from UQLab: https://www.uqlab.com/pce-user-manual

Metsä. (2025, May). Kerto LVL - Kerto-Ripa - Prefabricated building elements. Finland.

Miller, R. (2019). 1430 Q: Engineering the first 6-over-2 podium building in the US. Sacramento, California: Woodworks.org.

Ministerie van Volkshuisvesting en Ruimtelijke Ordening. (2023, 07 24). *900.000 nieuwe woningen om aan groeiende vraag te voldoen*. Retrieved 11 14, 2025, from https://www.rijksoverheid.nl/onderwerpen/volkshuisvesting/nieuwe-woningen

Ministerie van Volkshuisvesting en Ruimtelijke Ordening. (2024, 08 12). *Berekening woningbouwopgave*. Retrieved 11 14, 2025, from https://www.volkshuisvestingnederland.nl/documenten/2024/08/12/berekening-woningbouwopgave

Moelven Limtre As. (2019). *Mjøstårnet.* Retrieved from moelven.com: https://www.moelven.com/mjostarnet/

NEN-EN 1991-1-1+C1/NB:2019 nl. (2019). *Eurocode 1: Belastingen op constructies - Deel 1-1: Algemene belastingen - Volumieke gewichten, eigen gewicht en opgelegde belastingen voor gebouwen inclusief Nationale Bijlage.* Nederlands Normalisatie-instituut.

NEN-EN 1991-1-4+A1+C2. (2011). *Eurocode 1: Loads on structures - Part 1-4: General Loads - Wind load .* Delft: Nederlands Normalisatie-instituut.

NEN-EN-1990-NB. (2019). *National Annex to NEN-EN 1990+A1:2006+A1:2006/C2:2019 Eurocode: Basis of structural design.* Delft: Koninklijk Nederlands Normalisatie-instituut.

NEN-EN-1995-1-1. (2011). *Eurocode 5: Design of timber structures – Part 1-1: General - Common rules and rules for buildings.* Delft: Nederlands Normalisatie-instituut.

NEN-EN-1995-1-1. (2025). *Eurocode 5 - Design of timber structures - Part 1-1: General rules and rules for buildings.* Brussels: EUROPEAN COMMITTEE FOR STANDARDIZATION.

O. Lang, e. a. (2019). *Development of a Design-Driven Parametric Mass Timber Construction System for Modular High-Rise Urban Housing.* Vancouver, Canada: Modular and Offsite Construction.

Paardekooper, N. (2025). *Stability Systems for Timber High-Rise Structures - Parametric study on the influence of complementary stabilizing.* Delft: TU Delft.

PAO. (2021, 11 10). Techniek houtcursus uitvoeringsaspecten.

Reed, P., & Hadjimichael, A. (2022). *3. Sensitivity Analysis: The Basics*. Retrieved from Addressing Uncertainty in MultiSector Dynamics Research: https://uc-ebook.org/docs/html/3_sensitivity_analysis_the_basics.html#sensitivity-analysis-methods

Rijksoverheid. (n.d.). *Klimaatverandering beperken*. Retrieved 11 17, 2025, from https://www.rijksoverheid.nl/onderwerpen/klimaatverandering/klimaatverandering-beperken

Rothoblaas. (2022). *WHT ANGLE BRACKET FOR TENSILE LOADS.*

Saltelli, & Tarantola. (2004). *SENSITIVITY ANALYSIS IN PRACTICE.* Wiley.

Saltelli, A. (2002). *Making best use of model evaluations.* Ispra (VA), Italy: ELSEVIER.

Saltelli, A. (2008). *Global Sensitivity Analysis - The Primer.* England: Wiley.

Sandhaas, C., & Munch-Andersen, J. P. (2018). *Design of Connections in Timber Structures: A state-of-the-art report by COST Action .* Aachen, Germany: COST Action FP1402 / WG3 FP1402.

Saxion. (2025). *WOODCORE*. Retrieved from saxion.nl: https://www.saxion.nl/onderzoek/projecten/w/woodcore#Over%20dit%20project

SCIA Engineer. (n.d.). *Interpolation of FEM results on 2D members*. Retrieved from scia.net: https://www.scia.net/en/support/faq/scia-engineer/results/interpolation-fem-results-2d-members#:~:text=A%20basic%20rule%20for,plate.

SCIA Engineer. (n.d.). *Orthotropic behaviour of plates*. Retrieved from scia.net: https://www.scia.net/en/support/faq/scia-engineer/modelling/orthotropic-behaviour-plates

SciKit. (n.d.). *1.7. Gaussian Processes*. Retrieved from scikit-learn.org: https://scikit-learn.org/stable/modules/gaussian_process.html

Stora Enso. (n.d.). *Glued laminated timber (GLT)*. Retrieved from storaenso.com: https://www.storaenso.com/en/products/mass-timber-construction/building-products/glulam

Sudret, B. (2007). *Global sensitivity analysis using polynomial chaos expansions.* Moret-sur-Loing Cedex, France: ELSEVIER.

TKI. (2025). Innovatief HSB-geÏnspireerd kernexoskelet systeem voor emissiearme. Nederland.

Urban Climate Architects. (2026). *HANDBOEK HOUTBOUW IN DETAIL.*

Verhaegh, R. (2021). *Haut Amsterdam – a 21-Storey Timber.* Berlin: Holzbau Kongress Berlin DHK 2021.

Wagemans, L. (2014). *Quick Reference.* Delft: Section Structural and Building Engineering, Delft.

WEBO. (n.d.). *Prefab Timber-Frame Facade Element.* Rijssen.

Williams, B., & Cremaschi, S. (2019). *SURROGATE MODEL SELECTION FOR DESIGN.* Copper Mountain, Colorado, USA: Elsevier.

WoodWorks. (2020). *Sacramento Developer Builds First Six-Storey Light Wood-Frame Residential Building in the U.S.* Retrieved from Woodworks.org: https://www.woodworks.org/resources/1430-q-light-frame-maximizes-space-and-profitability-in-a-competitive-market/

Xia, B., & O'Neill, T. (2014). *Perceived obstacles to multi-storey timber-frame construction: an Australian study.* Brisbane, Australia: Taylor & Francis.

Yan, L., & Chen, H. (2025). *High-rise timber buildings: Benchmarks in structural systems, fire safety, prefabrication efficiency and environmental insights of world's 10 tallest completed mass timber projects.* Braunschweig: ScienceDirect.

Appendix A – Calculation wind load on the building

The wind load on the building will be considered as the load having the largest effect on the horizontal deflection of the building. This section describes how the wind load can be calculated for the building. The wind load will be determined according to the guidelines of EN 1991-1-4 in combination with the corresponding National Annex.

A.1 Wind pressure distribution over the height

Depending on the slenderness of the building, the Eurocode provides different profiles for the wind load on the building façade. The building from the case study has a footprint of 21.5 x 23.5 m^2. The height of the building will vary from 18 to 45 meters. Most variants that will be considered can be assigned to the profile where b < h < 2*b. Therefore, it is assumed that this profile can be applied for all variants with varying heights. This wind profile divides the wind load into two parts with constant values over the height as displayed in Figure A.1.

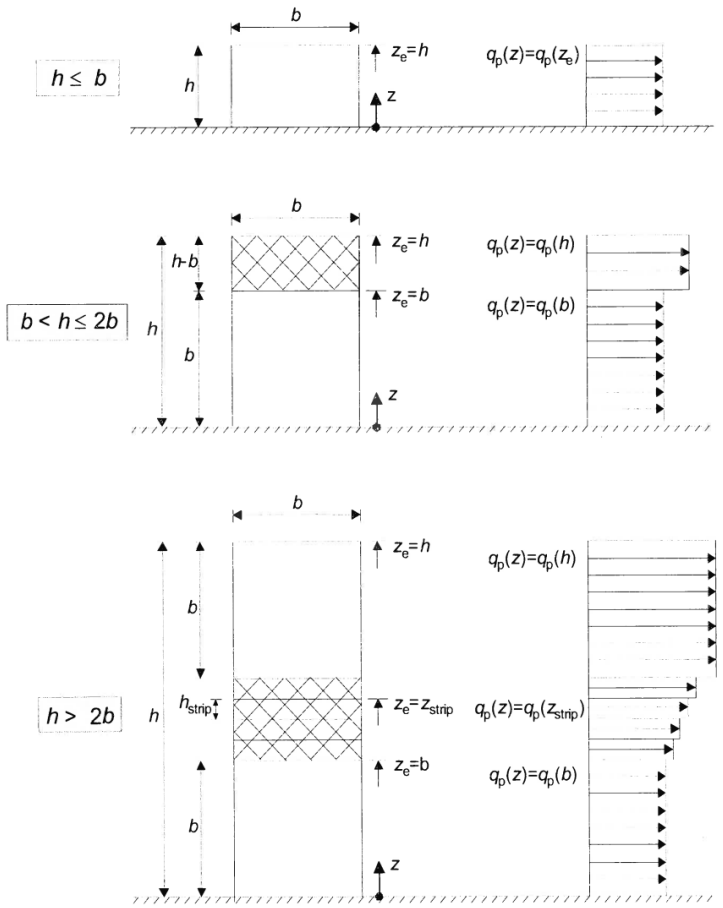

Figure A.1: Wind-load profiles for varying building heights (NEN-EN 1991-1-4+A1+C2, 2011).

A.2 General formula characteristic wind-load

According to EN 1991-1-4, the wind force F_w on a structure can be determined in multiple ways. Since the building in this case study is a mid- to high-rise building, the formula where the force coefficient c_f is determined per component will be used. The general formula for calculating the wind load is displayed in equation A.1 (NEN-EN 1991-1-4+A1+C2, 2011).

$$F_w = c_s c_d * \sum_{elements} c_f * q_p(z_c) * A_{ref} \quad \text{(A.1)}$$

Where:

$c_s c_d$	[-]	=	Structural factor
c_f	[-]	=	Force coefficient
$q_p(z_c)$	[N/m^2]	=	Peak wind pressure
A_{ref}	[m^2]	=	The reference area of the construction element

A.3 Determination structural factor $c_s c_d$:

The structural factor $c_s c_d$ takes into account the effects of the non-simultaneous occurrence of peak wind pressures on the surface (size factor c_s) together with the effect of the vibrations of the structure due to turbulence (dynamic factor c_d). The Eurocode states that for buildings with a frame structure of with shear walls which are less than 100 m high and whose height is less than 4 times the building depth in the wind direction, the structural factor $c_s c_d$ can be assumed to be equal to 1.0 . (NEN-EN 1991-1-4+A1+C2, 2011).

A.4 Determination expected wind velocity v_m and peak wind pressure q_p

In addition to the structural factor, the total wind load is dependent on the expected wind velocity and the corresponding peak wind pressure. De wind velocity is dependent on the wind region where the building is located a dependent on the terrain category which gives an identification of the roughness of the terrain surrounding the building. The peak wind pressure indicates the load of the wind velocity in a undisturbed wind field. The peak wind pressure can be determined using equation A.2 (NEN-EN 1991-1-4+A1+C2, 2011).

$$q_p(z) = [1 + 7 * I_V(z)] * \frac{1}{2} * \rho * v_m^2(z) \quad \text{(A.2)}$$

Where:

I_V	[-]	=	Factor for turbulence intensity
ρ	[kg/m^3]	=	Volumetric mass of air = 1.25
v_m	[m/s]	=	Average wind velocity on height z
z	[m]	=	height in z-direction

Turbulence intensity factor I_v:

The turbulence intensity factor can subsequently be determined using equation A.3.

$$I_V = \frac{1}{c_0 * \ln(\frac{z}{z_0})} \quad \text{(A.3)}$$

Where:

z	[m]	=	height in z-direction
c_0	[-]	=	Orography factor
z_0	[m]	=	Roughness length

In equation 8.3, the orography factor accounts for height differences in the terrain. It is assumed that the terrain around the building is flat. Therefore, it holds that $c_0 = 1.0$.

The roughness length z_0 is dependent on the terrain category surrounding the building. As there was no location assigned to the building from this case-study, assumptions need to be made. It is assumed that the building is surrounded by a rural area which corresponds to terrain category II. Using Table A.1, it can be obtained that the corresponding roughness length z_0 is equal to 0.2 m and the minimum height z_{min} is equal to 4 m. Below the minimum height the wind pressure needs to be determined by multiplying the fundamental wind pressure with the constant exposure factor $c_e(z_{min})$. As this load only applies on the lowest 5 meters of the building, the effect of the exposure factor will have a limited effect on the lateral deformation of the building. Therefore, it is assumed that the wind pressure below z_{min} is equal to the wind pressure above z_{min}.

Terrain Category		z_0 [m]	z_{min} [m]
0	Sea or coastal area	0.005	1
II	Rural area	0.2	4
III	Urban area	0.5	7

Table A.1: Terrain categories according to (NEN-EN 1991-1-4+A1+C2, 2011).

Average wind velocity $v_m(z)$:
The average wind velocity can be determined using equations A.4 to A.7.

$$v_m(z) = c_r(z) * c_0(z) * v_b \quad \text{(A.4)}$$

$$c_r(z) = k_r * \ln(\frac{z}{z_0}) \quad \text{(A.5)}$$

$$k_r(z) = 0.19 * \left(\frac{z_0}{0.05}\right)^{0.07} \quad \text{(A.6)}$$

$$v_b(z) = c_{dir} * c_{season} * v_{b,0} \quad \text{(A.7)}$$

Where:

$c_r(z)$	[-]	=	Roughness factor
$c_0(z)$	[-]	=	Orography factor, flat terrain is assumed = 1.0
v_b	[m/s]	=	Standard wind velocity at reference height of 10 m.
k_r	[-]	=	Terrain factor
z	[m]	=	height in z-direction
z_0	[m]	=	Roughness length
c_{dir}	[-]	=	Direction factor = 1.0
c_{dir}	[-]	=	Season factor = 1.0
$v_{b,0}$	[-]	=	Fundamental wind velocity

The standard wind velocity v_b is dependent on the wind region in which the building is located and can be obtained by multiplying the fundamental wind velocity with the directional and seasonal factor, which are taken as 1.0 The fundamental value of the standard wind velocity $v_{b,0}$ can be determined using Table A.2. It is assumed that the building is located in wind region II.

Wind region	I	II	III
$v_{b,0}$ [m/s]	29.5	27.0	24.5

Table A.2: standard wind velocity for different wind regions (NEN-EN 1991-1-4+A1+C2, 2011).

The average wind velocity can subsequently be determined by multiplying the standard wind velocity with the orography factor $c_o(z)$ and roughness factor $c_r(z)$. Using the roughness factor and the orography factor, the average velocity can subsequently be calculated.

A.5 Determination of force coefficient c_f

The last step in calculating the wind load on the building is by multiplying the peak wind pressure with factors the force coefficients c_f that accounts for aerodynamic effects of the building. To determine the force coefficients, the facades of the building are divided into different areas dependent on the wind direction and the main dimensions of the building. In Figure A.2, the wind pressure zones the facades is displayed.

In addition, to the wind pressure on the facades perpendicular to the wind direction (areas D and E), the Eurocode accounts also for the wind pressure on the facades parallel to the wind direction (areas A, B and C). As the length of the facades is relatively short and as the parallel wind pressure have no significant effect on the lateral deformation, the wind pressure on the parallel facades are assumed to be equal to zero for this study.

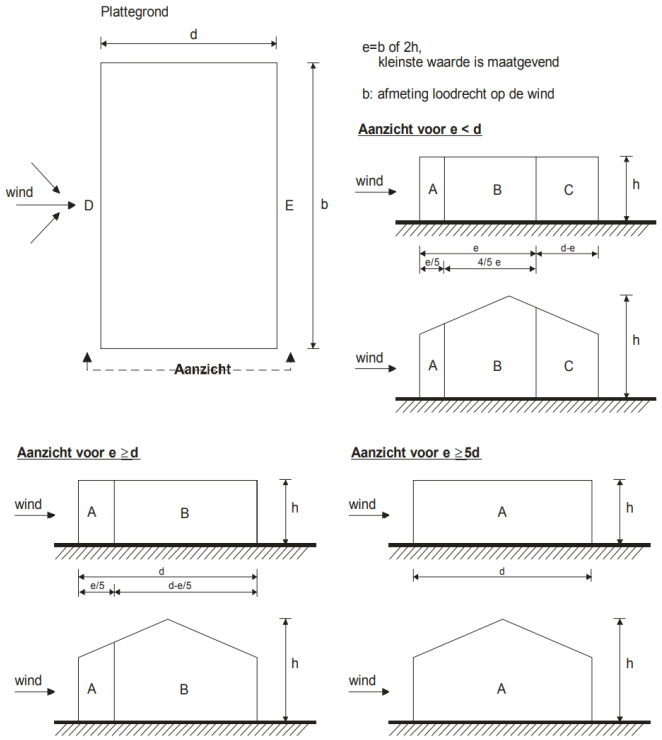

Figure A.2: Wind pressure zones for walls (NEN-EN 1991-1-4+A1+C2, 2011).

In Table A.3, the corresponding values for the pressure coefficients are displayed. As the area of the facades is much larger than 10 m^2, the factors $c_{pe,10}$ apply. The factors are also dependent on the slenderness of the building. Between the factors of column E, linear interpolation can be applied. For the reference building with a height of 45 meters, the slenderness is approximately equal to 2. Therefore $c_{pe,10,E}$, will be equal to -0.55. The pressure coefficient for the façade directly facing the wind direction is equal to $c_{pe,10,D}$ = +0.8.

Zone	A		B		C		D		E	
h/d	$C_{pe,10}$	$C_{pe,1}$	$C_{pe,10}$	$C_{pe,1}$	$C_{pe,10}$	$C_{pe,1}$	$C_{pe,10}$	$C_{pe,1}$	$C_{pe,10}$	$C_{pe,1}$
5	-1,2	-1,4	-0,8	-1,1	-0,5		+0,8	+1,0	-0,7	
1	-1,2	-1,4	-0,8	-1,1	-0,5		+0,8	+1,0	-0,5	
≤ 0,25	-1,2	-1,4	-0,8	-1,1	-0,5		+0,7	+1,0	-0,3	

Table A.3: Values for the external pressure coefficients on facades (NEN-EN 1991-1-4+A1+C2, 2011).

In the Dutch National Annex, it is stated that the pressure coefficients may be reduced by multiplying the total pressure coefficient with a factor 0.85 (NEN-EN 1991-1-4+A1+C2, 2011). The total pressure coefficient that can be applied is therefore equal to (+0.8 – (-0.55)) * 0.85 = 1.15. The factor cannot be applied for both the D and E façade simultaneously. The Eurocode describes two ways to apply this reduction coefficient. In this study it is assumed that façade D is fully loaded by the wind. The wind pressure on façade E is then equal to the remaining such that the total of pressure coefficient is equal to 1.15 (1.15–0.80=0.35).

Appendix B – Design of timber members

B.1 Material properties timber

The characteristic material properties of glulam which will be used for the design of the building are displayed in Table B.1 (EN 14080, 2013).

Property	Symbol	Glulam strength class						
		GL 20h	GL 22h	GL 24h	GL 26h	GL 28h	GL 30h	GL 32h
Bending strength	$f_{m,g,k}$	20	22	24	26	28	30	32
Tensile strength	$f_{t,0,g,k}$	16	17,6	19,2	20,8	22,3	24	25,6
	$f_{t,90,g,k}$	0,5						
Compression strength	$f_{c,0,g,k}$	20	22	24	26	28	30	32
	$f_{c,90,g,k}$	2,5						
Shear strength (shear and torsion)	$f_{v,g,k}$	3,5						
Rolling shear strength	$f_{r,g,k}$	1,2						
Modulus of elasticity	$E_{0,g,mean}$	8 400	10 500	11 500	12 100	12 600	13 600	14 200
	$E_{0,g,05}$	7 000	8 800	9 600	10 100	10 500	11 300	11 800
	$E_{90,g,mean}$	300						
	$E_{90,g,05}$	250						
Shear modulus	$G_{g,mean}$	650						
	$G_{g,05}$	540						
Rolling shear modulus	$G_{r,g,mean}$	65						
	$G_{r,g,05}$	54						
Density	$\rho_{g,k}$	340	370	385	405	425	430	440
	$\rho_{g,mean}$	370	410	420	445	460	480	490

Table B.1: Characteristic strength and stiffness properties [MPa] and densities kg/m^3 for homogeneous glulam (EN 14080, 2013)

B.2 Overview verification

For the design of the timber building every timber element needs to be dimensioned to resist the design loads which are applied on the structure. The dimensions of the elements in the exoskeleton and the core skeleton will be used as lower-bound for the sensitivity analysis and the optimization and will therefore be determined for every variant. The dimensions of the remaining elements are only determined once for the main variant of 15 stories. In Table B.2, an overview of the checks which are determined for every element is displayed. The equations for every Unity Check are displayed in Table B.3.

	Compression	Tension	Buckling pure compression	Buckling compression + bending	Shear	Bending + tension	Vertical deflection
Beams Exoskeleton	X	X		X		X	X
Columns Exoskeleton	X	X	X				
Diagonals Exoskeleton	X	X	X				
Beams Core	X	X		X		X	X
Columns Core	X	X	X				
Diagonals Core	X	X	X				
Beams Wall	X			X	X	X	X
Beams Floor	X			X	X	X	X
Columns Remaining	X	X	X				

Table B.2: Overview of calculated Unity Check for every structural element.

ULS Check	***Formula***
Cross-section verification for one stress in one principal direction	
Compressive stress:	
parallel to the grain	$\sigma_{c,0,d} \leq f_{c,0,d}$
perpendicular to the grain	$\sigma_{c,90,d} \leq k_{c,90} * f_{c,90,d}$ $\sigma_{c,90,d} = \frac{F_{c,90,d}}{A_{ef}}$
at an angle to the grain	$\sigma_{t,\alpha,d} \leq f_{c,\alpha} = \frac{f_{c,0} * f_{c,90}}{f_{c,0} * \sin^2(\alpha) + f_{c,90} * cos^2(\alpha)}$
Tensile stress:	
parallel to the grain	$\sigma_{t,0,d} \leq f_{t,0,d}$
at an angle to the grain	$\sigma_{t,\alpha,d} \leq \frac{f_{t,0,d}}{\frac{f_{t,0,d}}{f_{t,90,d}} * \sin^2 \alpha + \frac{f_{t,0,d}}{f_{v,d}} * \sin \alpha * \cos \alpha + \cos^2 \alpha}$
Bending:	
both equations should be satisfied	$\frac{\sigma_{m,y,d}}{f_{m,y,d}} + k_m * \frac{\sigma_{m,z,d}}{f_{m,z,d}} \leq 1$ $k_m * \frac{\sigma_{m,y,d}}{f_{m,y,d}} + \frac{\sigma_{m,z,d}}{f_{m,z,d}} \leq 1$

Shear:	
parallel and perpendicular to the grain	$\tau_d \leq f_{v,d}$
Cross-section verification for combined stresses	
Combined bending and axial tensile stresses	$\frac{\sigma_{t,0,d}}{f_{t,0,d}} + \frac{\sigma_{m,y,d}}{f_{m,y,d}} + k_m * \frac{\sigma_{m,z,d}}{f_{m,z,d}} \leq 1$ $\frac{\sigma_{t,0,d}}{f_{t,0,d}} + k_m * \frac{\sigma_{m,y,d}}{f_{m,y,d}} + \frac{\sigma_{m,z,d}}{f_{m,z,d}} \leq 1$
Combined bending and axial compressive stresses	$\left(\frac{\sigma_{c,0,d}}{f_{c,0,d}}\right)^2 + \frac{\sigma_{m,y,d}}{f_{m,y,d}} + k_m * \frac{\sigma_{m,z,d}}{f_{m,z,d}} \leq 1$ $\left(\frac{\sigma_{c,0,d}}{f_{c,0,d}}\right)^2 + k_m * \frac{\sigma_{m,y,d}}{f_{m,y,d}} + \frac{\sigma_{m,z,d}}{f_{m,z,d}} \leq 1$
Tensile stress at an angle to the grain	$\frac{\sigma_{t,0,d}}{f_{t,0,d}} + \frac{\sigma_{t,90,d}}{k_{vol} * k_{dis} * f_{t,90,d}} \leq 1$ $\sigma_{t,0,d} = \sigma_{t,\alpha,d} * \cos^2 \alpha$ $\sigma_{t,90,d} = \sigma_{t,\alpha,d} * \sin^2 \alpha$
Stability of elements	
Buckling of column subjected to compression or compression and bending:	$\frac{\sigma_{c,0,d}}{k_{c,y} * f_{c,0,d}} + \frac{\sigma_{m,y,d}}{f_{m,y,d}} + k_m * \frac{\sigma_{m,z,d}}{f_{m,z,d}} \leq 1$ $\frac{\sigma_{c,0,d}}{k_{c,z} * f_{c,0,d}} + + k_m * \frac{\sigma_{m,y,d}}{f_{m,y,d}} + \frac{\sigma_{m,z,d}}{f_{m,z,d}} \leq 1$
Lateral torsional buckling of beam subjected to bending or compression and bending:	$\left(\frac{\sigma_{m,d}}{k_{crit} * f_{m,d}}\right)^2 + \frac{\sigma_{c,0,d}}{k_{c,z} * f_{c,0,d}} \leq 1$

Table B.3: Overview ULS verifications of timber members.

Where:

$\sigma_{c,0,d}$	[MPa]	=	Design compressive stress parallel to the grain
$f_{c,o,d}$	[MPa]	=	Design compressive strength parallel to the grain
$\sigma_{c,90,d}$	[MPa]	=	Design compressive stress perpendicular to the grain
$k_{c,90}$	[-]	=	Factor accounting for load configuration, splitting risk and the extent of deformation. Equals 1.0 for standard load conditions.
$f_{c,90,d}$	[MPa]	=	Design compressive strength perpendicular to the grain
$F_{c,90,d}$	[N]	=	Design compressive force perpendicular to the grain
A_{ef}	[mm^2]	=	Effective contact area for compression perpendicular to the grain
$\sigma_{c,\alpha,d}$	[MPa]	=	Design compressive stress under an angle α between the load and grain direction
$\sigma_{t,0,d}$	[MPa]	=	Design tensile stress parallel to the grain
$f_{t,o,d}$	[MPa]	=	Design tensile strength parallel to the grain

$\sigma_{t,90,d}$	[MPa]	=	Design tensile stress perpendicular to the grain
$f_{t,90,d}$	[MPa]	=	Design tensile strength perpendicular to the grain
$\sigma_{t,\alpha,d}$	[MPa]	=	Design tensile stress under an angle α between the load and grain direction
$f_{v,d}$	[MPa]	=	Design shear strength
$\sigma_{m,y,d}$	[MPa]	=	Design bending stress in y-direction
$\sigma_{m,z,d}$	[MPa]	=	Design bending stress in z-direction
$f_{m,y,d}$	[MPa]	=	Design bending strength in y-direction
$f_{m,z,d}$	[MPa]	=	Design bending strength in z-direction
k_m	[-]	=	Factor accounting for redistribution of stresses and heterogeneity of material. Equals 0.7 for rectangular glulam cross-sections
τ_d	[MPa]	=	Design shear stress
k_{vol}	[-]	=	Factor accounting for the influence of volume
k_{dis}	[-]	=	Factor accounting for the distribution of tensile stresses perpendicular to the grain
$k_{c,y}$, $k_{c,z}$	[-]	=	Factors in y and z-direction accounting for the reduction in compressive strength due to buckling
k_{crit}	[-]	=	Factor accounting for the reduction in bending strength due to lateral torsional buckling

B.3 Design calculation for the governing failure mode

For the columns and diagonals in both the exoskeleton as the braced core, buckling under pure compression was the governing failure mode. In this appendix the calculation of the unity check fort his failure mode will be displayed. As the connection between the timber elements are assumed to be hinged, the buckling length of the diagonals and columns is assumed to be equal to the length of the element itself. All cross-sections are assumed to be square for his calculation.

Radius of gyration:

$$i = \sqrt{\frac{I}{A}} \tag{B.1}$$

Where:

I	[mm^4]	=	The moment of inertia of the cross-section
A	[mm^2]	=	The area of the cross-section

Slenderness:

$$\lambda = \sqrt{\frac{l_{buc}}{i}} \tag{B.2}$$

Where:

l_{buc}	[mm]	=	The buckling length of the member
i	[mm]	=	The radius of gyration

Relative slenderness

$$\lambda_{rel} = \frac{\lambda}{\pi}\sqrt{\frac{f_{c,0,k}}{E_{0,05}}} \tag{B.3}$$

Where:

λ	[-]	=	The slenderness of the member
$f_{c,0,k}$	[MPa]	=	The characteristic compressive strength
$E_{0,05}$	[MPa]	=	The characteristic Young's modulus

Buckling factors:

$$k = 0{,}5 * (1 + \beta_c * (\lambda_{rel} - 0.3) + \lambda_{rel}^2) \tag{B.4}$$

$$k_c = \frac{1}{k_y + \sqrt{k^2 - \lambda_{rel}^2}} \tag{B.5}$$

Where:

λ_{rel}	[-]	=	The relative slenderness of the member
β_c	[-]	=	Straightness factor

Resulting Unity Check:

$$\frac{\sigma_{c,0,d}}{k_c * f_{c,0,d}} \leq 1 \tag{B.6}$$

Where:

$\sigma_{c,0,d}$	[MPa]	=	The design compressive stress in the member
$f_{c,0,d}$	[MPa]	=	The design compressive strength of the member

Appendix C – Modelling of floors

As the Kerto-Ripa floors in the building consists of ribs and plates, the floors have orthotropic stiffness properties: the stiffness in the x-direction is different than the stiffness in y-direction. To implement this behaviour the floors are modelled in SCIA using orthotropic plates as described in paragraph 5.1.1.

In Figure C.1, one single floor element including the dimensions in mm is displayed. The Youngs modulus of the plates and ribs in the floor elements are respectively equal to 10500 MPa and 12000 MPa (Metsä, 2025). The shear modulus is assumed to be equal to 600 MPa. As the Kert-Ripa floors are hollow it is assumed that the Poisson factor for the interaction between the stiffness in x and y direction is equal to 0.

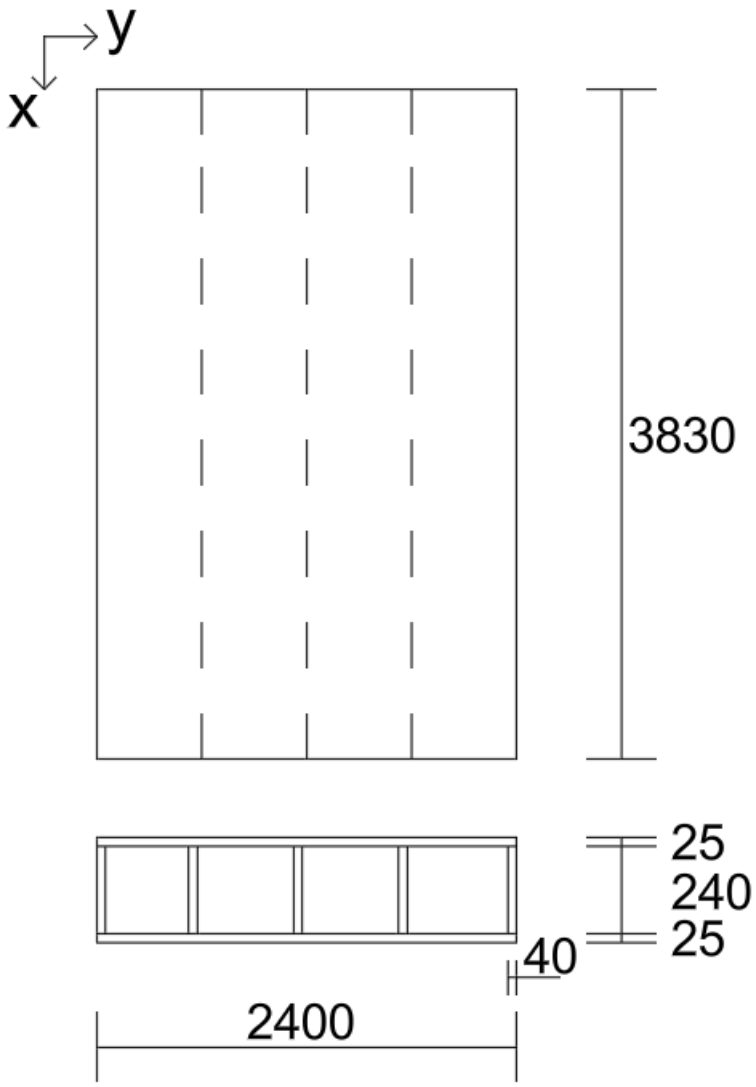

Figure C.1: Visualisation of a Kerto-Ripa floor element including dimensions.

Bending stiffness in x and y-direction D_{11} and D_{22} :

The LVL rib and plate elements of the Kerto-Ripa floors are glued together due to which full composite action between the ribs and plates can be obtained resulting to a gamma factor of 1. Therefore, the bending stiffness of the floors can simply be computed by combining the bending stiffness of every element in the floor using Steiner displacement rule as displayed in equation C.1.

$$\begin{aligned} EI_{tot,x} &= E_r * 5 * (\frac{1}{12} * b * h_r^3) + E_p * 2 * (\frac{1}{12} * b_p * h_p^3 + \left(\frac{1}{2} * h_r + \frac{1}{2} * h_p\right)^2 * b_p * h_p) \\ EI_x = D_{11} &= \frac{EI_{tot,x}}{b_p} = 10.74\ MNm^2/m \\ EI_{tot,y} &= E_p * 2 * (\frac{1}{12} * l_p * h_p^3 + \left(\frac{1}{2} * h_r + \frac{1}{2} * h_p\right)^2 * l_p * h_p) \\ EI_y = D_{22} &= \frac{EI_{tot,y}}{l_p} = 2.11\ MNm^2/m \end{aligned} \quad \text{(C.8)}$$

Combined bending stiffness factor D_{12}:

This factor is calculated using equation C.2. As the Poisson factor is assumed to be equal to 0 the combined bending stiffness is equal to 0.

$$D_{12} = \nu * \sqrt{D_{11} * D_{22}} = 0 \quad \text{(C.2)}$$

Torsional stiffness D_{33}:

The torsional bending stiffness of the plate is the most difficult to determine as the plate consist of multiple hollow compartments. As the torsional stiffness of the floors have only limited effect on the global horizontal displacement of the building, a simplified approach was chosen where every compartment of the floor was assumed to be equal to a hollow rectangular cross-section, and the stiffness was calculated using the formula of Bredt. Interaction between these compartments is not considered. In equation C.3 the torsional stiffness is computed.

$$\begin{aligned} GI_{t,comp} &= G * \frac{4 * \left(b_{comp} * h_{comp}\right)^2}{2 * \frac{b_{comp}}{t_p} + 2 * \frac{h_{comp}}{\frac{1}{2} * t_r}} \\ D_{33} &= \frac{GI_{t,comp}}{b_{comp}} = 1{,}00\ MNm \end{aligned} \quad \text{(C.3)}$$

Shear flexural stiffness in x- and y-direction D_{44} and D_{55}

Using the shear flexural factors for modelling orthotropic plates shear deformation of the plates can be accounted for. However, as the plates have a slenderness ratio bigger than 10, shear deformation of the floors can be neglected (Hendriks, 2021). Therefore, it is assumed that the shear flexural stiffness in both x and y-direction is close to infinite. The resulting chosen parameters for the shear flexural stiffness are displayed in equation C.4.

$$\begin{aligned} D_{44} &= 1\,000\,000\ MN/m \\ D_{55} &= 1\,000\,000\ MN/m \end{aligned} \quad \text{(C.4)}$$

Axial stiffness in x- and y-direction d_{11} and d_{22}:

The most important stiffness property of the orthotropic floor elements for the global lateral behaviour of the building is the axial stiffness of the floors. The axial stiffness is calculated by simplify multiplying the cross-sectional area of the elements of the floor with the Young's modulus of the plates and ribs in the floor. As the ribs only span in x-direction, the axial stiffness in x-direction Is greater than the axial stiffness in y-direction as displayed in equation C.5.

$$\begin{gathered} EA_{tot,x} = E_p * 2 * b_p * h_p + E_r * 5 * b_r * h_r \\ EA_{eq,x} = \frac{EA_{tot,x}}{b_p} = \ d_{11} = 836\ MN/m \\ EA_{tot,y} = E_p * 2 * l_p * h_p \\ EA_{eq},y = \frac{EA_{tot,y}}{l_p} = \ d_{22} = 159\ MN/m \end{gathered} \tag{C.5}$$

Shear membrane stiffness parameter d_{33}:

The shear membrane stiffness parameter for the orthotropic plate can be computed using equation C.6. As explained before the Poisson ratio is assumed to be equal to 0.

$$d_{33} = (1 - \nu) * \sqrt{d_{11} * d_{22}} = 158\ MN/m \tag{C.6}$$

Combined axial stiffness in x- and y-direction d_{12}:

The combined axial stiffness for the orthotropic plate can be computed using equation C.7. As the Poisson ratio is assumed to be equal to 0, this stiffness parameter is equal to 0.

$$d_{33} = \nu * \sqrt{d_{11} * d_{22}} = 0\ MN/m \tag{C.7}$$

Appendix D – Modelling of timber frame walls

As described in paragraph 5.1.2 and 6.2.4, the timber frame shear walls will be modelled using the equivalent diagonal method as the stiffness of the timber frame shear walls is dependent on many factors which cannot be efficiently modelled in detail using the finite element software. The calculation used to determine the stiffness and resulting dimensions of the equivalent diagonal is explained in this Appendix. In Figure D.1 the schematisation of the timber frame wall is displayed (Hoekstra, 2012).

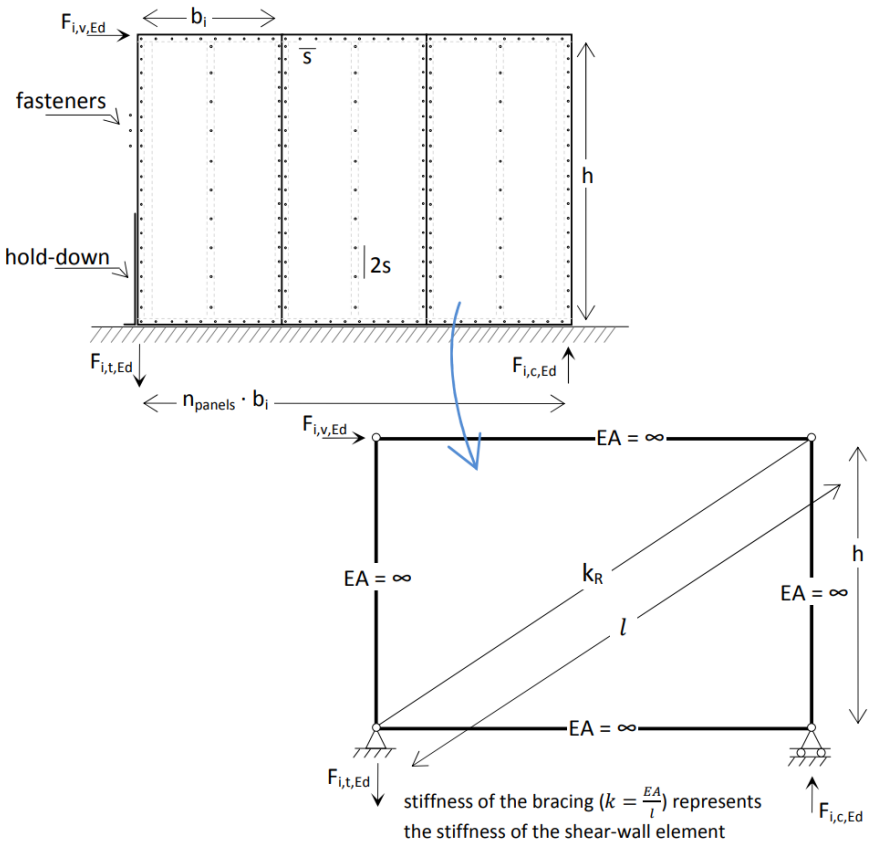

Figure D.1: Model for the structural analysis of timber-frame shear walls in a framework program (Hoekstra, 2012)

Influence of slip modulus nails

The slip modulus for one individual nail can be calculated according to Eurocode 1995 (NEN-EN-1995-1-1, 2011) and can be rewritten as a function of the racking stiffness using equation D.1.

$$K_{ser} = \rho_{mean}^{1,5} * \frac{d^{0.8}}{30}$$
$$R_n = \frac{n_{panels} * n_{faces} * b_1}{2 * (1 + \frac{h}{b_1})} * \frac{K_{ser}}{s} = 8670\ N/mm \quad \text{(D.1)}$$

Stiffness due to compression perpendicular to the bottom rail:
The influence on the racking stiffness due to perpendicular to the bottom rail at the corner of the wall in compression can be computed using equation D.2.

$$K_{c,90} = 1{,}33 * \left(n_{studs,corner} * b_1\right) + 30) * h$$
$$R_c = \frac{(n_{panels} * b_1)^2}{h^2} * K_{c,90} = 109230\ N/mm \quad \text{(D.2)}$$

Hold down stiffness:
The hold down stiffness is based on the catalogue for a hold-down anchor for timber frame shear walls (Rothoblaas, 2022). Hold-down anchor WHT620 with a hold-down stiffness of 47800 N/mm was chosen.

$$K_{hd} = n_{hd} * K_{hd,1}$$
$$R_{hd} = \frac{(n_{panels} * b_1)^2}{h^2} * K_{hd} = 441130\ N/mm \quad \text{(D.3)}$$

Shear deformation of plates:
The shear deformation of the plates can be computed using equation D.4.

$$R_G = \frac{n_{panels} * b_1 * t_{panel}}{h} * G_{mean} = 8589\ N/mm \quad \text{(D.4)}$$

Flexural stiffness of the studs:
The influence of the flexural deformation of the studs on the shear stiffness of the walls can be computed using equation D.5.

$$R_{str} = \frac{n_{studs} * b_{stud} h_{stud} * (n_{panels} * b_1)^2}{h^3} * E_{stud} = 8589\ N/mm \quad \text{(D.5)}$$

Total racking stiffness:
The total racking stiffness of the timber frame shear wall can subsequently be determined by summing every individual effect using equation D.6.

$$R_{tot} = \frac{1}{\frac{1}{R_n} + \frac{1}{R_c} + \frac{1}{R_{hd}} + \frac{1}{R_G} + \frac{1}{R_{str}}} = 4100\ N/mm \quad \text{(D.6)}$$

Equivalent diagonal stiffness:
The racking stiffness can be rewritten to a diagonal stiffness of the wall using equation D.7. The factor n_{frames} indicates the number of timber frames at the location of the wall.

$$k_{eq,dia} = n_{frames} * R_{tot} * (1 + \frac{h^2}{b^2}) = 9980\ N/mm \quad \text{(D.7)}$$

Equivalent diagonal dimension:
Assuming that the diagonal is made out of glulam with strength class GL24h the dimensions of the equivalent diagonal can be calculated using equation D.8.

$$A_{eq,dia} = \frac{k_{eq,dia} * L_{eq,dia}}{E}$$
$$h_{eq,dia} = \sqrt{A_{eq,dia}} = 75\ mm \quad \text{(D.8)}$$

Appendix E – Additional results

E.1 Results global sensitivity analysis of the base-line model with average lower-bounds

For the average lower-bound a minimum cross-sectional dimension of 100 mm is considered for the parameter ranges diagonals in the exoskeleton and braced core. This appendix is an addition to the results of the global sensitivity analysis in Section 6.4.4. In Figure E.1, the first order and total order Sobol-indices are displayed. In figure E.2, the second order Sobol-indices are displayed indicating the interaction between the parameters.

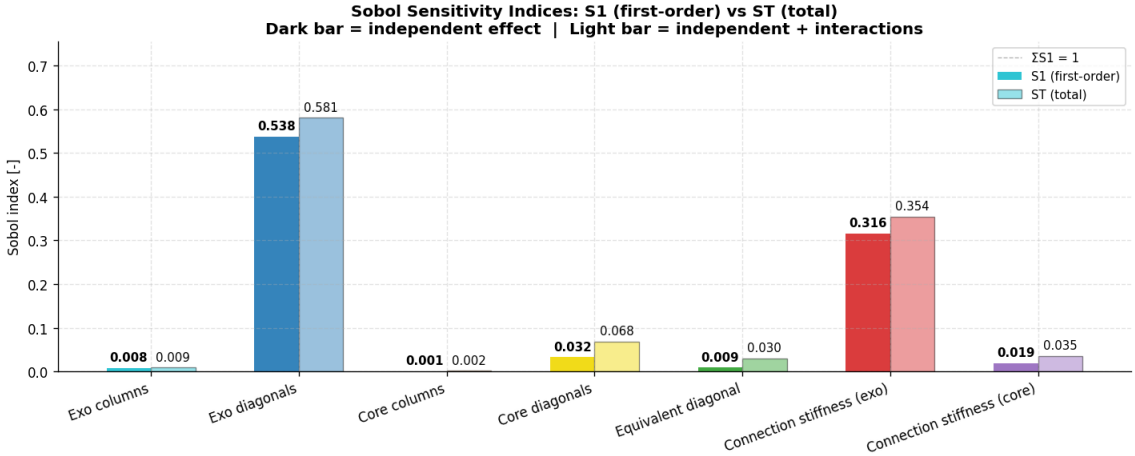

Figure E.1: Results of global sensitivity analysis for the base-line variant with average lower-bounds. The left bar for every parameter indicates the first order Sobol-index and the right bar of every parameter indicates the total Sobol-index.

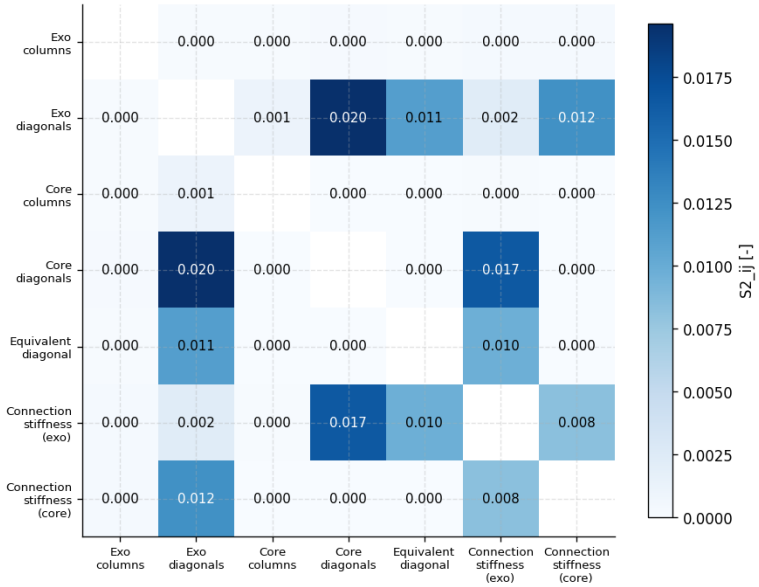

Figure E.2: Interaction diagram of every parameter with each other for the GSA with average lower bounds. The darker the colour of the square, the stronger the interaction.

Appendix F – Access to parametric model

The Python-script, the SCIA Engineer model, and the XML files which are developed for this study can be accessed using the link or the QR-code below. For a more detailed explanation of the parametric workflow is referred to Section 4.4.

https://github.com/JanKarsemeijer/Python-Script-Parametric-Model-Timber-building-concept-using-exoskeleton-and-braced-core.git